ANALYTICAL MODELING OF CONTAMINANT TRANSPORT AND HORIZONTAL WELL HYDRAULICS

A Dissertation

by

EUNGYU PARK

Submitted to the Office of Graduate Studies of
Texas A&M University
in partial fulfillment of the requirements for the degree of

DOCTOR OF PHILOSOPHY

August 2002

Major Subject: Geology

ANALYTICAL MODELING OF CONTAMINANT TRANSPORT AND HORIZONTAL WELL HYDRAULICS

A Dissertation

by

EUNGYU PARK

Submitted to Texas A&M University
in partial fulfillment of the requirements
for the degree of

DOCTOR OF PHILOSOPHY

Approved as to style and content by:

Hongbin Zhan (Chair of Committee)	Bruce E. Herbert (Member)
Mark E. Everett (Member)	Anthony T. Cahill (Member)
Jianxin Zhou (Member)	Andrew Hajash, Jr. (Head of Department)

August 2002

Major Subject: Geology

ABSTRACT

Analytical Modeling of Contaminant Transport and
Horizontal Well Hydraulics. (August 2002)
Eungyu Park, B.S., Yonsei University, Korea;
M.S., Yonsei University, Korea
Chair of Advisory Committee: Dr. Hongbin Zhan

This dissertation is composed of three parts of major contributions.

In Chapter II, we discuss analytical study of contaminant transport from a finite source in a finite-thickness aquifer. This chapter provides analytical solutions of contaminant transport from one-, two-, and three- dimensional finite sources in a finite-thickness aquifer using Green's function method. A library of unpublished analytical solutions with different finite source geometry is provided. A graphically integrated software CTINT is developed to calculate the temporal integrations in the analytical solutions and obtain the final solutions of concentration.

In Chapter III, we obtained solutions of groundwater flow to a finite-diameter horizontal well including wellbore storage and skin effect in a three-dimensionally anisotropic leaky aquifer. These solutions improve previous line source solutions by considering realistic well geometry and offer better description of drawdown near the horizontal well. These solutions are derived on the basis of the separation of the source and the geometric functions. The graphically integrated computer program FINHOW is written to generate type curves of groundwater flow to a finite-diameter horizontal well.

The influence of the finite-diameter of the well, the wellbore storage, the skin effect, the leakage parameter, and the aquifer anisotropy is thoroughly analyzed.

In Chapter IV, a general theory of groundwater flow to a fractured or non-fractured aquifer considering wellbore storage and skin effect is provided. Solutions for both leaky confined and water table aquifers are provided. The fracture model used in this study is the standard double-porosity model. The storage of the aquitard (the leaky confining layer) is included in the formula. A program denoted FINHOW2 is written to facilitate the calculation. Sensitivity of the solution to the confined versus unconfined conditions, fractured versus non-fractured conditions, and wellbore storage and skin effects is analyzed.

DEDICATION

To my beloved parents, my wife, Suho Cho, and my son, Joshua Park.

ACKNOWLEDGMENTS

I, at first, thank my graduate advisor, Dr. Hongbin Zhan, for his unstinting support in both academy and philosophy. During my three years of graduate courses, he has taught me how to be a decent scientist. He is also the coauthor of the publications from this dissertation.

I would like to thank my family. They all patiently supported my endeavor in spiritual and physical aspects. I especially thank my wife, Suho Cho. She has patiently supported my studying in the Unite States by her great sacrifices. She also gave me the most precious present of my life, our son, Joshua Park. They have shared my joy and sorrow during my graduate courses.

Many thanks go to Jinwook Kim and Sungwhan Yuh who counseled me through out my tough time. I have learned a lot from them out of their prudent thoughts. The people in my group also helped me a lot in many ways, and I would like to appreciate our friendship through this writing. I also would like to thank my previous teachers who educated and taught me.

Finally, my sincere appreciation and thanks go to my five advisory members for their services. The constructive discussions will greatly contribute to my future research career.

TABLE OF CONTENTS

Page

Page

LIST OF TABLES

LIST OF FIGURES

FIGURE Page

FIGURE Page

FIGURE Page

CHAPTER I

GENERAL INTRODUCTION

Through all over the world, groundwater is one of most precious resources for human being to sustain its life. Unfortunately, these invaluable resources are abused by human activity in both quality and quantity. There are uncountable numbers of contaminants induced by agriculture, industry, and daily human activity. Also with the growth of human society, we seek for the larger quantity of groundwater which results in depletion of the groundwater from its aquifer.

It seems that the development and industrialization, and healthy groundwater environments are generally incompatible. The heavy metals, organic solvents, and fuels used by industry; the agricultural chemicals, hormone preparations and artificial fertilizers by agriculture; waste materials and acid drainages from mining industry; and municipal landfills, urban runoff and leaking underground storage tanks from urbanization are all typical examples of potential sources of groundwater contaminations. Groundwater resources are also quantitatively suffered by excessive water use with the growth of human society. These cause many problems over the many developed countries. Those typical problems are salt water intrusions in coastal area, land subsidence by losing effective stress, enhancement of aquifer contamination, and depletion or uneven distributions of groundwater.

This chapter of the dissertation follows the style and format of the Journal of Hydrology.

Hydrogeologists struggle to resolve these many problems by taking advantage of current advanced technology. In this endeavors, the most fundamental starting point is to understand the groundwater flow and the transport phenomenon, and develop those theories applicable to current problems and remedial techniques. Currently, numerous field methods have been being developed and tested and will be developed in the near future.

The effort to monitor the contaminant transport in the subsurface is one of our major practical interests. Through the precise prediction of the movement of contaminant plume, we can save a lot of effort and time to guide and collect data and monitor water quality (Wexler, 1992). In most cases, the contaminant sources in the subsurface have their particular geometries and dimensions. For instance, the problems caused by non-aqueous phase liquids (NAPLs) are currently hot issue in environmental science and engineering because of their toxicity. They have typically very low solubility while their toxicity is extremely high. In many cases, the maximum contaminated levels (MCL) of the NAPLs are several orders higher than its solubility. Therefore, once they are intruded into groundwater system, they can serve as long-term contaminant source with the highest virulence. The NAPLs can be classified into two groups by their density. LNAPLs are the NAPLs which have lighter density than water and DNAPLs are heavier than water. Once the LNAPLs are intruded into groundwater system, they usually form pools right on top of the water table. On the other hand, DNAPLs usually form pools on the bottom of the aquifers or on top of the impermeable

layers. Because of these characteristics, they usually have the particular geometries and three dimensional configurations.

When applying field remedial techniques to the fields problems, the efficiency and effectiveness of the techniques are the main concern. Most frequently, the techniques are associated with wells which are the passages of the materials to and from the subsurface. Typical examples of using wells include pump and treat methods, soil vapor extraction (SVE), free product recovery, enhanced bioremediation, air sparging, and soil flushing. Therefore, it is not exaggerated to say that the efficiency of those passageways to subsurface, wells, are the primary factors for deciding the total system efficiency. Horizontal wells are proved in terms of efficiency by having good coupling with the aquifer systems due to its horizontal geometries. They are used in many places for the environmental remediation and many supporting data of their superiority to vertical wells have been reported in most aquifer configurations.

In this study, we like to investigate the two major hydrogeologic problems, i.e. contaminant transport from finite sources and well hydraulics of finite diameter horizontal wells, by considering more realistic aquifer and source conditions. In the study, we use as less assumption on the source geometries and boundary conditions as possible to meet this purpose. In Chapter II, we provide analytical solutions and computational code of contaminant transport from one-, two-, and three- dimensional finite sources in a finite-thickness aquifer that are previously not published.

A library of analytical solutions is provided with corresponding source geometries. In the computational code, we include this library for various comparisons among the

geometries and graphical user interface (GUI) is integrated to facilitate the input and the output of these calculations. The sensitivities of the line source solutions to source geometry, dispersion coefficients, and distance to the source are tested.

In Chapters III and IV, we provide a general theory of groundwater flow to a fractured or non-fractured, aquifer considering wellbore storage and skin effect. The analytical solutions for confined, leaky confined, and water table aquifers are provided. The developed analytical solutions are compared with previous theories. The sensitivity analyses are performed over wide range of hydrogeologic parameters and well parameters.

This research provides better tools for understanding the contaminant transport from a finite source in a finite thickness aquifer and well hydraulics of the horizontal wells by considering finite diameter of the horizontal wellbores.

CHAPTER II

ANALYTICAL SOLUTIONS OF CONTAMINANT TRANSPORT FROM FINITE ONE-, TWO-, AND THREE- DIMENSIONAL SOURCES IN A FINITE-THICKNESS AQUIFER*

Analytical study of contaminant transport from a finite source in a finite-thickness aquifer is most useful in hydrological and environmental sciences and engineering, but rarely investigated in previous studies. This paper provides analytical solutions of contaminant transport from one-, two-, and three- dimensional finite sources in a finite-thickness aquifer using Green's function method. A library of unpublished analytical solutions with different finite source geometry is provided. A graphically integrated MATLAB script is developed to calculate the temporal integrations in the analytical solutions and obtain the final solutions of concentration. The analytical solutions are examined by reproducing the solutions of some special cases discussed in previous studies. The sensitivities of the line source solutions to source geometry, dispersion coefficients, and distance to the source are tested.

---

*Reprinted with permission from "Analytical Solutions of Contaminant Transport from Finite One-, Two-, and Three- Dimensional Sources in A Finite-Thickness Aquifer" by Eungyu Park and Hongbin Zhan, 2001, *Journal of Contaminant Hydrology*, 53(1-2), p. 41-61, Copyright 2001 by the Elsevier Science B.V.

The contaminant concentration in the near field is found to be sensitive to the source geometry and anisotropy of the dispersion coefficients. The contaminant concentration in the far field is found to be much less sensitive to the source geometry. The physical insights of the analytical solutions are interpreted.

2.1 Introduction

Contaminant transport in the subsurface has been one of the most important research topics in the hydrological sciences and engineering in the last four decades (Bear, 1972; Gelhar, 1993; Domenico and Schwartz, 1998; Fetter, 1999). Although many transport problems must be solved numerically, analytical solutions are still pursued by many scientists because they can provide better physical insights into problems. Analytical solutions are usually derived from the basic physical principles and free from numerical dispersions and other truncation errors that often occurred in numerical simulations (Zheng and Bennett, 1995). With help of analytical solutions to estimate movements of contaminant plumes, we can save a lot of effort to guide and collect data and monitor water quality despite complexities of hydrogeologic systems (Wexler, 1992). Using analytical solutions, we can better understand the mechanism of contaminant transport, predict the movement of contaminant plumes, measure the field parameters related to solute transport, and verify the results of numerical modeling.

The solutions of one-, two-, and three- dimensional deterministic advection-dispersion equations have been investigated in numerous publications before and are still actively studied (Ogata and Banks, 1961; Bear, 1972; Sauty, 1980; Van Genuchten, 1981; Domenico and Robbins, 1984; Domenico, 1987; Batu, 1993; Leij et al., 1993;

Domenico and Schwartz, 1998; Fetter, 1999; Leij et al., 2000). Although most of the source bodies of contaminants are usually three-dimensional and finite, the advection-dispersion equation is commonly solved either with an infinitely large source (Ogata and Banks, 1961) or with a one- or two- dimensional source (Domenico and Robbins, 1984, Domenico, 1987; Batu, 1993; Leij et al., 1993; Leij et al, 2000). A three-dimensional source is rarely considered. Beside that, many of the previous solutions assume that either the sources are fully penetrated through the entire thickness of the aquifer (Ogata and Banks, 1961) or the aquifers are infinite or semi-infinite along the vertical axis (Leij et al., 2000). In reality, aquifers are finite vertically.

Previous works closely related to our study were carried out by Domenico and Robbins (1984), Domenico (1987), Batu (1989, 1993), and Leij et al. (2000). Domenico and Robbins (1984), and Domenico (1987) considered finite sources as boundary conditions when solving the advection-dispersion equation. They did not include the effect from the upper and lower boundaries of an aquifer. Batu (1989, 1993) provided a two-dimensional analytical solute transport model in a bounded aquifer by using the same source dimension as the aquifer thickness along the *z*-axis and included the contaminant source as a boundary condition. The general solutions were derived there through the help of Fourier analysis and Laplace transform (Batu, 1989, 1993). Leij et al. (2000) also used the Green's function method by including the contaminant source as a boundary condition. In their study, a vertically semi-infinite aquifer and a vertically infinitely thin source are assumed. In this study, we assume a three-dimensionally finite

source within a vertically finite-thickness aquifer, and include the source as a source term in the advection-dispersion equation.

The first goal of this paper is using Green's function method to solve the general form of contaminant transport from three-dimensionally finite, instantaneous or continuous sources in a finite-thickness aquifer. Using the same methodology, we derive the solutions for the point, line, and area sources in a finite-thickness aquifer. The Green's function method is a convenient way to solve three-dimensional flow and transport problems that include source terms. With a parallelepiped shape of source, the three-dimensional Green's function can be obtained from three separate one-dimensional Green's functions. Such one-dimensional solutions have been provided in previous works (Gringarten and Ramey, 1973).

The second objective of this paper is, using the established general methodology, to derive various solutions for point, line, and area sources. By generating concentration curves using the derived solutions, we can observe how each of the different source geometries and aquifer conditions influence the concentration distribution. A library of unpublished analytical solutions will be provided.

2.2 Conceptual and Mathematical Models

The general geometry of the problem is shown in Figure 2.1. The origin of the coordinate system is at the upper boundary. The positive *z*-axis is downward. The aquifer is assumed infinite in the *x*- and *y*- directions but finite in the *z*-direction with a thickness of *d*. The aquifer is horizontal without curvature. A no-flow boundary exists at

the bottom of the aquifer ($z=d$). A no-flow or a water table boundary exists at the top of the aquifer. If a water table boundary exists, we assume that the slope of the water table is so small that we can assume the water table to be parallel to the lower boundary. The shape of the contaminant source is a parallelepiped body with $x \in [0, x_0]$, $y \in [-y_0, y_0]$, and $z \in [z_0, z_1]$. Steady-state groundwater flow is along the x-axis. The three-dimensional deterministic advection-dispersion equation, which describes equilibrium solute transport within a vertically finite aquifer from a finite source, is written as follows:

$$\frac{\partial C}{\partial t} - D_x \frac{\partial^2 C}{\partial x^2} - D_y \frac{\partial^2 C}{\partial y^2} - D_z \frac{\partial^2 C}{\partial z^2} + v \frac{\partial C}{\partial x} + \lambda C = q_v(x, y, z, t) \tag{2.1}$$

with boundary conditions:

$$C(\pm\infty, y, z, t) = 0, \qquad -\infty < y < \infty,\ 0 < z < d, \text{ and } t > 0 \tag{2.2}$$

$$C(x, \pm\infty, z, t) = 0, \qquad -\infty < x < \infty,\ 0 < z < d, \text{ and } t > 0 \tag{2.3}$$

$$\frac{\partial}{\partial z} C(x, y, 0, t) = \frac{\partial}{\partial z} C(x, y, d, t) = 0, \qquad t > 0 \tag{2.4}$$

and initial condition:

$$C(x, y, z, 0) = 0, \qquad 0 < z < d \tag{2.5}$$

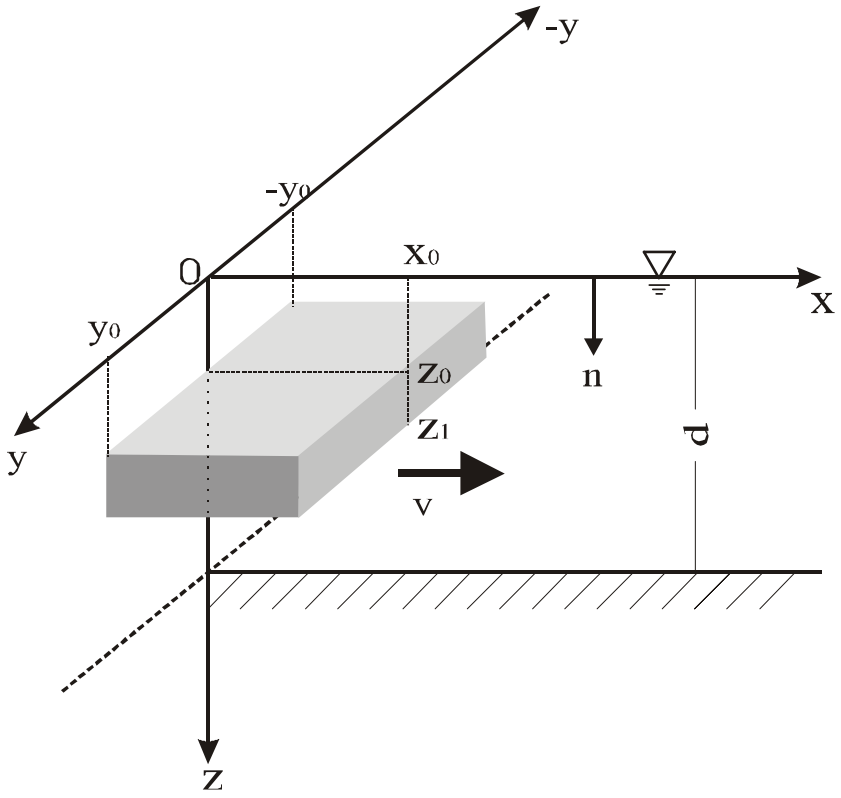

Figure 2.1. A schematic diagram of a three-dimensional source body within parallel non-penetrable boundaries for the solute. The upper boundary is a no-flow boundary or a water table boundary. The lower boundary is a no-flow boundary.

where C is the solute concentration (kg/m^3); t is time (day); D_x, D_y, and D_z are the principal dispersion coefficients in the x-, y-, and z- directions, respectively (m^2/day); v is the ground water flow velocity(m/day); λ is the first order reaction or decay constant (1/day); $q_v(x, y, z, t)$ is the volumetric source strength function (SSF) (kg/(m^{3}day)) (q_v>0 means producing contaminant mass in the source volume, q_v<0 means removing contaminant mass from the source volume); and d is the thickness of the saturated aquifer (m).

For a three dimensionally finite source, q_v is defined as the mass removed or added to a unit aqueous volume at a unit time interval. q_v is assumed to have the characteristics of Heaviside function (see Figure 2.1):

$$q_v(x,y,z,t) = \begin{cases} q_0 f(t) & 0 < x < x_0,\ -y_0 < y < y_0,\ z_0 < z < z_1, \text{ and } t > 0 \\ 0 & \text{otherwise} \end{cases}, \qquad (2.6)$$

where q_0 is a constant and $f(t)$ is a function of time.

The concentrations at laterally infinite distances are assumed zero. Along the z-direction, both the upper and lower boundaries are assumed non-penetrable for the solute. By transforming x to $\bar{x} = x - vt$, C to $\bar{C} = \exp(\lambda t)C$, q_v to $\bar{q}_v = \exp(\lambda t)q_v$ and doing the following dimensionless transformations:

$$\bar{x}_D = \frac{\bar{x}}{d}\sqrt{\frac{D_z}{D_x}},\ y_D = \frac{y}{d}\sqrt{\frac{D_z}{D_y}},\ z_D = \frac{z}{d},\ t_D = \frac{D_z}{d^2}t,\ \bar{C}_D = \frac{D_z}{q_0 d^2}\bar{C},\ \bar{q}_{vD} = \frac{\bar{q}_v}{q_0},\ v_D = \frac{vd}{\sqrt{D_x D_z}} \qquad (2.7)$$

above Eqs. (2.1)-(2.5) become

$$\frac{\partial \overline{C}_D}{\partial t_D} - \frac{\partial^2 \overline{C}_D}{\partial \overline{x}_D{}^2} - \frac{\partial^2 \overline{C}_D}{\partial y_D{}^2} - \frac{\partial^2 \overline{C}_D}{\partial z_D{}^2} = \begin{cases} \overline{q}_{vD} & \text{inside the source} \\ 0 & \text{outside the source} \end{cases} \tag{2.8}$$

$$\overline{C}_D(\pm\infty, y_D, z_D, t_D) = 0, \qquad -\infty < y_D < \infty,\ 0 < z_D < 1 \tag{2.9}$$

$$\overline{C}_D(\overline{x}_D, \pm\infty, z_D, t_D) = 0, \qquad -\infty < \overline{x}_D < \infty,\ 0 < z_D < 1 \tag{2.10}$$

$$\frac{\partial}{\partial z_D}\overline{C}_D(\overline{x}_D, y_D, 0, t_D) = \frac{\partial}{\partial z_D}\overline{C}_D(\overline{x}_D, y_D, 1, t_D) = 0, \tag{2.11}$$

$$\overline{C}_D(\overline{x}_D, y_D, z_D, 0) = 0, \qquad 0 < z_D < 1 \tag{2.12}$$

2.3 Solutions Derived Using Green's Function Method

2.3.1 Three-dimensional solutions

Above mathematical model can be solved using Green's function method. Green's function in this problem is defined as the concentration at (x, y, z, t) due to an instantaneous point source of strength unity generated at the point (x', y', z', τ), the aquifer being initially kept at zero concentration and boundary surface being kept at zero concentration (Gringarten and Ramey, 1973). This method has been used in fewer previous studies of contaminant transport (Yeh, 1981; Leij, 2000). Detailed description of the Green's function method can be found from Carslaw and Jaeger (1959), Gringarten and Ramey (1973); and Arfken and Weber (1995).

Recently, Leij et al. (2000) used the Green's function method to solve the transport equation with an infinitesimally thick source in a semi-infinite space along the *z*-direction. In their study, the contaminant sources are included as boundary conditions.

Thus, their solutions are not suitable to handle the sources inside the studied domain. In this study, we consider various shapes of sources inside the studied domain.

The Green's function of this problem can be obtained by solving the following differential equation with initial and boundary conditions (2.9)-(2.12).

$$\frac{\partial^2 G}{\partial \bar{x}_D{}^2}+\frac{\partial^2 G}{\partial y_D{}^2}+\frac{\partial^2 G}{\partial z_D{}^2}-\frac{\partial G}{\partial t_D}=\delta(\bar{x}_D-\bar{x}'_D)\delta(y_D-y'_D)\delta(z_D-z'_D)\delta(t_D-t'_D) \tag{2.13}$$

The three-dimensional Green's function can be expressed as the product of three one-dimensional Green's functions. The one-dimensional Green's function in an infinite aquifer is (Carslaw and Jaeger, 1959):

$$G(j_D,j'_D,t_D)=\frac{1}{2\sqrt{\pi t_D}}\exp\left(-\frac{(j_D-j'_D)^2}{4t_D}\right),\quad j=\bar{x},y\quad or\quad z \tag{2.14}$$

where, j'_D and j_D denote the coordinates of the source point and measured point, respectively.

The Green's function method is commonly applied using the source function (SF), which is defined as the integration of the Green's function over the volume or area or length of the source (Carslaw and Jaeger, 1959; Gringarten and Ramey, 1973). Using the Green's function method, the concentration in Eq. (2.8) can be written as follows (Carslaw and Jaeger, 1959; Gringarten and Ramey, 1973):

$$\bar{C}_D(\bar{x}_D,y_D,z_D,t_D)=\int_0^{t_D}\bar{q}_D(\tau_D)\int_\Omega G(\bar{x}_D,y_D,z_D,t_D-\tau_D;\bar{x}'_D,y'_D,z'_D)d\Omega d\tau_D=\int_0^{t_D}\bar{q}_D(\tau_D)S(\bar{x}_D,y_D,z_D,t_D-\tau_D)d\tau_D \tag{2.15}$$

where Ω is the source domain, *G* is the Green's function, and *S* is the source function.

The physical meaning of Eq. (2.15) deserves discussion. This equation shows that the three-dimensional Green's function is the solution at point ($\bar{x}_D$, y_D, z_D, t_D) with a unit strength, instantaneous, point source at ($\bar{x}'_D$, y'_D, z'_D,τ_D); the three-dimensional source function is the solution at ($\bar{x}_D$, y_D, z_D, t_D) with a unit strength, instantaneous, volume source at time τ_D. The continuous source solution is the temporal integration of the instantaneous source solutions. Eq. (2.15) also shows that the continuous source solution is simply the temporal convolution of the source strength function $\bar{q}_D$ and the source function *S*. Therefore the resultant dimensionless concentration of $\bar{C}_D$ can be thought as the summation of the product of the effect of pulse source, $\bar{q}_D d\tau_D$, and the temporal difference kernel, $S(\bar{x}_D, y_D, z_D, t_D - \tau_D)$, that is related to the system of hydrogeologic setting.

Applying Neumann's product rule, the three-dimensional source function is expressed as the product of three one-dimensional source functions:

$$S(\bar{x}_D, y_D, z_D, t_D - \tau_D) = S(\bar{x}_D, t_D - \tau_D) S(y_D, t_D - \tau_D) S(z_D, t_D - \tau_D) \tag{2.16}$$

Through the *z*-axis, the one-dimensional source function, $S(z_D, t_D - \tau_D)$, is represented as an integration of the one-dimensional Green's function, $G(z_D, z'_D, t_D - \tau_D)$, from z_{0D} to z_{1D}, where z_{0D} and z_{1D} are the dimensionless source dimensions in the *z* direction, defined in Eq. (2.7). Along the vertical direction, there are two boundaries that contaminant cannot penetrate through. To solve the boundary value problem, the

method of image is applied (Bear, 1972). The method of image uses infinite numbers of image sources along the *z*-axis to replace the upper and lower boundaries (Zhan, 1999). The source function along the *z*-axis is a summation of the source function of the original source and the source functions of all the image sources. The resulting source function in the *z*-axis is given by Eq. (2.17) (Carslaw and Jaeger, 1959, p. 275).

$$S(z_D, t_D - \tau_D) = \int_{z_{0D}}^{z_{1D}} \left[1 + 2 \sum_{n=1}^{\infty} \cos n\pi\zeta_D \cos n\pi z_D \exp\left[-n^2\pi^2 (t_D - \tau_D) \right] \right] d\zeta \tag{2.17}$$

Through the *y*-axis, the source function is an integration of the corresponding one-dimensional Green's function from $-y_{0D}$ to y_{0D} along the *y*-axis (Gringarten and Ramey, 1973):

$$S(y_D, t_D - \tau_D) = \frac{1}{2\sqrt{\pi (t_D - \tau_D)}} \int_{-y_{0D}}^{y_{0D}} \exp\left[-\frac{(y_D - \psi_D)^2}{4(t_D - \tau_D)} \right] d\psi_D \tag{2.18}$$

where y_{0D} is the dimensionless y_0, defined in Eq. (2.7).

The source function along the *x*-axis is derived as follows. The source along the $\bar{x}_D$ -axis is between -$v_D \tau_D$and x_{0D} -$v_D \tau_D$ in the coordinate system ($\bar{x}_D$, y_D, z_D) at time τ_D . Notice that the source function S($\bar{x}_D$, t_D- τ_D) is referred to an instantaneous source at time τ_D and it is the spatial integration of the corresponding Green's function at that time τ_D. Thus when calculating $S(\bar{x}_D, t_D - \tau_D)$, τ_D is treated as a fixed value. Therefore, $S(\bar{x}_D, t_D - \tau_D)$ is (Gringarten and Ramey, 1973):

$$S(\bar{x}_D, t_D - \tau_D) = \frac{1}{2\sqrt{\pi}} \int_{-v_D\tau_D}^{x_{0D} - v_D\tau_D} \frac{1}{\sqrt{t_D - \tau_D}} \exp\left[-\frac{(\bar{x}_D - \xi_D)^2}{4(t_D - \tau_D)} \right] d\xi_D \tag{2.19}$$

The ultimate solution of our problem is given by the integration of product of Eqs. (2.17)-(2.19).

$$\overline{C}_D(\bar{x}_D, y_D, z_D, t_D) = \frac{1}{4\pi}\int_0^{t_D} \overline{q}_{vD}(\tau_D) \int_{-v_D\tau_D}^{x_{0D}-v_D\tau_D} \int_{-y_{0D}}^{y_{0D}} \int_{z_{0D}}^{z_{1D}} \frac{1}{t_D-\tau_D} \exp\left[-\frac{(\bar{x}_D-\xi_D)^2+(y_D-\psi_D)^2}{4(t_D-\tau_D)}\right] \times$$
$$\left[1+2\sum_{n=1}^{\infty}\cos n\pi\zeta_D \cos n\pi z_D \exp\left[-n^2\pi^2(t_D-\tau_D)\right]\right] d\xi_D d\psi_D d\zeta_D d\tau_D \tag{2.20}$$

Changing the integration parameter from τ_D to $\tau'_D = t_D - \tau_D$ in Eq. (2.20) and finishing the spatial integration first, we have

$$\overline{C}_D(\bar{x}_D, y_D, z_D, t_D) = \frac{1}{4}\int_0^{t_D} \overline{q}_{vD}(t_D-\tau'_D)\left[erfc\frac{\bar{x}_D - x_{0D} + v_D(t_D-\tau'_D)}{2\sqrt{\tau'_D}} - erfc\frac{\bar{x}_D + v_D(t_D-\tau'_D)}{2\sqrt{\tau'_D}}\right] \times$$
$$\left[erfc\frac{y_D-y_{0D}}{2\sqrt{\tau'_D}} - erfc\frac{y_D+y_{0D}}{2\sqrt{\tau'_D}}\right] \times \left[z_{1D}-z_{0D} + \frac{2}{\pi}\sum_{n=1}^{\infty}\frac{1}{n}\left(\sin n\pi z_{1D} - \sin n\pi z_{0D}\right)\cos n\pi z_D \exp\left[-n^2\pi^2\tau_D\right]\right] d\tau'_D \tag{2.21}$$

If expressed in a dimensional format, Eq. (2.21) becomes

$$C(x,y,z,t) = \frac{1}{4d}\int_0^t q_v(t-\tau')\exp(-\lambda\tau')\left[erfc\frac{x-v\tau'-x_0}{2\sqrt{D_x\tau'}} - erfc\frac{x-v\tau'}{2\sqrt{D_x\tau'}}\right]\left[erfc\frac{y-y_0}{2\sqrt{D_y\tau'}} - erfc\frac{y+y_0}{2\sqrt{D_y\tau'}}\right]$$
$$\times\left[z_1 - z_0 + 2\sum_{n=1}^{\infty}\frac{d}{n\pi}\left(\sin\frac{n\pi z_1}{d} - \sin\frac{n\pi z_0}{d}\right)\cos\frac{n\pi z}{d}\exp\left[-\left(\frac{D_z n^2\pi^2}{d^2}\right)\tau'\right]\right] d\tau' \tag{2.22}$$

Eqs. (2.21) and (2.22) are the dimensionless and dimensional solutions of contaminant transport in a finite-thickness aquifer with a three-dimensional finite source.

If an instantaneous source exists, the SSF, $q_v(t) = C_0\delta(t)$, where C_0 is the source concentration at time t, and $\delta(t)$ is the Dirac Delta function. Therefore, the instantaneous

source solution is expressed by the same equation as Eq. (2.22) without doing the integration and q_v is replaced by C_0. If the source is eliminated at a certain time t', we can get the solution by changing the lower limit of the integration from 0 to $t - t'$ in Eq. (2.22).

The following discussion explains how to determine q_v and source concentration C_0 at some hypothetical cases. If doing a tracer test with a continuously adding tracer, q_v is the amount of mass added to the source zone per unit volume of pore water per unit time. If doing a tracer test with an instantaneous tracer, C_0 is the mass of tracer added to the source zone per unit volume of pore water per unit time. If free phase contaminants such as LNAPLs and DNAPLs exist in the aquifer, then dissolved free phase contaminants become the sources of aqueous phase contamination. The dissolution process cannot be easily handled by solution (2.22) because of the difficulty of accurately determining the source strength function. However, that process can be handled by Leij et al.'s solution (Leij, 2000) if treating the source as a boundary condition rather than a source term inside the studied domain.

2.3.2 One- and two- dimensional solutions

Using Eq. (2.22) as a base, a library of analytical solutions for different source types are derived and shown in Table 2.1. The source types in Table 2.1 include a point source (Case A, Figure 2.2a); three line sources (Cases B-D, Figures 2b-2d); and two area sources (Cases E-F, Figures 2e-2f).

Table 2.1. Solutions of several general types of sources

Solution of given geometry	Source Type
$C(x,y,z,t)=\frac{1}{4d\pi\sqrt{D_xD_y}}\int_0^t q_p(t-\tau)\exp(-\lambda\tau)\exp\left[-\frac{(x-v\tau)^2}{4D_x\tau}\right]\times\exp\left[-\frac{y^2}{4D_y\tau}\right]$ $\times\left[1+2\sum_{n=1}^{\infty}\cos\frac{n\pi z_0}{d}\cos\frac{n\pi z}{d}\exp\left[-\frac{D_zn^2\pi^2}{d^2}\tau\right]\right]\frac{d\tau}{\tau}$	Case A Point source (Fig. 2.2a)
$C(x,y,z,t)=\frac{1}{4d\sqrt{D_y\pi}}\int_0^t q_l(t-\tau)\exp(-\lambda\tau)\left[erfc\frac{x-v\tau-x_0}{2\sqrt{D_x\tau}}-erfc\frac{x-v\tau}{2\sqrt{D_x\tau}}\right]\times$ $\exp\left[-\frac{y^2}{4\tau D_y}\right]\times\left[1+2\sum_{n=1}^{\infty}\cos\frac{n\pi z_0}{d}\cos\frac{n\pi z}{d}\exp\left[-\frac{D_zn^2\pi^2}{d^2}\tau\right]\right]\frac{d\tau}{\sqrt{\tau}}$	Case B Line source (Fig. 2.2b)
$C(x,y,z,t)=\frac{1}{4d\sqrt{D_x\pi}}\int_0^t q_l(t-\tau)\exp(-\lambda\tau)\exp\left[-\frac{(x-v\tau)^2}{4D_x\tau}\right]\times$ $\left[erfc\frac{y+y_0}{2\sqrt{D_y\tau}}-erfc\frac{y-y_0}{2\sqrt{D_y\tau}}\right]\times\left[1+2\sum_{n=1}^{\infty}\cos\frac{n\pi z_0}{d}\cos\frac{n\pi z}{d}\exp\left[-\frac{D_zn^2\pi^2}{d^2}\tau\right]\right]\frac{d\tau}{\sqrt{\tau}}$	Case C Line source (Fig. 2.2c)
$C(x,y,z,t)=\frac{1}{4d\pi\sqrt{D_xD_y}}\int_0^t q_l(t-\tau)\exp(-\lambda\tau)\exp\left[-\frac{(x-v\tau)^2}{4D_x\tau}\right]\times\exp\left[-\frac{y^2}{4D_y\tau}\right]$ $\left[z_1-z_0+\frac{2d}{\pi}\sum_{i=1}^{\infty}\frac{1}{n}\left(\sin\frac{n\pi z_1}{d}-\sin\frac{n\pi z_0}{d}\right)\cos\frac{n\pi z}{d}\exp\left[-\frac{D_zn^2\pi^2}{d^2}\tau\right]\right]\frac{d\tau}{\tau}$	Case D Line source (Fig. 2.2d)
$C(x,y,z,t)=\frac{1}{4d\sqrt{D_x\pi}}\int_0^t q_a(t-\tau)\exp(-\lambda\tau)\exp\left[-\frac{(x-v\tau)^2}{4D_x\tau}\right]\times$ $\left[erfc\frac{y+y_0}{2\sqrt{D_y\tau}}-erfc\frac{y-y_0}{2\sqrt{D_y\tau}}\right]\times$ $\left[z_1-z_0+\frac{2}{\pi}\sum_{n=1}^{\infty}\frac{1}{n}\left(\sin\frac{n\pi z_1}{d}-\sin\frac{n\pi z_0}{d}\right)\cos\frac{n\pi z}{d}\exp\left[-\frac{D_zn^2\pi^2}{d^2}\tau\right]\right]\frac{d\tau}{\sqrt{\tau}}$	Case E Area source (Fig. 2.2e)
$C(x,y,z,t)=\frac{1}{4d}\int_0^t q_a(t-\tau)\exp(-\lambda\tau)\left[erfc\frac{x-x_0-v\tau}{2\sqrt{D_x\tau}}-erfc\frac{x-v\tau}{2\sqrt{D_x\tau}}\right]\times$ $\times\left[erfc\frac{y+y_0}{2\sqrt{D_y\tau}}-erfc\frac{y-y_0}{2\sqrt{D_y\tau}}\right]\left[1+2\sum_{n=1}^{\infty}\cos\frac{n\pi z_0}{d}\cos\frac{n\pi z}{d}\exp\left[-\frac{D_zn^2\pi^2}{d^2}\tau\right]\right]d\tau$	Case F Area source (Fig. 2.2f)

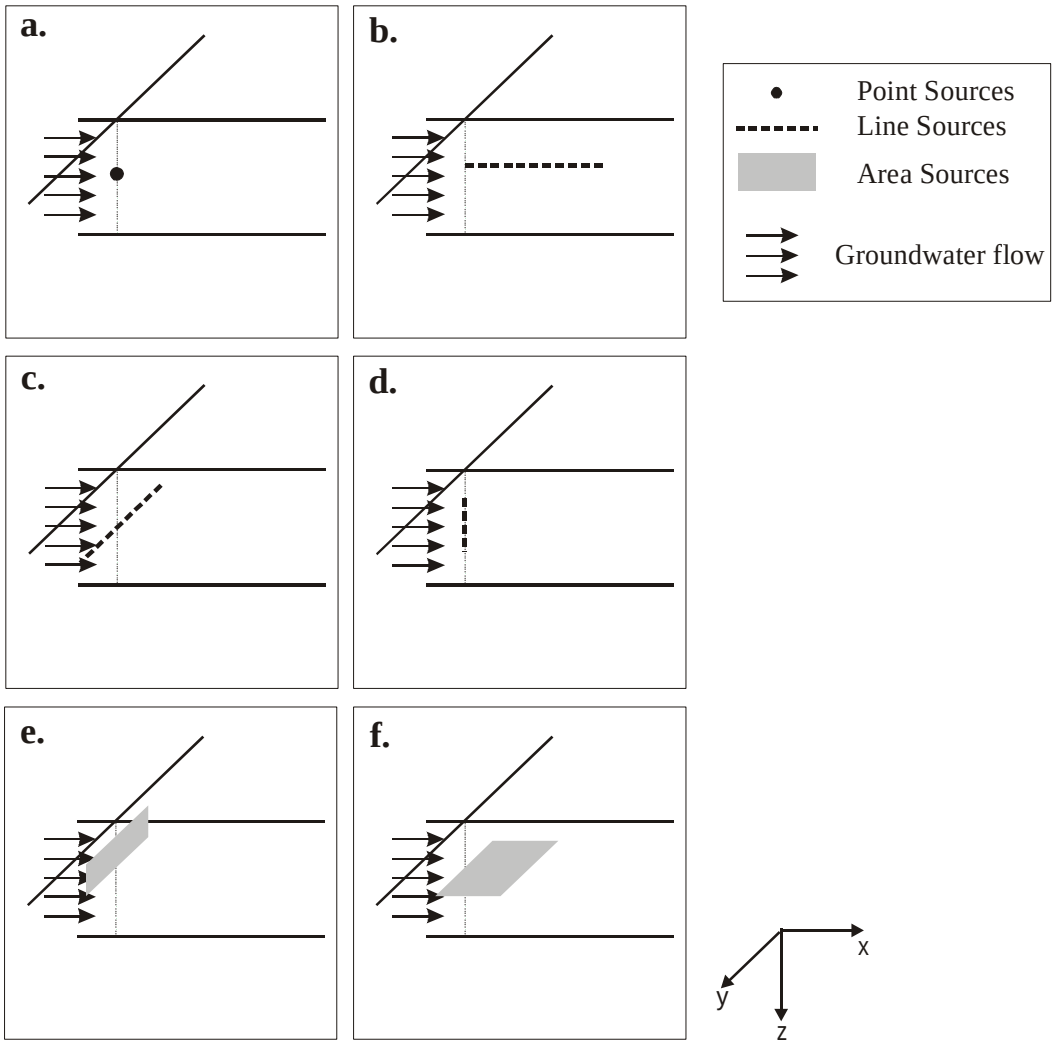

Figure 2.2. Schematic diagrams of various source shapes within two parallel non-penetrable boundaries for the solute. (a) A point source; (b) a horizontal line source parallel to the regional flow; (c) a horizontal line source perpendicular to the regional flow; (d) a vertical line source perpendicular to the regional flow; (e) an area source perpendicular to the regional flow; and (f) an area source parallel to the upper and lower boundaries.

The SSF for a point case, denoted as q_p, is defined as the produced or removed mass per unit time at the point [M/T]; the SSF for a line source, denoted as q_l, is defined as the produced or removed mass per unit length per unit time [M/(LT)]; and the SSF for an area source, denoted as q_a, is defined as the produced or removed mass per unit area per unit time [M/(L^{2}T)].

The point source in Figure 2.2a is located at (0, 0, z_0). The sources in Figures 2b, 2c, and 2d are line sources with infinitesimal radius. The source in Figure 2.2b spans along the *x*-direction, from (0, 0, z_0) to (x_0, 0, z_0), parallel to the groundwater flow. The source in Figure 2.2c spans along the *y*-direction, from (0, -y_0, z_0) to (0, y_0, z_0), normal to the groundwater flow. The source in Figure 2.2d spans along the *z*-direction, from (0, 0, z_0) to (0, 0, z_1), normal to the groundwater flow. The sources in Figures 2e and 2f are rectangular area sources. The source in Figure 2.2e is on the *yz*-plane with infinitesimal thickness along the *x*-direction; it is from $-y_0$ to y_0 along the *y*- direction; and from z_0 to z_1 along the *z*-direction. The source in Figure 2.2f is located on the *xy*-plane with a distance z_0 below the upper boundary; it is from $-y_0$ to y_0 along the *y*-direction; and from 0 to x_0 along the *x*-direction.

Eq. (2.22) can be simplified in certain special cases. For instances, if the source dimension in the vertical direction is the same as the aquifer thickness, the solution becomes independent of the vertical coordinate. If the source dimension in the *y* direction is infinite, then the solution is independent of the *y* coordinate. Through these manipulations, the general solution (2.22) will converge to some typical solutions

derived before by other investigators (Morgenau and Murphy, 1956; Ogata and Banks, 1961; Leij et al., 2000). Time-dependent source strength function can be applied to our solution to simulate the loading history of the contaminant sources. Some typical cases are discussed below and their results are compared with previous solutions.

Case 1 (a continuous area source located at the upper boundary in a semi-infinite aquifer). In this special case, the continuous source has an infinitesimal thickness along the *z*-direction; an extension from zero to x_0 along the *x*-direction; and an extension from $-y_0$ to y_0 along the *y*-direction. The source is located at the upper boundary. The lower impermeable boundary is assumed to be far from the source thus its influence upon the transport is negligible. Therefore, the source function along the *z*-direction becomes:

$$S(z,t) = \frac{1}{\sqrt{\pi D_z \tau}} \exp\left(- \frac{z^2}{4 D_z \tau} \right) \tag{2.23}$$

If including the first-order decay, the concentration then becomes

$$C(x,y,z,t) = \frac{1}{4\sqrt{\pi D_z}} \int_0^t q(t-\tau) \exp\left(- \lambda \tau - \frac{z^2}{4 D_z \tau} \right) \left[erfc \frac{x - v\tau - x_0}{2\sqrt{D_x \tau}} - erfc \frac{x - v\tau}{2\sqrt{D_x \tau}} \right] \times$$
$$\times \left[erfc \frac{y - y_0}{2\sqrt{D_y \tau}} - erfc \frac{y + y_0}{2\sqrt{D_y \tau}} \right] \frac{d\tau}{\sqrt{\tau}} \tag{2.24}$$

Eq. (2.24) is identical to the equation of the second type source solution given by Leij et al. (2000, p.166, Eq. (24)) but $q(t-\tau)$ is replaced by the mass flux, $D_z \frac{\partial C}{\partial z}$ at *z*=0, given

by Fick's law, in their equation. Notice that the *y*- and *z*- axes used in Leij et al. (2000, Figure 2.1 there) are equivalent to the *z*- and *y*- axes in our coordinate system, respectively (Figure 2.1).

Case 2 (a fully penetrated instantaneous source). If we extend the source length along the *z*-axis to the aquifer thickness and exclude the first-order decay and sorption,

$$S(z,t)=\frac{1}{d}\left[d+2\sum_{n=1}^{\infty}\frac{d}{n\pi}\sin\frac{n\pi d}{d}\cos\frac{n\pi z}{d}\exp\left[-\frac{D_z n^2\pi^2 t}{d^2}\right]\right]=1 \tag{2.25}$$

For a problem with an instantaneous source, $q_v(t)=C_0\delta(t)$. Eq. (2.22) becomes the following Eq. (2.26).

$$C(x,y,t)=\frac{C_0}{4}\left[erfc\frac{x-vt}{2\sqrt{D_x t}}-erfc\frac{x-vt-x_0}{2\sqrt{D_x t}}\right]\left[erfc\frac{y+y_0}{2\sqrt{D_y t}}-erfc\frac{y-y_0}{2\sqrt{D_y t}}\right] \tag{2.26}$$

Eq. (2.26) agrees with the two-dimensional solution derived by Morgenau and Murphy (1956).

Case 3 (an instantaneous semi-infinite source). For a problem with an instantaneous source, if we extend the source length along the *z*-axis to the aquifer thickness, the source length along the *y*-axis to infinity, the source length along the *x*-axis from zero to negative infinity, and exclude the first order-decay and sorption, we can reproduce the solution derived by Ogata and Banks (1961). In this case

$$S(y,t)=\frac{1}{2}\left[erfc\frac{y-\infty}{2\sqrt{D_y t}}-erfc\frac{y+\infty}{2\sqrt{D_y t}}\right]=1 \tag{2.27}$$

$$S(x,t)=\frac{1}{2}\left[erfc\frac{x-vt}{2\sqrt{D_x t}}-erfc\frac{x-vt+\infty}{2\sqrt{D_x t}}\right]=\frac{1}{2}erfc\frac{x-vt}{2\sqrt{D_x t}} \tag{2.28}$$

Therefore Eq. (2.22) becomes Eq. (2.29), which is the well-known Ogata and Banks' solution (Ogata and Banks, 1961; Domenico and Schwartz, 1998).

$$C(x,y,z,t)=\frac{C_0}{2}erfc\frac{x-vt}{2\sqrt{D_x t}} \tag{2.29}$$

where C_0 is the concentration of the source.

2.3.3 Numerical calculation of the concentration

The analytical solutions shown in above Eq. (2.22) and in Table 2.1 include the temporal integrations. A numerical integration program using the Gaussian Quadrature method (Abramowitz and Stegun, 1972) is written in a MATLAB M-file (MathWorks, 2000). A visual graphical interface is built in the program so that input and output handling becomes straightforward. This program has the following characteristics.

1. It can calculate concentration at any given time for any given type of sources presented in Figures 1 and 2.
2. It can calculate concentration for both continuous and instantaneous sources including the first-order decay.
3. It can automatically calculate the abscissas and weights used in the Gaussian Quadrature to achieve the desired accuracy of integration.

The program and its user's manual are available from the author's website http://geoweb.tamu.edu/Faculty/Zhan/Research.html.

2.4 Characteristics and Applications of the Solutions

2.4.1 Characteristics and applications of the three-dimensional solution

The results of this study have many applications. For instance, Eq. (2.22) can be directly applied to sources located within or on the boundaries. Typical cases of this kind could be a smear zone of a chemical spill, formed by a changing water table, or a leaking landfill. The solutions for the line sources can be applied to wells, abandoned mines, utility pipes, ditches, etc.

Figure 2.3 shows the results of a contaminant plume caused by a source similar to a smear zone of a continuous chemical spill, calculated from eq. (2.22) using the numerical program described above. Two cases are presented here for comparison. Figures 3a-3b are the results in a finite-thickness aquifer in which the lower boundary is at $z=d$, Figures 2.3c-2.3d are the results in a semi-infinite aquifer in which the lower boundary is at $z = \infty$. As expected, the plume spreads out with time and the plume movement depends on the regional flow velocity. The degree of spreading depends on the dispersion coefficients of each direction. Because the source is closer to the upper boundary, the expansion of the plume along the $+z$ direction is prohibited. The iso-concentration profiles in Figure 2.3b are perpendicular to the upper and lower boundaries, reflecting the influence of impermeable conditions at $z=0$ and $z=d$. The iso-concentration profiles in Figure 2.3d are semi-elliptic shapes, reflecting the impermeable condition at $z=0$ and an infinitely far lower boundary.

Domenico and Schwartz (1998, p. 379) also discussed the influence of a finite aquifer thickness upon the evolution of a plume. They gave an order-of-magnitude estimation of the distance at which the plume will "touch" the lower boundary. The Eq. (2.22) in this paper is a rigorous solution including the influence of the upper and lower boundaries upon the concentration.

2.4.2 Effects of source geometry, dispersion coefficients, and distance from the source

Figures 4 and 5 show the influence of source geometry and dispersion coefficients on the concentration distribution. Figure 2.6 shows the influence of distance from the source on the concentration distribution. Three line sources are included in Figures 2.4-2.6.

The following parameters are used in Figures 2.4-2.6. The source mass per unit length is 0.09 g/m for the instantaneous line source in Figure 2.4. The source strength function q_l is 0.09 ($gm^{-1}d^{-1}$) for the continuous line source in Figure 2.5. The line source along the *x*–axis is from (0, 0, 8 m) to (8 m, 0, 8 m); the line source along the y-axis is from (0, -4 m, 8 m) to (0, 4 m, 8 m); and the line source along the *z*-axis is from (0, 0, 0) to (0, 0, 8 m).

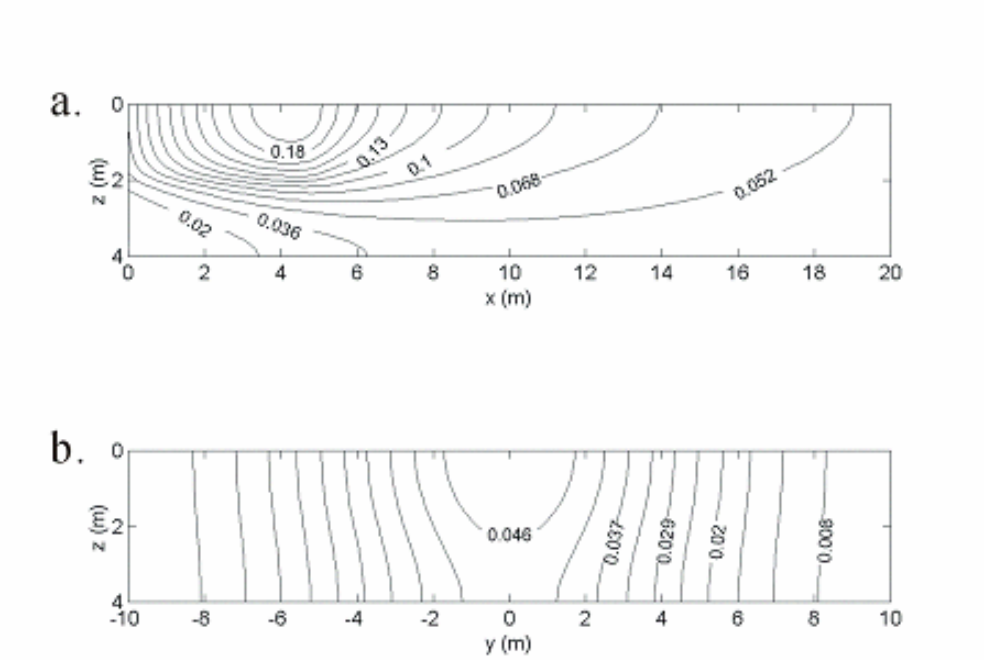

Figure 2.3. Iso-concentration contours on the *xz* plane (y=0) and *yz* plane (x=20 m) in 2 years after injecting of solute. The source strength is q_v=0.01 g m^{-3} d^{-1}. The source dimensions are $x \in [0, x_0]$, $y \in [-y_0, y_0]$ $y \in [-y_0, y_0]$, and $z \in [0, z_0]$ where x_0=5, y_0=1, and z_0=2 m. The aquifer parameters are d=5 m, D_x=0.1 $m^2 d^{-1}$, D_z/D_x=0.5, and D_z/D_x=0.3. (a) *xy*-slice plane passing through the center of the source along the *z*-axis in a finite-thickness aquifer; (b) *yz*-slice plane passing through x=20 m in a finite-thickness aquifer; (c) *xy*-slice plane passing through the center of the source along the *z*-axis in a semi-infinite aquifer.; and (d) *yz*-slice plane passing through x=20 m in a semi-infinite aquifer.

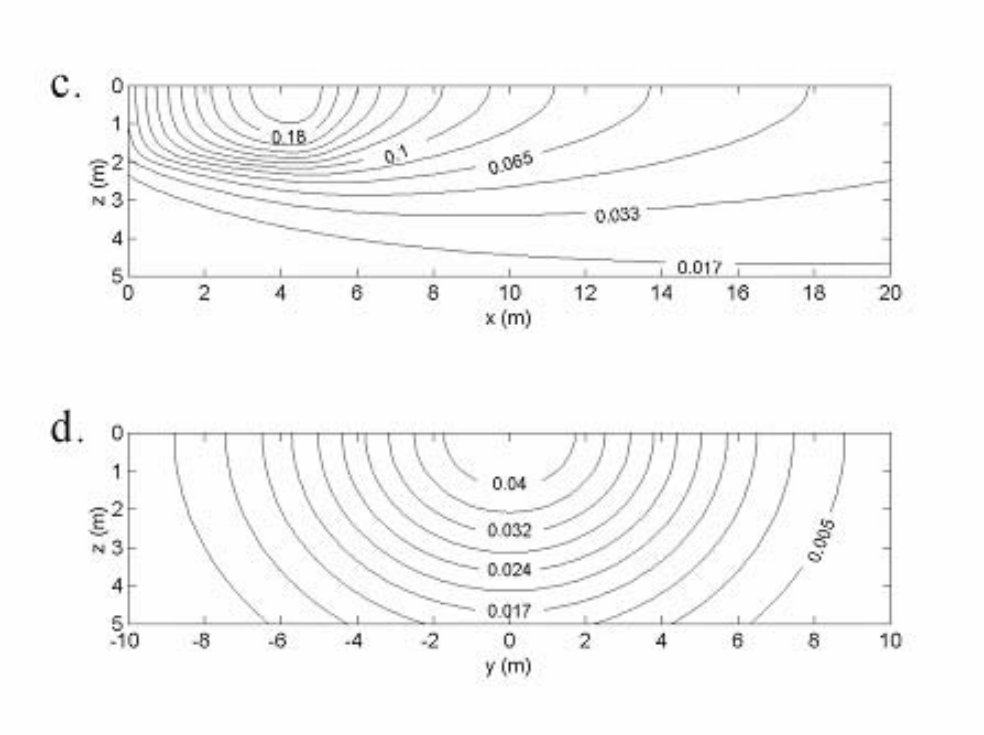

Figure 2.3. Continued

The concentration profiles of instantaneous sources in Figure 2.4 show left skewed bell shapes. This is consistent with what was found before for a finite-length source in the *x* direction (Zhan, 1998). Such left skewed bell shapes are caused by the subtraction of two *x*-dependent complementary error functions in Eq. (2.22) and in Table 2.1. If $x_0 \to 0$, the skewed bell shapes will become symmetric bell shapes.

As shown in Figures 2.4a and 2.5a, difference of the source geometry affects the concentration distribution significantly if dispersion coefficients are anisotropic. The horizontal line source along the regional flow shows the highest concentration, the horizontal line source normal to the regional flow shows the second highest concentration, and the vertical source shows the lowest concentration. If $D_x=D_y=D_z$, Figures 4b and 5b show that the difference of the source geometry has less significant influence upon the concentration distributions.

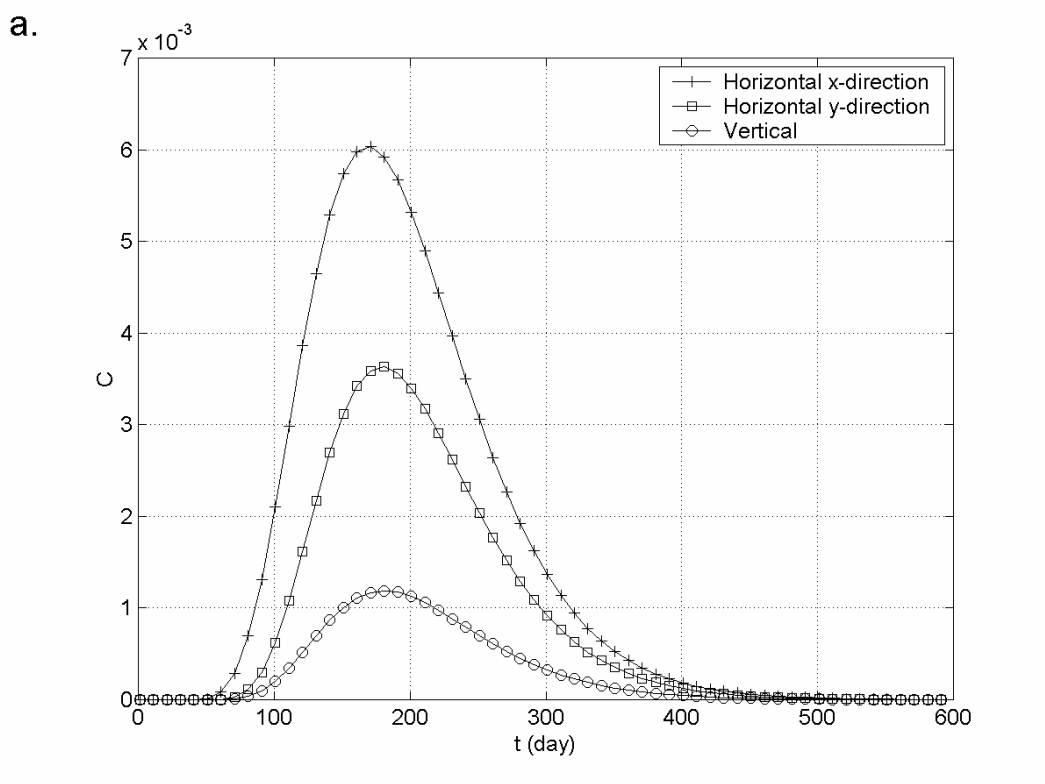

Figure 2.4. Theoretical concentration measured at 20 m downstream from the center of the sources that is released instantaneously. The released mass per unit length of the source C_0=0.09 gm^{-1}, D_x=0.1 m^2 d^{-1}, d=10 m. (a) Comparison of concentrations from 3 different types of sources, the ratio of D_y/D_x and D_z/D_x are 0.1 and 0.01, respectively; (b) comparison of concentrations from 3 different types of sources, the ratio of D_y / D_x and D_z/D_x are all 1.

b.

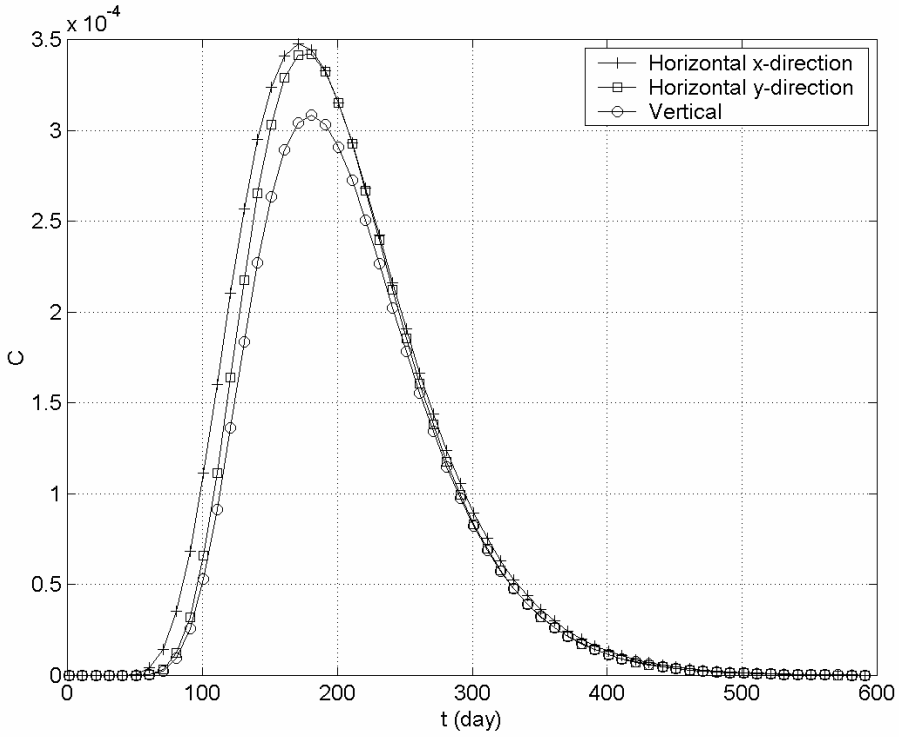

Figure 2.4. Continued

a.

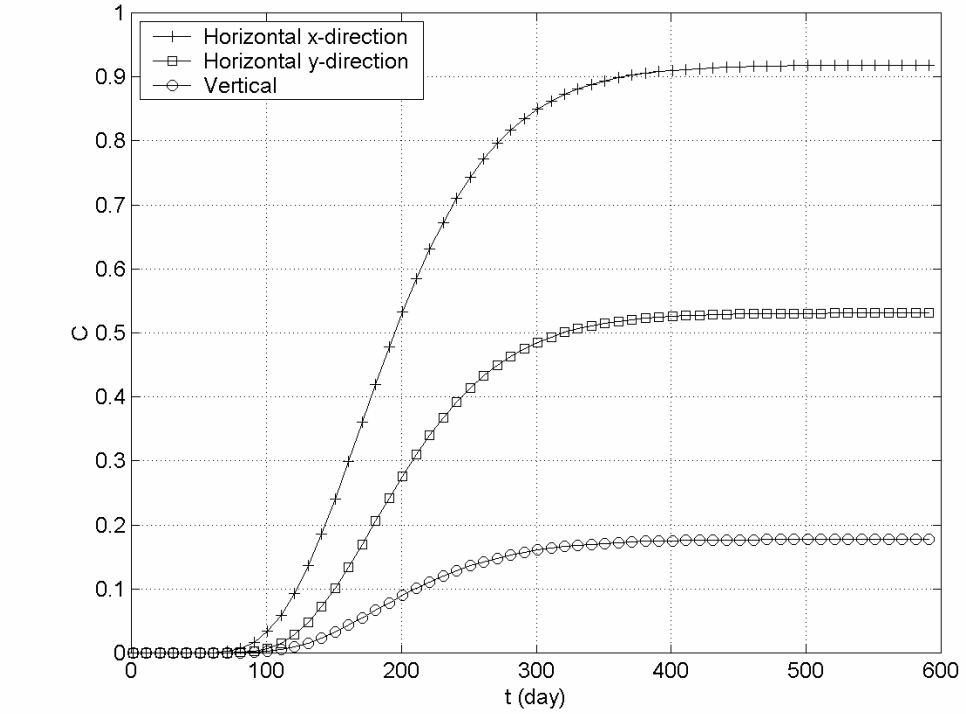

Figure 2.5. Theoretical concentration measured at 20 m downstream from the center of the sources that is released continuously. q=0.09 m^{-1} d^{-1}, D_x=0.1 m^2 d^{-1}, and d=10 m. (a) Comparison of concentrations from 3 different types of sources, the ratio of D_y/D_x and D_z/D_x are 0.1 and 0.01, respectively; (b) Comparison of concentrations from 3 different types of sources, the ratio of D_y/D_x and D_z/D_x are all 1.

b.

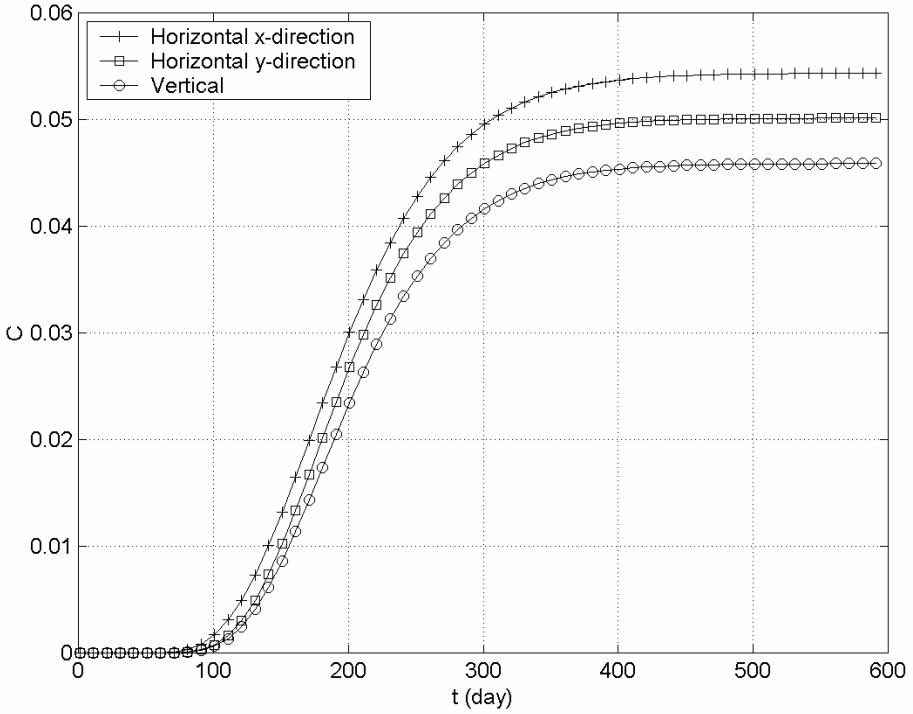

Figure 2.5. Continued

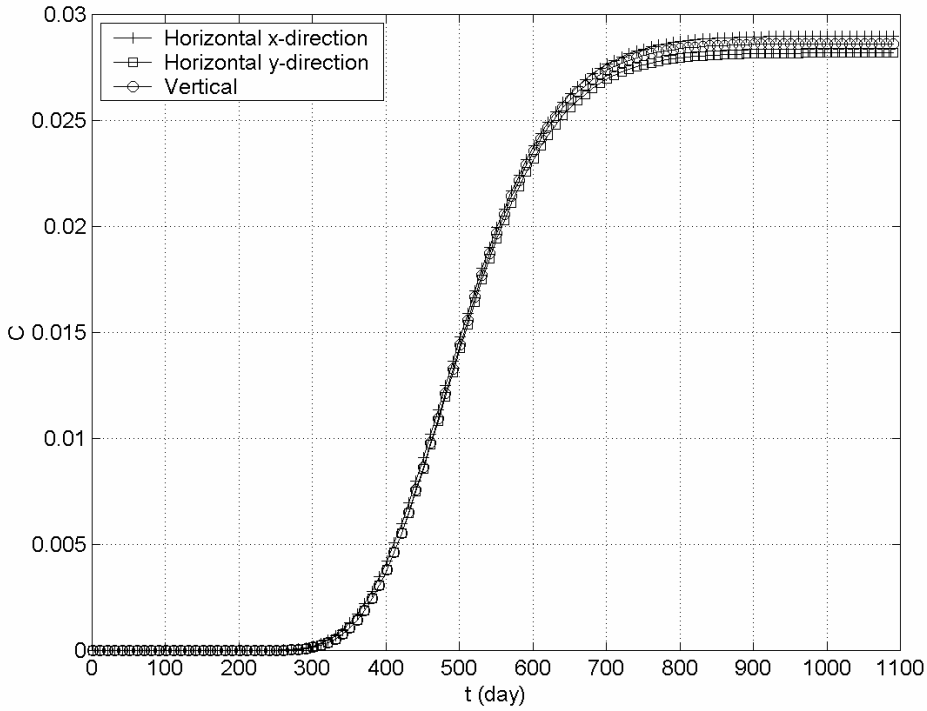

Figure 2.6. Comparison of the theoretical concentration measured at 50 m downstream from the center of the source with 3 different types of continuous line sources. q=0.09 $m^{-1}d^{-1}$, D_x =0.1 m^2 d^{-1}, d=10 m, the ratio of D_y/D_x and D_z/D_x are all 1.

The results of Figures 2.4 and 2.5 can be explained as follows. Let's compare the line sources in Figure 2.2b and Figure 2.2c first. The contaminant dispersive flux is $D_x(-\partial C/\partial x) + D_y(-\partial C/\partial y) + D_z(-\partial C/\partial z)$, if D_x is much larger than D_y and D_z ($D_x : D_y : D_z = 1 : 0.1 : 0.01$), $D_x(-\partial C/\partial x)$ is the leading term in the dispersive flux. The line sources in Figure 2.2b and Figure 2.2c are along the regional flow and perpendicular to the regional flow, respectively, thus $(-\partial C/\partial x)$ near the line source in Figure 2.2b should be less than that in Figure 2.2c. Therefore, the dispersive flux in Figure 2.2b should be less than that in Figure 2.2c. Notice that the dispersive effect is the only mechanism causing dilution for the non-reactive contaminant transport in Figure 2.2, thus the dilution effect in Figure 2.2b should be less than that in Figure 2.2c at the same downstream point. In another word, the concentration in Figure 2.2b should be higher than that in Figure 2.2c, as shown in Figures 2.4a and 2.5a.

Similar rationale can be used to explain the difference between Figures 2c and 2d. Now the *x* components of the dispersive fluxes in Figures 2c and 2d are nearly the same, but the *y*-component of the dispersive flux in Figure 2.2c is less than that in Figure 2.2d. If D_y is much larger than D_z ($D_z / D_y = 0.1$) , the overall dilution effect caused by the dispersion in Figure 2.2b should be less than that in Figure 2.2c. Therefore, the concentration is higher in Figure 2.2b than that in Figure 2.2c for a given downstream point.

When the dispersion coefficients are isotropic, the differences of concentration distributions are less significant for different line source orientations. The remaining

slight differences in Figures 2.4b and 2.5b are caused by the finite aquifer dimensions in the *z* direction. If the aquifer thickness is infinite, those differences will disappear.

Figures 2.4-2.5 indicate that the source geometry has a profound influence on the concentration profiles when the dispersion coefficients are anisotropic. Such influence is insignificant when the dispersion coefficients are isotropic.

Figure 2.6 is similar to Figure 2.5b except that the measuring point is 50 m downstream in Figure 2.6, while it is 20 m downstream in Figure 2.5b. Comparison of Figures 2.5b and 2.6 shows that at a near field point (Figure 2.5b), the source geometry influences the concentration distribution, but at a far field point (Figure 2.6), the source geometry has an almost negligible influence upon the concentration distribution.

2.5 Summary and Conclusions

We generated analytical solutions of multidimensional concentration fields originated from one- two-, and three-dimensional, finite sources within finite-thickness aquifers using the Green's function method. Our solution is examined by reproducing the special solutions of previous works. Based on the general three-dimensional solutions (Eq. (2.22)), a library of analytical solutions for different source shapes is published in Table 2.1. The temporal integrations in the analytical solutions are calculated using a graphically integrated MATLAB program. The program is available from the author's website http://geoweb.tamu.edu/Faculty/Zhan/Research.htm.

The derived analytical solutions show that the upper and lower aquifer boundaries have a profound influence upon the concentration distribution. We also find that the

concentration at a near field point is sensitive to the source geometry when the dispersion coefficients are anisotropic; it is less sensitive to the source geometry when the dispersion coefficients are isotropic. The concentration at a far field is found to be almost independent of the source geometry.

The limitation of these analytical solutions is that they assume simplified aquifer geometry with no slope, and a uniform one-dimensional groundwater flow. Dispersion coefficients are assumed to be constants at all scales rather than scale-dependent variables as described by Gelhar (1993), Zhan (1998), and many others.

CHAPTER III

HYDRAULICS OF A FINITE-DIAMETER HORIZONTAL WELL WITH WELLBORE STORAGE AND SKIN*

We have obtained solutions of groundwater flow to a finite-diameter horizontal well including wellbore storage and skin effect in a three-dimensionally anisotropic leaky aquifer. These solutions improve previous line source solutions by considering realistic well geometry and offer better description of drawdown near the horizontal well. These solutions are derived on the basis of the separation of the source and the geometric functions. The source function is analyzed using Laplace transformation, and the geometric function is derived based on the method of superposition. The solution in a confined aquifer is derived as a special case of the solution in a leaky aquifer. The graphically integrated computer program FINHOW is written to generate type curves of groundwater flow to a finite-diameter horizontal well. The influence of the finite-diameter of the well, the wellbore storage, the skin effect, the leakage parameter, and the aquifer anisotropy is thoroughly analyzed.

---

*Reprinted with permission from "Hydraulics of A Finite-Diameter Horizontal Well with Wellbore Storage and skin" by Eungyu Park and Hongbin Zhan, 2002, Advances in Water Resources, 25 (4), p. 389-400, Copyright 2002 by the Elsevier Science B.V.

The well diameter, the wellbore storage, the skin effect, and the aquifer anisotropy substantially affect the near-well early time drawdown if compared to the line source solution, but they have negligible influence upon the far field or late time drawdown. This research provides a better tool for interpreting finite-diameter horizontal well pumping tests.

3.1 Introduction

Horizontal wells have screen sections parallel to the horizontal directions. These wells have been widely used in petroleum engineering (Joshi, 1988; Maurer, 1995; Seines et al., 1994), and agricultural and civil engineering (Hantush and Papadopulos, 1962; Murdoch, 1994) in the past. They have gained significant interests among hydrogeologists, environmental scientists, and engineers in recent years (Falta, 1995; Hunt B, Massmann, 2000; Sawyer and Lieuallen-Dulam, 1998; Zhan, 1999; Zhan and Cao, 2000; Zhan et al., 2001). Horizontal wells have advantages that are irreplaceable by vertical wells at some circumstances. For instance, they can be used at sites where ground surfaces are obstructed by permanent structures such as buildings, highways, railways, wetlands, landfills, etc.; they can have great contact areas with the thin ground water aquifers; they can be effective in recovering thin layer contaminants; they can perform better recovery in vertically fractured aquifers; etc.

Hantush and Papadopulos (1962) have initially investigated the hydraulics of a collector well, which is a series of horizontal wells distributed in a horizontal plane. Petroleum engineers have studied fluid flow to horizontal wells in oil and gas reservoirs (Daviau et al., 1988; Goode and Thambynayagam, 1987; Rosa and Carvalho, 1989). In

recent years, hydrogeologists have studied hydraulics of horizontal wells in shallow ground water aquifers (Cleveland, 1994; Sawyer and Lieuallen-Dulam, 1998; Zhan, 1999; Zhan and Cao, 2000; Zhan et al., 2001). In most of these studies, the horizontal well is treated as a line source and the well storage and skin effect are not included. The wellbore storage refers to water initially stored inside the well; the skin effect refers to the alteration of hydraulic conductivity at a thin layer immediately outside the wellbore during the well-installation process. The well skin serves as a barrier separating the wellbore from the aquifer.

Extensive studies on hydraulics of finite or large diameter vertical wells, including the wellbore storage and skin effect, have been reported before (Cassiani and Kabala, 1998; Cassiani et al., 1999; Dougherty and Babu, 1984; Ehlig-Economides and Joseph, 1987; Kabala and Cassiani, 1997; Moench, 1985; Moench, 1997; Moench and Hsieh, 1985; Novakowski, 1989; Papadopulos and Cooper, 1967; Wilkinson D, Hammond, 1990). The analytical solution for the drawdown produced by a large-diameter vertical well including fluid storage capacity was first presented by Van Everdingen and Hurst (1949) in petroleum, and by Papadopulos and Cooper (1967) in groundwater literature. Those studies have been extensively applied to oil and gas well problems later (Agarwal et al., 1970; Jargon, 1976; Ramey, 1965; Ramey, 1970; Ramey and Agarwal, 1972; Streltsova, 1988). Large diameter wells have been used for hydrological applications in homogeneous aquifers (Jiao and Rushton, 1995; Moench, 1985; Moench, 1997; Papadopulos and Cooper, 1967) and in heterogeneous aquifers (Hemker, 1999). They have been applied in confined aquifers (Papadopulos and Cooper, 1967; Sen, 1992),

leaky aquifers (Lai and Su, 1974; Moench, 1985), and water table aquifers (Moench, 1997). They have also been used to study problems with non-Darcian fluid flow (Ramey, 1965; Sen, 1992).

However, hydraulics of a finite-diameter horizontal well, including the wellbore storage and skin effect, has rarely been studied before. The available references in this field include an analytical study for horizontal wells with wellbore storage and skin in a layered petroleum reservoir (Kuchuk and Habashy, 1996); and an analysis of horizontal wells in a bounded naturally fractured reservoir (Ng and Aguilera, 1999). But those analytical studies only reflect the measurement of drawdown inside the wellbore based on the previous study on wellbore storage and skin effect (van Everdingen and Hurst, 1949). Solutions for monitoring piezometers or wells were not available from those studies. Those solutions did not explicitly consider the finite diameter of the horizontal wellbore, and they were not suitable for studying leaky confined aquifers.

It is the purpose of this paper to study hydraulics of horizontal wells under a more realistic circumstance, i.e., considering the actual diameter of a horizontal well and including the effect of the wellbore storage and the skin effect. The results derived in this paper will be closer to the physical reality of the horizontal well performance. These results will be compared with previous line source solutions to assess the sensitivity of ground water flow on the horizontal well diameter, the wellbore storage, the skin effect, and the aquifer anisotropy.

3.2 Conceptual and Mathematical Model

The general geometry of the problem is shown in Figure 3.1. The origin of the coordinate system is at the lower boundary below the center of the horizontal wellbore, and the positive *z*-direction is upward. The aquifer is assumed laterally infinite but vertically finite with a thickness of *d*. The aquifer is homogeneous, and the principal directions of the hydraulic conductivity tensor are generally assumed to coincide with the coordinate axes. A no-flow boundary exists at the bottom, and a leaky confining layer is at the top of the aquifer. The aquifer and the fluid are slightly compressible and have constant physical properties. We assume that the horizontal well has a finite-diameter and a finite screen length. The central axis of the well is along the *x*-axis from *– L/2* to *L/2*, where *L* is the screen length of the horizontal wellbore, and the cross section of the horizontal well is a circular area with the diameter of $2r_w$. The depth from the central axis of the horizontal well to the lower boundary is z_w.

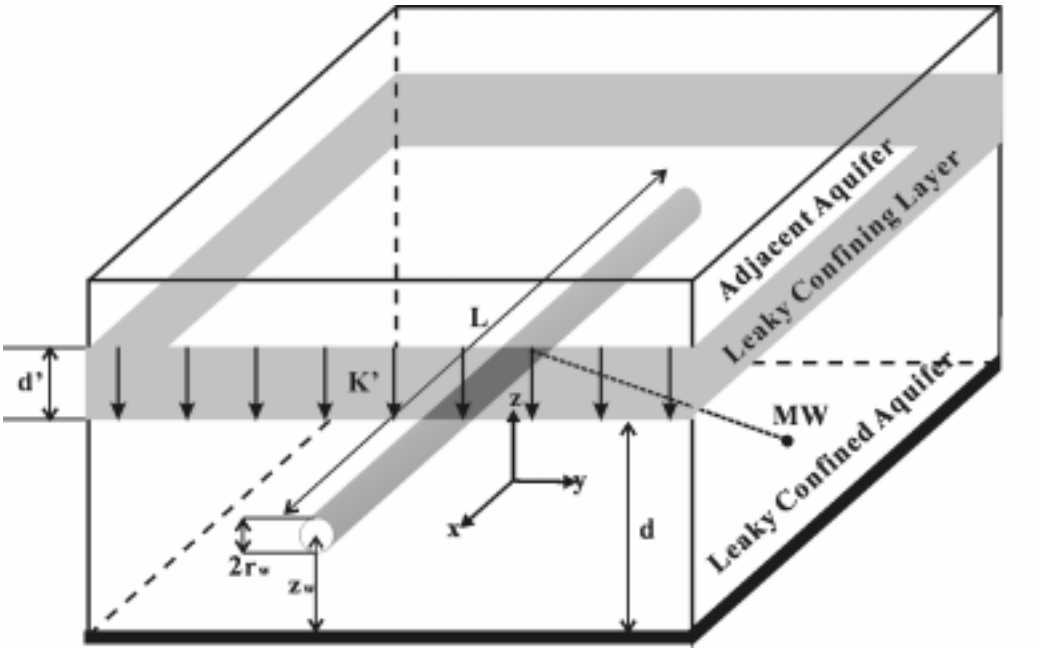

Figure 3.1. General geometry of a finite-diameter horizontal well in a homogeneous, anisotropic, leaky confined aquifer. A leaky confining layer separates the leaky confined aquifer from an adjacent aquifer. MW is the location of the monitoring point.

We separate the problem-solving process into two parts (the rationale of doing so is explained later in section 2.1). The first part is finding the geometric function (GF) that is related to the geometry of the well and characteristics of the aquifer. In this part, we study ground water flow to a point source first, and then superpose the point source solution to obtain the solution of a horizontal well. The second part of the process is about the source function (SF) that includes the production rate, wellbore storage, and skin effect.

Now we briefly discuss the way to handle the leaky aquifer. Hantush (1964, p. 348) pointed out that studying flow in a leaky aquifer must consider a combined problem of flow in the leaky aquifer, flow in the leaky confining layer, and flow in the adjacent aquifer simultaneously. The solution of this problem is difficult to use in practice. Hantush (1964) suggested that the leakage may be substituted as a source/sink which is located inside the aquifer whose boundary is fully impermeable. We should point out that Hantush's assumption (1964) about leakage is usually thought to be "sufficiently accurate for practical purposes" for the vertical well solutions developed by him. However, whether this assumption is accurate enough for a horizontal-well problem is unknown. If treating a finite-length, finite-diameter horizontal well as a superposition of many partially penetrating vertical wells whose screen lengths equal the diameter of the horizontal well, then it is reasonable to extend Hantush's assumption to a horizontal-well problem. In this study, we assume that such a treatment is sufficiently accurate for practical purposes for a horizontal as well as vertical wellbore.

The hydrological system is assumed to be static before pumping; thus the initial hydraulic head of the leaky aquifer equals the head in the adjacent aquifer above the leaky confining layer (h_0). Based on this, the governing equation of ground water flow to a point source in a three-dimensionally anisotropic leaky aquifer is (Hantush, 1964)

$$K_x \frac{\partial^2 h}{\partial x^2} + K_y \frac{\partial^2 h}{\partial y^2} + K_z \frac{\partial^2 h}{\partial z^2} - K' \frac{h_0 - h}{dd'} - S_s \frac{\partial h}{\partial t} = q_f(t)\delta(x - x_0)\delta(y - y_0)\delta(z - z_0), \quad (3.1)$$

where K_x, K_y, K_z are the principal hydraulic conductivities (m/sec) in the x-, y-, and z-directions, respectively, h is hydraulic head (m), K' is hydraulic conductivity of the leaky confining layer (m/sec), h_0 is the head in the adjacent aquifer above the leaky confining layer and is assumed to be constant (m), d and d' are the thickness of the leaky aquifer and the leaky confining layer, respectively, S_s is specific storativity of the aquifer (m^{-1}), t is time (sec), q_f is the aquifer pumping rate for a point source (m^3/sec) (q_f>0 means pumping), $\delta(u)$ is the Dirac delta function, and (x_0, y_0, z_0) is the point source location.

The outer boundaries that are located infinity from the source along the horizontal directions are

$$h(x,y,z,t)\big|_{x=\pm\infty} = h_0, \; h(x,y,z,t)\big|_{y=\pm\infty} = h_0, \quad (3.2)$$

and the conditions at the upper and lower boundaries are

$$\partial h(x,y,z,t)/\partial z\big|_{z=0} = 0, \; \partial h(x,y,z,t)/\partial z\big|_{z=d} = 0. \quad (3.3)$$

The initial condition is

$$h(x,y,z,t)\big|_{t=0} = h_0. \quad (3.4)$$

If $K'/d' \to 0$, Eq. (3.1) converges into the governing equation of a confined aquifer.

3.2.1 Solution in a leaky aquifer

For the convenience of calculation, we change the variable from head, h, to drawdown, $s=h_0-h$, and define the dimensionless parameters in List of Symbols where all the parameters are explained in the List of Symbols. The solution of Eq. (3.1) can be obtained either using a Laplace transform (Dougherty and Babu, 1984; Moench, 1997, 1998) or Green's function methods (Gringarten and Ramey, 1973; Ozkan and Raghavan, 1991). By applying a Laplace transform to Eqs. (3.1)-(3.4) and using above defined dimensionless parameters, one has

$$p\bar{s}'_D = \frac{\partial^2 \bar{s}'_D}{\partial x_D^2} + \frac{\partial^2 \bar{s}'_D}{\partial y_D^2} + \frac{\partial^2 \bar{s}'_D}{\partial z_D^2} + 4\pi \bar{q}'_{fD}(p)\delta(x_D - x_{0D})\delta(y_D - y_{0D})\delta(z_D - z_{0D}), \quad (3.5)$$

$$\partial \bar{s}'_D(x_D, y_D, 0, p)/\partial z_D = 0, \quad (3.6)$$

$$\partial \bar{s}'_D(x_D, y_D, 1, p)/\partial z_D = 0, \quad (3.7)$$

$$\bar{s}'_D(\pm\infty, y_D, z_D, p) = \bar{s}'_D(x_D, \pm\infty, z_D, p) = 0, \quad (3.8)$$

where p is the Laplace transform variable referred to as the dimensionless time, over bar means Laplace transformation, s'_D and q'_{fD} are defined in List of Symbols, and x_{0D}, y_{0D}, and z_{0D} are defined in the same way as x_D, y_D, and z_D, respectively.

Eqs. (3.5)-(3.8) are solved in the appendix, and the dimensionless drawdown is

$$s_D(t_D) = \int_0^{t_D} q_{fD}(t_D - \tau)\exp\left[-\frac{\tau}{B_D^2} - \frac{r_D^2}{4\tau}\right]\left[1 + 2\sum_{n=1}^{\infty}\cos[n\pi z_D]\cos[n\pi z_{0D}]\exp\left[-n^2\pi^2\tau\right]\right]\frac{d\tau}{\tau}, \quad (3.9)$$

where r_D is the dimensionless horizontal distance from point source to monitoring location, and B_D^2 is defined in Table 3.1.

The first term inside the integration sign of Eq. (3.9), $q_{fD}(t_D-\tau)$, is the source function (SF) for a point source; while the product of all the rest of the terms inside the integration sign of Eq. (3.9) is the dimensionless point geometric function, $g_0(x_D, y_D, z_D; x_{0D}, y_{0D}, z_{0D}, t_D)$:

$$g_0(x_D, y_D, z_D; x_{0D}, y_{0D}, z_{0D}, t_D) = \exp\left[-\frac{t_D}{B_D^2}-\frac{r_D^{\ 2}}{4t_D}\right]\left[1+2\sum_{n=1}^{\infty}\cos[n\pi z_D]\cos[n\pi z_{0D}]\exp\left[-n^2\pi^2 t_D\right]\right]\frac{1}{t_D} \quad , \tag{3.10}$$

and in Laplace domain

$$\bar{g}_0(x_D, y_D, z_D; x_{0D}, y_{0D}, z_{0D}, p) = 2K_0(r_D\sqrt{p+1/B_D^2}) + 4\sum_{n=1}^{\infty}\cos[n\pi z_D]\cos[n\pi z_{0D}]K_0(r_D\sqrt{p+n^2\pi^2+1/B_D^2}) \quad . \tag{3.11}$$

where $\bar{g}_0$ is the Laplace transform of g_0, K_0 is the second kind, zero order modified Bessel function. Eq. (3.9) indicates that the dimensionless drawdown is simply the convolution of the source function and geometric function in dimensionless time domain. If represented in Laplace domain, the dimensionless drawdown is the product of source function and geometric function. Such a problem-solving mechanism can be extended to other types of sources such as line or volume sources. One can reproduce the line source solution of a partially penetrating vertical well in a leaky aquifer (Bear, 1979, p.349, Hantush, 1964, p.350) by integrating z_{0D} along the vertical direction of Eq. (3.9).

3.2.2 Solution for a point source in a confined aquifer

As a special case of the leaky aquifer solution, if assuming that the conductance of the leaky confining layer, *K′/d′,* goes to zero, Eq. (3.1) becomes the governing equation of flow in a confined aquifer and Eq. (3.9) reduces to the solution for a confined aquifer. By assigning $B_D \to \infty$ in Eq. (3.9), one obtains

$$s_D(x_D, y_D, z_D; x_{0D}, y_{0D}, z_{0D}, t_D) = \int_0^{t_D} q_{fD}(t_D - \tau) \exp\left[-\frac{r_D^2}{4\tau}\right]\left[1 + 2\sum_{n=1}^{\infty} \cos[n\pi z_D]\cos[n\pi z_{0D}]\exp\left[-n^2\pi^2\tau\right]\right]\frac{d\tau}{\tau}$$

, (3.12)

which is the point source solution in a confined aquifer.

3.3 Solution of a Finite-Diameter Horizontal Well with Wellbore Storage and Skin Effect

The point source solution Eq. (3.9) is the foundation for the following work. A finite-diameter horizontal well can be visualized as superposition of many point sources, and the aquifer pumping rate from the horizontal well, Q_f, is defined as

$$Q_f(t) = \frac{1}{V}\int_v q_f(x, y, z, t)dV \,, \quad (3.13)$$

where V is the volume of the horizontal wellbore and $q_f(x, y, z, t)/V$ is the point source strength. Before proceeding, we need to answer the following two questions:

1. How is the pumping rate distributed inside a horizontal wellbore?
2. How is the aquifer pumping rate, $Q_f(t)$, related to the total pumping rate, Q, and the pumping time?

3.3.1 Pumping rate distribution inside a horizontal well

There are traditionally two different methods to treat a pumping well. One method is to treat it as a uniform flux boundary, and another is to treat it as a uniform head boundary. Hantush (1964) pointed out that these two treatments were two extremes and a realistic wellbore was a mixed-type boundary between these two extremes because of flow inside the wellbore. Several researches have studied the mixed-type boundary value problems for the partially penetrating vertical well (Cole and Zlotnik, 1994; Haitjema and Kraemer, 1988; Kirkham, 1959; Muskat, 1937). In recent years, great advancements have been made in using the mixed-type boundary to treat a vertical wellbore (Cassiani and Kabala, 1998; Cassiani and Kabala, 1999; Rund and Kabala, 1997; Wilkinson and Hammond, 1990). Intensive computational power is still needed to perform the numerical calculation when using this method. No effort is made in this study to incorporate the mixed-type boundary method to treat the horizontal wellbore. However, because the mixed-type boundary is assumed to be closer to the physical boundary, additional research is needed to apply this method for horizontal-well study in the future.

As a result, scientists favor the uniform flux boundary because of its simple implementation in the analytical study. However, the true distribution of pumping rate is non-uniform because the pumping rate at both ends of the screen is higher than the average over the screen length. Thus, it is important to know the errors associated with the uniform flux boundary assumption. Previous studies indicated that the error is usually less than a few percent if the screen length-to-well radius is large enough: $L/r_w>40$ (Cole and Zlotnik, 1994; Rund and Kabala, 1997). This condition is almost

always satisfied for a horizontal pumping well case because the horizontal wells used in hydrological and environmental studies usually have long screen lengths. Because of this, the uniform flux boundary can be safely used for treating horizontal wells in practical cases. If using the uniform flux to treat a horizontal well, $q_f(x, y, z, t)$ in Eq. (3.13) is independent of (x, y, z), and Eq. (3.13) becomes $Q_f(t)=q_f(t)$.

3.3.2 Consideration of wellbore storage and skin effect

The wellbore storage is one of the important parameters that mask early time or near to pumping well pressure data by distorting the aquifer water levels in pumping tests (Moench, 1997; Ramey and Agarwal, 1972; Van Everdingen and Hurst, 1949).

The total pumping rate, Q, is the summation of the aquifer pumping rate, $Q_f(t)$, and the wellbore storage pumping rate, $Q_w(t)$: $Q_w(t)+Q_f(t)=Q$. The wellbore storage supplies most of the initial pumped water, and $Q_w(t)$ initially equals Q and gradually decreases to zero when pumping continues (Streltsova, 1988).

$$Q_w = \pi r_c^2 \frac{\partial s_w}{\partial t}, \tag{3.14}$$

where r_c is the radius of the casing connected with the horizontal-well screen, and s_w is the drawdown inside the wellbore. r_c may or may not equal to the radius of the horizontal-well screen, r_w. In contrast, $Q_f(t)$ is initially zero and gradually approaches Q when pumping continues. Using Darcy's Law, the aquifer-pumping rate is proportional to the head difference at wellbore (Dougherty and Babu, 1984; Moench, 1997; Streltsova, 1988):

$$Q_f = (2\pi r_w L C_s)(s_w - f), \tag{3.15}$$

where L is the screen length of the horizontal well, C_s is the conductance of wellbore skin (K_s/d_s), K_s and d_s are the hydraulic conductivity and the thickness of the skin, respectively, and f is averaged drawdown at the outside surface of the wellbore skin.

The skin is assumed to be infinitesimally thin when using Eq. (3.15). This treatment is similar to those used by Dougherty and Babu (1984), Ehlig-Economides and Joseph (1987), Kabala and Cassiani (1997), and many others in studying vertical wells. However, it is different from the finite-thickness skin effect treatment used by Novakowski (1989), and Moench and Hsieh (1985). Using the similar notation employed by Kabala and Cassiani (1997) to define the skin effect, η, in an isotropic aquifer:

$$-\eta r_w \frac{\partial f(r_w,t)}{\partial r} + f(r_w,t) = s_w, \tag{3.16}$$

and recall Darcy's Law: $Q_f = -2\pi r_w L K(\partial f / \partial r)$, where K is the aquifer hydraulic conductivity, then the skin effect corresponding to Eq. (3.15) becomes

$$\eta = \frac{K}{r_w C_s}. \tag{3.17}$$

Using the notation of Moench and Hsieh (1985), defining $r_{\sin} = r_w + d_s$, and considering an infinitesimal skin, then $\lim_{d\to 0} \ln\left[r_s / r_w\right] = \lim_{d\to 0} \ln\left[(r_w + d_s)/r_w\right] \simeq d_s / r_w$. Thus the skin effect given by Moench and Hsieh (1985) becomes

$\eta = \frac{K}{K_s}\ln[r_s / r_w] \simeq \frac{K}{K_s} \times \frac{d_s}{r_w} = \frac{K}{r_w C_s}$, which is identical to our Eq. (3.17).

The dimensionless form of Eq. (3.15) becomes

$$Q_{fD} = \alpha[s_{wD} - f_D(t)], \tag{3.18}$$

where Q_{fD} and α are defined in List of Symbols, and s_{wD} and f_D are defined in the same way as the dimensionless drawdown given in List of Symbols. The dimensionless wellbore pumping rate is

$$Q_{wD} = \partial s_{wD} / \beta \partial t_D, \tag{3.19}$$

where Q_{wD} and β are defined in List of Symbols.

The summation of Q_{fD} and Q_{wD} is

$$Q_{wD} + Q_{fD} = 1. \tag{3.20}$$

Substituting Eqs. (3.18)-(3.19) into Eq. (3.20) results in a differential equation of s_{wD}. Solving the equation in Laplace domain and substituting the solution of s_{wD} into Eq. (3.18) results in

$$\bar{Q}_{fD}(p) = -\frac{\alpha p \bar{f}_D(p)}{p + \alpha\beta} + \frac{1}{p} - \frac{1}{p + \alpha\beta}, \tag{3.21}$$

where the over bar implies the Laplace transform. The average drawdown (in Laplace domain) at the wellbore screen face is $\bar{f}_D(p) = \bar{Q}_{fD}(p)\bar{g}^*(p)$, where $\bar{g}^*(p)$ is the surface average of the geometric function of the finite-diameter well along the wellbore

screen face in Laplace domain. The geometric function of the finite-diameter well in Laplace domain, $\bar{g}(x_D, y_D, z_D, p)$, is

$$\bar{g}(x_D, y_D, z_D, p) = \frac{1}{V}\int_V \bar{g}_0(x_D, y_D, z_D; x_{0D}, y_{0D}, z_{0D}, p)dV\,, \tag{3.22}$$

where $\bar{g}_0(x_D, y_D, z_D; x_{0D}, y_{0D}, z_{0D}, p)$ is the point geometric function in Laplace domain defined in Eq. (3.11).

Therefore, Eq. (3.21) becomes

$$\bar{Q}_{fD}(p) = -\frac{\alpha p \bar{Q}_{fD}(p)\bar{g}^*(p)}{p+\alpha\beta} + \frac{1}{p} - \frac{1}{p+\alpha\beta}. \tag{3.23}$$

The resultant solution of the source function in Laplace domain is

$$\bar{Q}_{fD}(p) = \frac{\alpha\beta}{p\left[\, p\left\{1+\alpha\bar{g}^*(p)\right\}+\alpha\beta\,\right]}. \tag{3.24}$$

Two special cases deserve discussion:

1. If the well has a negligible wellbore storage, i.e., $r_c \to 0$ and $\beta \to \infty$, Eq. (3.24) converges to $\bar{Q}_{fD}(p) = 1/p$, which yields the constant pumping rate.

2. If the skin effect is negligible but the wellbore storage is not, i.e., $d_s \to 0$, so $\alpha \to \infty$, Eq. (3.24) becomes $\bar{Q}_{fD}(p) \to \beta/\left[\, p\left\{p\bar{g}^*(p)+\beta\right\}\,\right]$, which yields the pumping rate without skin.

3.3.3 Solution of a finite-diameter horizontal well

Eq. (3.24) indicates that if $\bar{g}^*(p)$ is known, then the aquifer pumping rate is also known. However, a rigorous analytical deviation of $\bar{g}^*(p)$ is extremely difficult for a finite-diameter horizontal well because of the change of head along the outside skin of the screened section of a wellbore. Fortunately, based on the following arguments, a close approximation of $\bar{g}^*(p)$ can be derived:

1. A finite-diameter horizontal well is a volume source that can be visualized as the superposition of many horizontal line sources. Thus the average geometric function of a finite-diameter horizontal well can be calculated from the average geometric functions of the superposed horizontal line sources.

2. Previous investigations about the horizontal line sources indicated that the drawdown at $x_D/(L_D/2) = 0.68$ offers an excellent approximation of the average drawdown at the horizontal wellbore (Daviau et al., 1988; Rosa AJ, Carvalho, 1989; Zhan et al., 2001), where L_D is the dimensionless well screen length defined in List of Symbols. Thus the average geometric function of a line source can be calculated by substituting $x_D/(L_D/2) = 0.68$, $y_D = 0$, $z_D = z_{wD}$, and $B_D \to \infty$ into the line source drawdown solution (Zhan et al., 2001, Eq. (18)). Considering the slight difference in the definitions of dimensionless drawdown used in Zhan et al. (2001) and in this work, the result is

$$\bar{g}^*(p)=\frac{2}{L_D}\left[\int_{-L_D/2}^{L_D/2}K_0[\sqrt{p}\,|0.34L_D-x'_D|]dx'_D +2\sum_{n=1}^{\infty}\cos^2[n\pi z_{wD}]\int_{-L_D/2}^{L_D/2}K_0[\sqrt{p+n^2\pi^2}\,|0.34L_D-x'_D|]dx'\right]. \tag{3.25}$$

Eq. (3.25) can be simplified if considering the fact that the wellbore storage and skin effect influence the early time drawdown the most; thus the above calculation will be targeted for p>>1. Under that condition, using the following identity $\int_0^u K_0(u)du \simeq \pi/2$, if $u \geq \pi$ (Hantush, 1964; Zhan et al., 2001), an approximate form of the average geometric function becomes

$$\bar{g}^*(p)=\frac{2\pi}{L_D}\left\{\frac{1}{\sqrt{p}}+2\sum_{n=1}^{\infty}\cos^2\left(n\pi z_{wD}\right)\frac{1}{\sqrt{p+n^2\pi^2}}\right\}. \tag{3.26}$$

Eq. (3.26) will be used as the approximate geometric function of a finite-diameter well, and it will be substituted into Eq. (3.24) to obtain $\bar{Q}_{fD}(p)$. The aquifer pumping rate $Q_{fD}(t_D)$ is numerically obtained through the inverse Laplace transform of $\bar{Q}_{fD}(p)$ using the Stehfest algorithm (Stehfest, 1970).

With these preparations, one can now calculate the drawdown near a finite-diameter horizontal pumping well by the volume integration of the point source solution:

$$s_{HD}(t_D)=\frac{1}{V}\int s_D(t_D)dx_0dy_0dz_0=\frac{d^3\sqrt{K_xK_y}/K_z}{\pi r_w^2L}\int s_D(t_D)dx_{0D}dy_{0D}dz_{0D}, \tag{3.27}$$

where s_{HD} is the horizontal-well dimensionless drawdown defined in List of Symbols with q replaced by Q. After performing the spatial integration, Eq. (3.27) becomes

$$s_{HD}(t_D)=\frac{\sqrt{K_y/K_z}}{L_D r_{wD}^2}\int_0^{t_D} Q_{fD}(t_D-\tau)\exp\left(-\frac{\tau}{B_D^2}\right)\left\{erf\left(\lambda_1\right)+erf\left(\lambda_2\right)\right\}\times \int_{z_{wD}-r_{wD}}^{z_{wD}+r_{wD}}\left\{erf\left(\mu_1\right)+erf\left(\mu_2\right)\right\}\left\{1+2\sum_{n=1}^{\infty}\cos\left(n\pi z_D\right)\cos\left(n\pi z_{0D}\right)\exp\left(-n^2\pi^2\tau\right)\right\}dz_{0D}d\tau \quad , \tag{3.28}$$

where r_{wD} is defined in List of Symbols; the aquifer pumping rate, $Q_{fD}(t_D)$, is the inverse Laplace transform of Eq. (3.24); and $\lambda_1=\frac{L_D/2+x_D}{2\sqrt{\tau}}$, $\lambda_2=\frac{L_D/2-x_D}{2\sqrt{\tau}}$, $\mu_1=\frac{\sqrt{r_{wD}^{\ 2}-(z_{0D}-z_{wD})^2}\sqrt{K_z/K_y}+y_D}{2\sqrt{\tau}}$, $\mu_2=\frac{\sqrt{r_{wD}^{\ 2}-(z_{0D}-z_{wD})^2}\sqrt{K_z/K_y}-y_D}{2\sqrt{\tau}}$.

When the well radius $r_{wD}\to 0$, Eq. (3.28) is simplified to

$$s_{HD}(t_D)=\frac{\sqrt{\pi}}{L_D}\int_0^{t_D} Q_{fD}(t_D-\tau)\exp\left(-\frac{\tau}{B_D^2}\right)\left\{erf\left(\lambda_1\right)+erf\left(\lambda_2\right)\right\}\times \exp\left(-\frac{y_D^2}{4\tau}\right)\left[1+2\sum_{n=1}^{\infty}\cos\left(n\pi z_D\right)\cos\left(n\pi z_{wD}\right)\exp\left(-n^2\pi^2\tau\right)\right]\frac{d\tau}{\sqrt{\tau}} \quad . \tag{3.29}$$

Eq. (3.29) is the line source solution including the wellbore storage, skin effect, and leakage. If excluding the wellbore storage, skin effect, and leakage, then Eq. (3.29) is identical to the solution derived by Zhan et al. (2001) if taking into account the slightly different definitions of the dimensionless drawdowns (we used $s_D=4\pi d\sqrt{K_x K_y}\,s/q$, and Zhan et al. (2001) used $s_D=2\pi d\sqrt{K_x K_y}\,s/q$).

For a confined aquifer, B_D^2 goes to infinity, the second term in Eq. (3.28) converges to unity, and the drawdown near a horizontal well in a confined aquifer is obtained.

3.4 Results and Discussion

The integration in Eq. (3.28) is computed using a numerical integration scheme (Press et al., 1989). The numerical evaluation of the drawdown is accomplished using a MATLAB program developed by the authors. This program, named FINHOW, together with the user's manual, is available from the author's website: http://park.tamu.edu/research.htm or by individual contact. This program is devised to calculate and plot a time-dependent drawdown curve at any measuring point in a leaky or confined aquifer near a horizontal well.

The influence of the finite well radius on the flow is most significant at near fields defined as the regions close to the horizontal well. The influence of the wellbore storage is most important at the early time during which the water is withdrawn from near fields. Thus in the following discussion, we will focus on the drawdown change at the near field and/or at the early time.

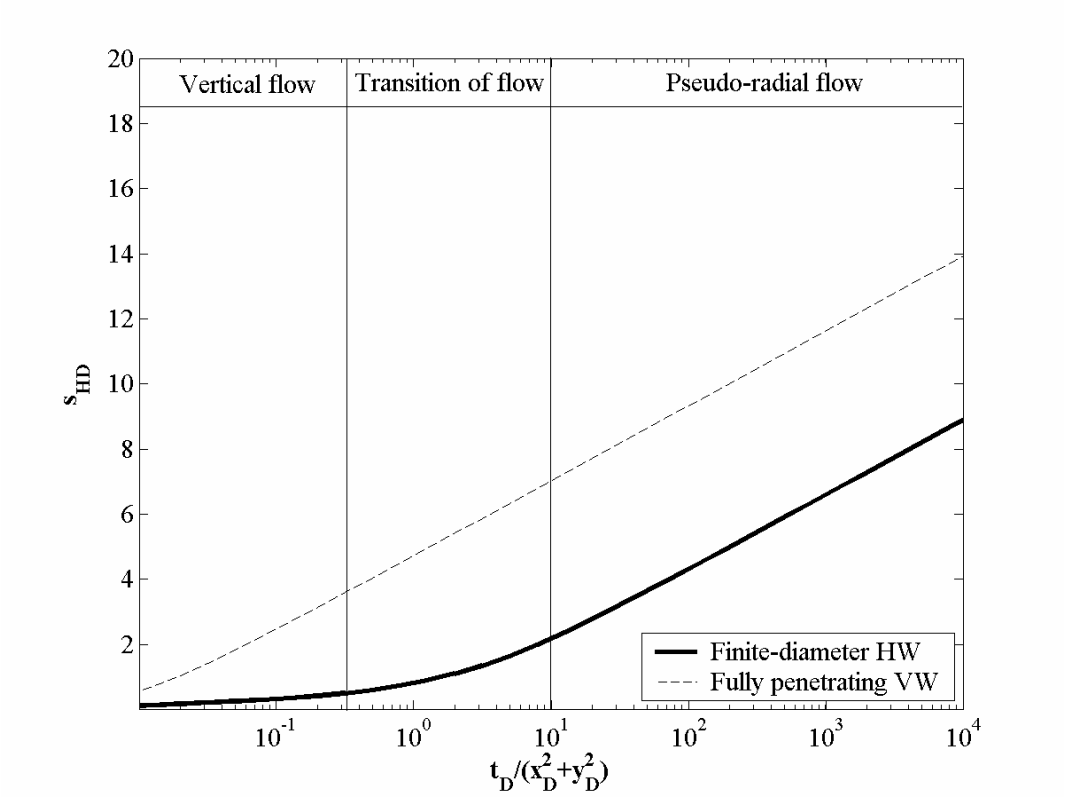

Figure 3.2. Comparison of dimensionless semi-log type curves of a finite-diameter horizontal well (HW) and a fully penetrating vertical well (VW).

Many interesting aspects of the results are shown in Figures 3.2-3.7. If not specified, the following default values of parameters are used in those figures: aquifer thickness is 10 m; aquifer is homogeneous and isotropic with hydraulic conductivities equal to 0.0001 m/s; specific storativity is 0.0002 m^{-1}; horizontal well is 100 m long and located at the middle elevation of the aquifer (z_w=5 m); pumping rate is 0.01 m^3/s; well radius is 0.1 m; for simplicity, the casing radius, r_c, is assumed to be the same as the horizontal-well radius, r_w, in the following discussion; conductance of the wellbore skin is 0.001 s^{-1} if skin effect is included; and monitoring point is at the same elevation as the horizontal well and is very close to the well at (1 m, 1 m, 5 m). For brevity of illustration, confined condition is used in most cases except that in section 4.5.

Figure 3.2 is the plot of dimensionless drawdown versus dimensionless time in a semi-log paper, and it shows three distinct sections reflecting the early flow, where all the direction of the flow caused by the pumping is perpendicular to the surface of the screened section, the intermediate transitional flow, where the drawdown is affected by the upper and lower boundaries, and the later time pseudo-radial flow. This result is identical to those found in previous studies using a line source, and the mechanism of this changing flow from vertical radial to pseudo-radial is explained thoroughly in previous works (Daviau et al., 1988; Goode and Thambynayagam, 1987; Kuchuk and Habashy, 1996; Zhan et al., 2001). Leakage effect is excluded in the following figures except Figure 3.7.

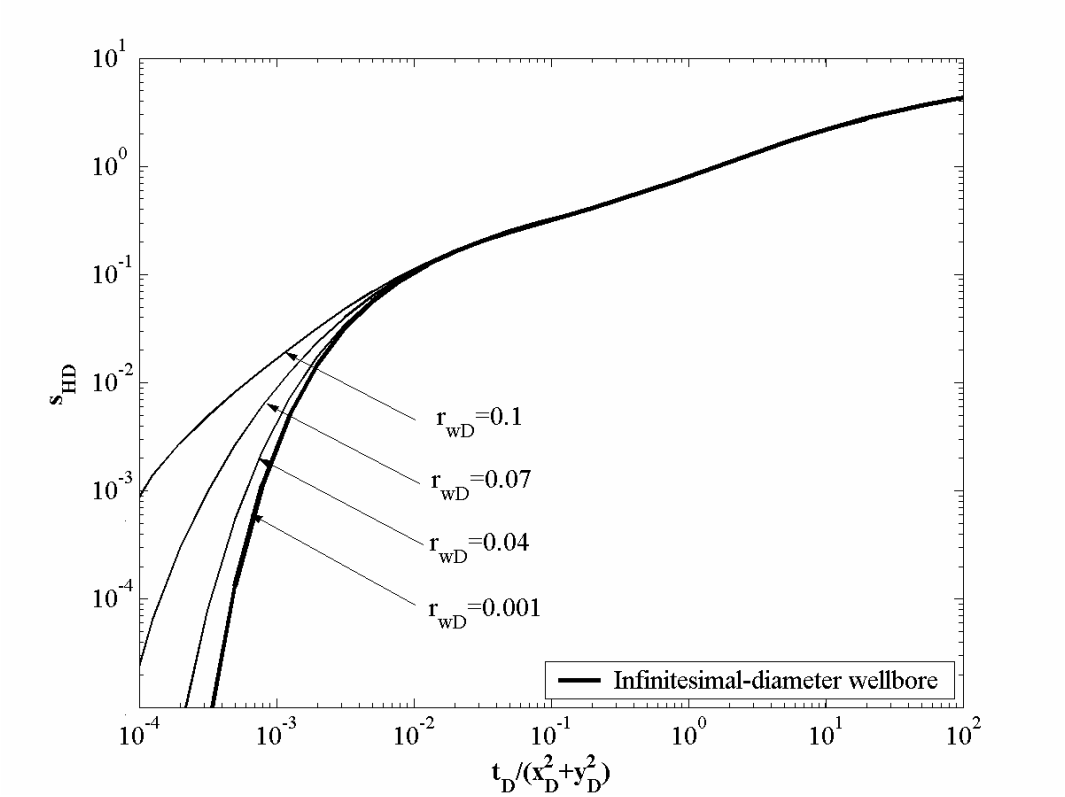

Figure 3.3. Dimensionless type curves with different wellbore radii in an isotropic aquifer. Wellbore storage and skin effects are excluded.

3.4.1 Effect of well radius on geometric function

The simulation of changing in the value of dimensionless geometric function with dimensionless time of different well radii in an isotropic aquifer is performed, and the results are shown in Figure 3.3. We tested the dimensionless well radii of 0.01, 0.04, 0.07, and 0.1. Wellbore storage and skin effects are excluded in this section. The purpose here is to compare our volume source solution Eq.(3.28) to a previous line source solution developed by Zhan et al. (2001).

The influence of the finite-diameter of the well on the geometric function in the near field case should be most profound at the early time during which water is withdrawn from the near field storage. When pumping time increases, the contribution to the geometric function comes from water withdrawn from fields with progressively increasing distances to the well, and the geometric function of the finite-diameter of the well will play a less important role. This rationale is verified in Figure 3.3, which shows that the finite-diameter well solution converges to the line source solution very fast in the isotropic case. After $t_D/(x_D^2 + y_D^2) = 0.01$, the line source solution can be safely used for a finite-diameter well case in an isotropic aquifer. Substituting the assigned parameters into $t_D/(x_D^2 + y_D^2) = 0.01$ results in t=0.04 sec. Thus, we prove that for any practical purpose, the volume-source geometric function can be safely replaced by the line-source geometric function, and Eq. (3.29) can be used to replace Eq. (3.28) for practical calculations.

3.4.2 Effect of wellbore storage

Given the same skin conductance of 10^{-4}/sec, a different well radius means a different wellbore storage. If the effect of wellbore storage is included, water withdrawn in the initial pumping is mostly from the wellbore storage and less from the aquifer storage; thus the drawdown at the monitoring well should be much smaller than that in Figure 3.3 at the early time. With increasing pumping time, the wellbore storage is gradually depleted and more water is withdrawn from the near field, and we should observe a rapid increase of drawdown. Thus, compared to the case excluding the wellbore storage (such as Figure 3.3), it seems that the influence of the horizontal well diameter on the drawdown is delayed by a period of time during which the wellbore storage supplies more water to the pumping than the aquifer. The largest well diameter has the longest delay. The masked section of the drawdown curve has almost a straight line with a unit slope when most of the water is deduced from wellbore. This coincides with previous works (Papadopulos and Cooper, 1967; Streltsova, 1988). This explanation is reflected in Figure 3.4. This finding is similar to those observed in vertical-well problems (Streltsova , 1988, p. 52, Figure 2.2).

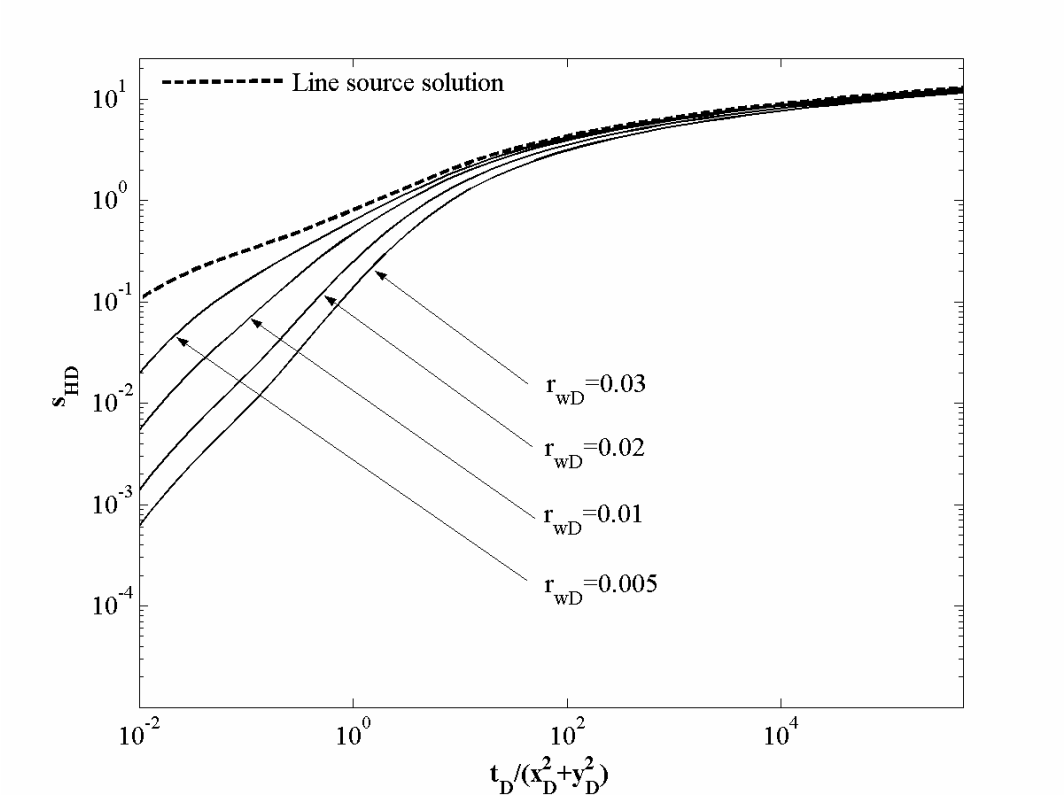

Figure 3.4. Comparison of dimensionless type curves with different dimensionless wellbore radii and the dimensionless type curve of the line source solution derived by Zhan et al. (2001) in an isotropic aquifer. Wellbore storage and skin effects are included.

3.4.3 Effect of skin

The wellbore storage effect deforms the early drawdown, and it depends on two parameters: the volume of the pumping wellbore and the conductance of the well skin K_s/d_s. Given the same wellbore volume, a higher skin conductance implies easier flow of water from the aquifer to the well and the rapid transformation of water withdrawal from the wellbore to the water withdrawal from the aquifer.

The sensitivity analysis of drawdown to the skin effect is tested with different skin conductance K_s/d_s. The aforementioned effect of masking early time drawdown by the skin effect is observed in Figure 3.5. By the analysis, one can find that the lower conductance of the skin causes less drawdown and longer delay of response to the pumping in the aquifer at early time. That is because it is difficult for groundwater to penetrate a lower conductance skin. When the skin conductance increases, the drawdown becomes less and less sensitive to the conductance and the type curves approach the asymptotic limit with an infinite conductance. In fact, Figure 3.5 shows that when the conductance is larger than 10^{-4}/s, the skin effect can be negligible for the given monitoring point.

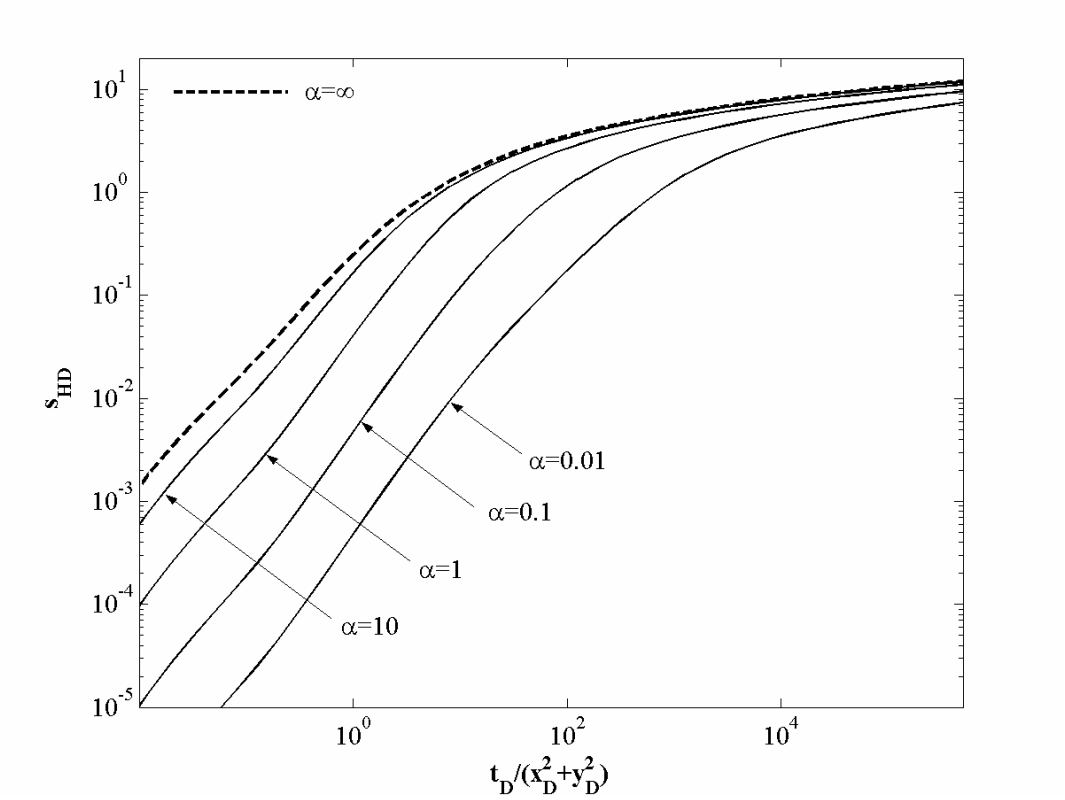

Figure 3.5. Dimensionless type curves with different skin effects. $\alpha \to \infty$ refers to the no-skin case.

3.4.4 Effect of anisotropy

The anisotropic aquifer used in Figure 3.6(a) has horizontal hydraulic conductivity of 0.0001 m/s and vertical hydraulic conductivity 0.00001 m/s; while the horizontal hydraulic conductivity, 0.00001 m/s, and vertical hydraulic conductivity, 0.0001 m/s, are used in Figure 3.6(b). Both wellbore storage and skin effects are included in this section. The ratio of vertical versus horizontal hydraulic conductivity is commonly found in the range of 0.01 to 1 in many rock types (Domenico and Schwartz, 1998, p. 40). If vertical fractures dominate, the vertical hydraulic conductivity could be larger than the horizontal hydraulic conductivity, and the ratio of vertical versus horizontal hydraulic conductivity could vary over a few orders of magnitude in such a fractured aquifer. Similarly, if horizontal fractures dominate in a certain orientation, the ratio of K_x/K_y could also vary over a few orders of magnitude in such a fractured aquifer.

If vertical hydraulic conductivity is much less than the horizontal hydraulic conductivity, it is more difficult to drain the water vertically; thus most water flow to the well comes from the horizontal direction, and we should observe larger drawdowns at the horizontal near field at the early time if compared to the isotropic case. This is true by comparing Figure 3.6(a) to Figure 3.4. On the contrary, if vertical hydraulic conductivity is larger than the horizontal hydraulic conductivity, it is easier to drain the water vertically; thus we should observe smaller drawdowns at the horizontal near field at the early time if compared to the isotropic case. This is confirmed by comparing Figure 3.6(b) to Figure 3.4. Figures 3.6(a) and 3.6(b) indicate that the near field

drawdown curves at the early time strongly depend on the vertical anisotropy because of the strong vertical flow near a horizontal well.

3.4.5 Effect of leaky aquifer

The sensitivity analysis of drawdown to leaking parameters is tested using five different leakage parameters $B_D^{2,}$ and the results are shown in Figure 3.7. The wellbore storage and skin effects are included in this section. The drawdowns in leaky aquifers follow similar curves observed in vertical well problems (Streltsova, 1988) at the late time when the water across the leaking bed becomes significant. The early and the intermediate time stages follow the same curves as that in the confined aquifers. In the case of the storage of the aquitard being considered, more complicated drawdown mechanisms are expected on the early and intermediate time stages. Further investigations including the aquitard storage are needed to provide better solutions to the problems in which the aquitard storage cannot be neglected. If the leakage parameter, B_D^2, goes to infinity, the leaky aquifer solution approaches that of the confined aquifer.

(A)

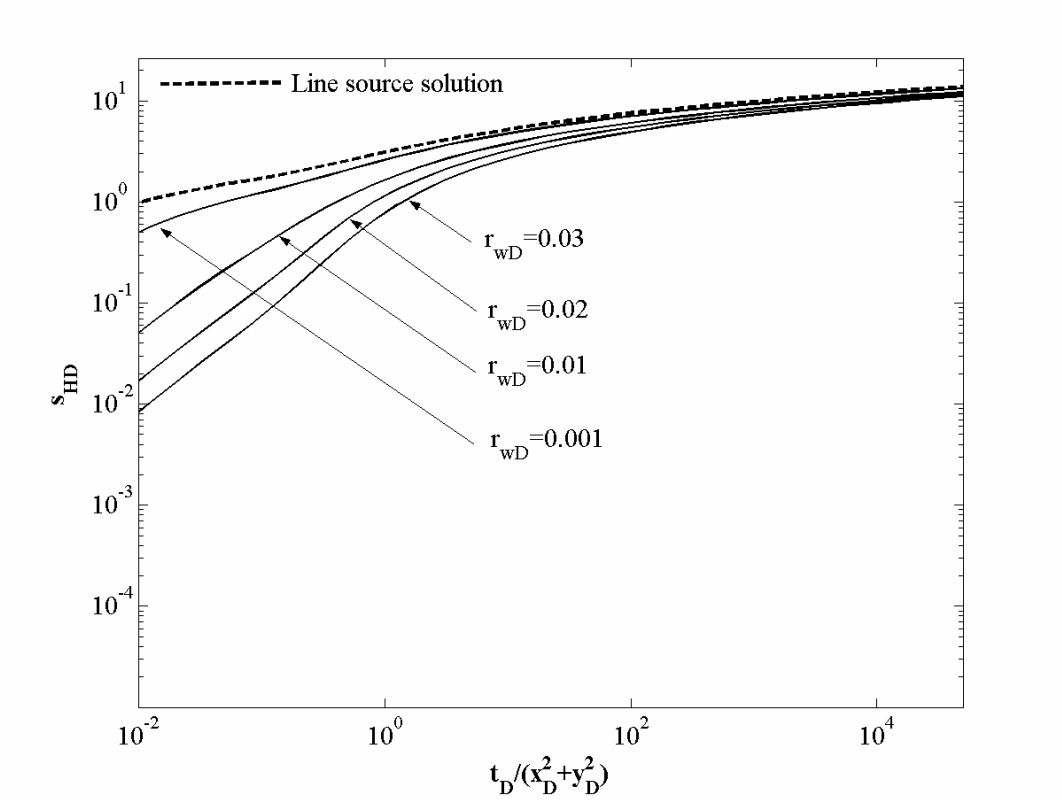

Figure 3.6. Comparison of dimensionless type curves with different wellbore radii and the dimensionless type curve of the line source solution derived by Zhan et al. (2001) in an anisotropic aquifer. (A) $K_z / K_x = 0.1$; (B) $K_z / K_x = 10$, and $K_x = K_y$ for both (A) and (B). Wellbore storage and skin effects are included.

(B)

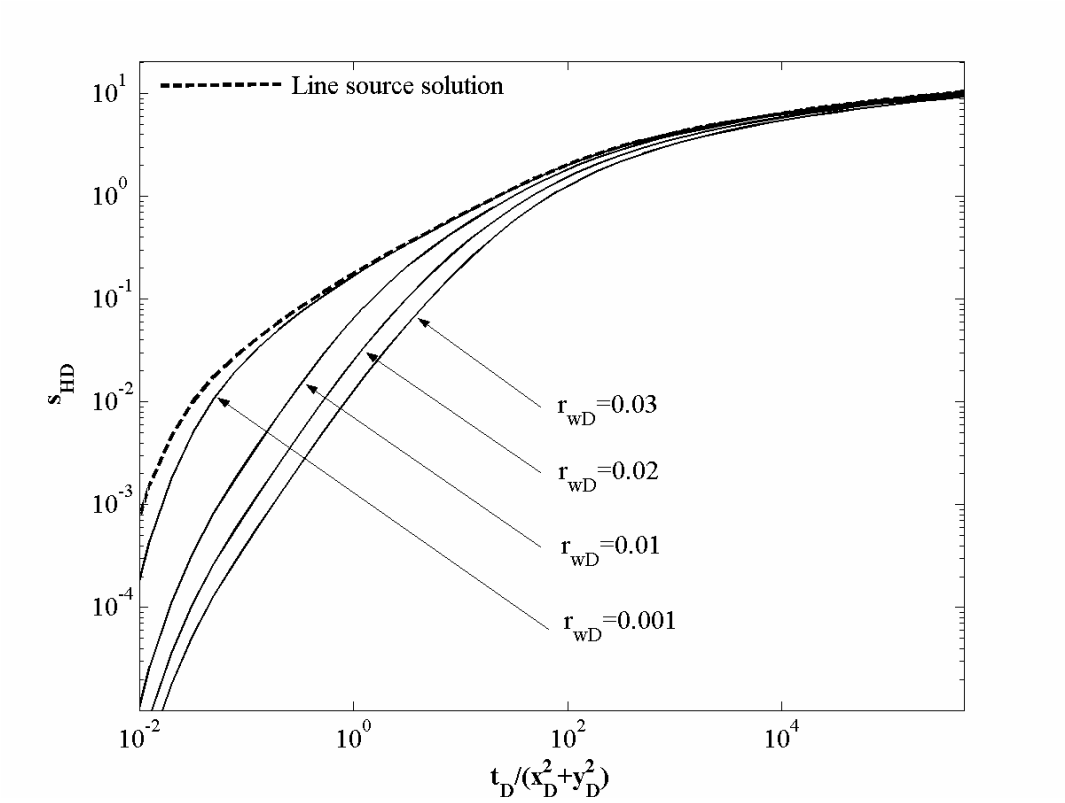

Figure 3.6. Continued

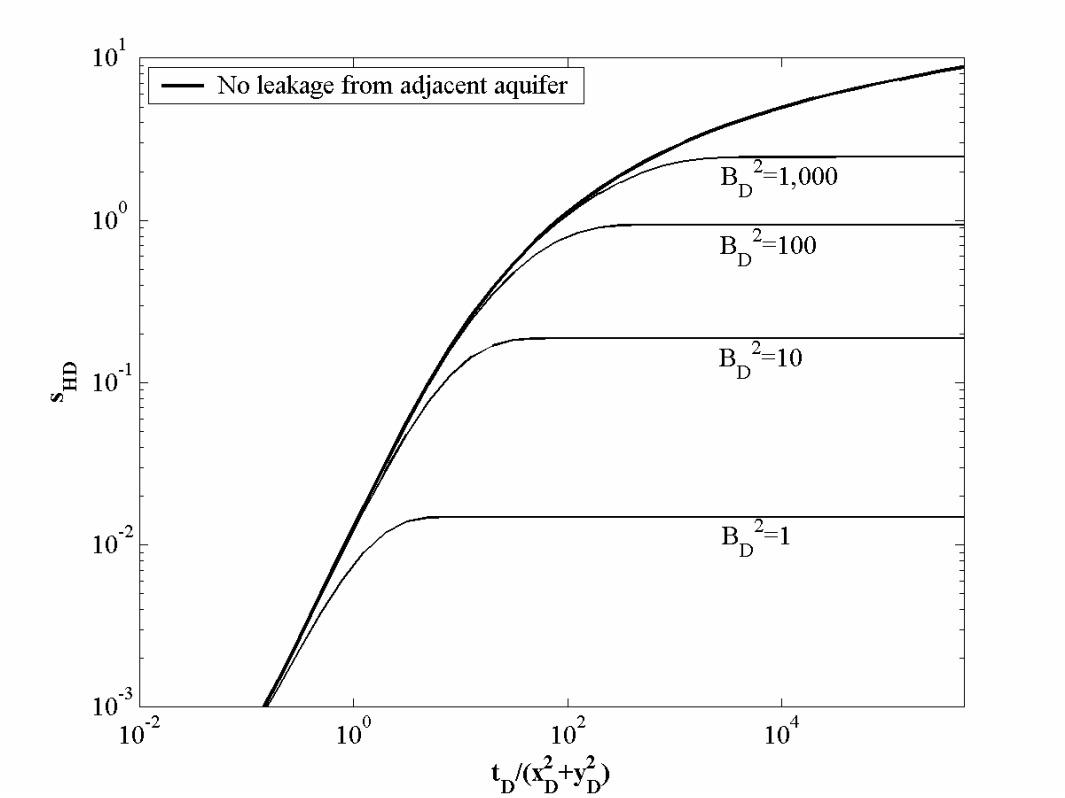

Figure 3.7. Comparison of dimensionless type curves with different leakage parameters and the dimensionless type curve of the line source solution derived by Zhan et al. (2001) in an isotropic aquifer. Wellbore storage and skin effects are included.

3.5 Summary and Conclusions

This paper provides solutions on groundwater flow to a finite-diameter horizontal well including wellbore storage and skin effect. These solutions offer better physical insights than previous line source solutions into the hydraulics of horizontal wells in three-dimensionally anisotropic leaky aquifers. They are more useful for describing the near field drawdown behavior.

The drawdown solution for a finite-diameter horizontal well is derived on the basis of volume integration of point-source solutions. A graphically integrated numerical MATLAB© program named FINHOW is written by the authors to compute the volume integration using the Gaussian quadrature method (Press et al., 1989) and to provide the type curves of groundwater flow to a finite-diameter horizontal well. The drawdown solution in a confined aquifer is obtained as a special case of the solution in the leaky aquifer.

Our solution shows that the finite-diameter of the well only influences the near field at the early flow time. The finite-diameter solution converges to the line source solution at $t_D/(x_D^2 + y_D^2) = 0.01$ in an isotropic aquifer if excluding the wellbore storage. If the wellbore storage is included, it will take a much longer time for the finite-diameter solution to converge to the line source solution.

The skin effect impacts flow through the conductance of the wellbore skin. A higher skin conductance means easier flow from the aquifer to the well and quicker response of the aquifer to the pumping. When the skin conductance increases, the

drawdown becomes less and less sensitive to the skin conductance, and the type curves approach the asymptotic limit that is corresponding to an infinite conductance case.

The anisotropy controls the relative strength of vertical and horizontal flows at the early time, and thus shows a strong influence on the early time near-field drawdown. The leakage parameter influences the late pseudo-radial flow substantially but has limited impact on the early and intermediate flows when excluding the storage in the leaky confining layer.

CHAPTER IV

HYDRAULICS OF HORIZONTAL WELLS IN FRACTURED SHALLOW AQUIFER SYSTEMS

A general theory of groundwater flow to a fractured or non-fractured aquifer considering wellbore storage and skin effect is provided. Solutions for both leaky confined and water table aquifers are provided. The fracture model used in this study is the standard double-porosity model. The storage of the aquitard (the leaky confining layer) is included in the formula. A MATLAB program denoted FINHOW2 is written to facilitate the calculation of drawdowns and the generation of type curves that plot the dimensionless drawdowns versus the dimensionless times over the squares of the dimensionless radial distances in log-log scales. Sensitivity of the solution to the confined versus unconfined conditions, fractured versus non-fractured conditions, and wellbore storage and skin effects is analyzed. This study improves previous solution found by Park and Zhan (2002) that only deals with a non-fractured confined aquifer scenario. It also improves the previous results found by Zhan and Zlotnik (2002) that only deals with a non-fractured water table aquifer that excludes wellbore storage and skin effect. Several findings of this study are summarized as follows. (1) The influence of wellbore storage and skin effects upon the drawdown is similar to what has been found in a previous study of a confined aquifer (Park and Zhan, 2002). (2) The aquitard storage affects the mid-time drawdown the most. (3) There is a significant difference between the type curves of fractured and non-fractured confined aquifers because of the contribution of matrix storage. The difference in type curves of fractured and non-

fractured water table aquifers disappears at the later-time because the unsaturated zone is the dominate water source at that time, and it surpasses the difference of the storage water contributions from the fractured and non-fractured media. (4) In general, the drawdowns are more sensitive to the hydraulic conductivity and storativity of the matrix in a fractured confined aquifer than in a fractured water table aquifer.

4.1 Introduction and Background Knowledge

The horizontal well applications in the environmental remediation are one of the most promising techniques. They have been successfully applied to many field remediation programs combined with the remedial techniques associated with vertical wellbores, e.g. pump and treat, soil vapor extraction (SVE), free product recovery, enhanced bioremediation, air sparging, soil flushing, etc (U.S.EPA, 1994). In most of these techniques, the contact area of the wellbore with the targeting zone is essential. Owing to its optimized contact with the targeting area through the up-to-date technology of the directional drilling, horizontal wells offer many advantages over vertical wells. By the field application reports, a horizontal well usually can substitute several to tens of vertical wells (Seines, 1994; Parmentier and Klemovich, 1996).

Although horizontal wells have been applied for environmental remedial purposes, the supporting theories are not sufficiently developed yet. Petroleum engineers have used horizontal wells for many years and have done numerous studies in this field (Goode and Thambynayagam, 1987; Daviau et al., 1988; Rosa and Carvalho, 1989; Ozkan and Raghavan, 1991). In hydrogeological sciences, due to its relatively short duration of interest on horizontal wells, most of the theories have been directly borrowed

from petroleum engineering. However, there are significant differences in terms of targets and the scopes of using horizontal wells in hydrogeology and in petroleum engineering due to different interests. Petroleum engineers do not apply horizontal wells in water-table and leaky confined aquifers, which are interested by hydrogeologists. A water-table aquifer is most vulnerable to the contaminant generated by surface activity; a leaky confined aquifer also has high potential to be impacted by overlying contaminated water-table aquifer. Moreover, when applying a horizontal well to a hydrogeologic study, the knowledge of hydrodynamics taking place near the well is crucial in a remediation work because the horizontal wellbore is installed directly into the contaminant. The geometry of the finite diameter of the well becomes an important factor influencing the near field problems, where a near field means an area close to the pumping well. In addition, the properties of the aquifer (i.e. porous or fractured), the wellbore storage and skin effects could be important for the near field and the early time problems, where the wellbore storage refers to water initially stored inside the well, and the skin effect refers to the alternation of hydraulic conductivity at a thin layer immediately outside the wellbore during the well-installation process. The well skin serves as a barrier separating the wellbore from the aquifer.

Hydrogeologists have studied hydraulics of horizontal wells in shallow ground water aquifers (Hantush and Papadopulos, 1962; Cleveland, 1994; Sawyer and Lieuallen-Dulam, 1998; Zhan, 1999; Zhan and Cao, 2000; Zhan et al., 2001) and in unsaturated zones (Falta, 1995; Zhan and Park, 2002). In most of these studies, the horizontal well is treated as a line sink/source and the wellbore storage and skin effects

are not included. Zhan and Zlotnik (2002) derived solutions of drawdowns in water-table aquifers due to horizontal-well and inclined-well pumping. By neglecting the wellbore storage and skin effects, their solutions may not be applied on early time and near field aquifer pumping data. Most recently, Park and Zhan (2002) derived a finite-diameter horizontal well solution that is useful for confined and leaky confined aquifer considering wellbore storage and skin effects. But their solution is also limited in application by neglecting the aquitard storage effect.

Park and Zhan (2002) have done a detailed review of previous works on wellbore storage and skin effects. The conceptual model used for dealing with a fractured aquifer in this study is the double-porosity approach. This concept is first introduced by Barenblatt et al. (1960). Later on, it is established as a pseudo-steady state model by Warren and Root (1963) and as a transient model by Kazemi (1969). The double-porosity concept is widely applied in petroleum and groundwater literature on vertical wells in fractured aquifer or reservoir systems (Boulton and Streltsova, 1977; Deruyck et al., 1982; Moench, 1984; Cleveland, 1994). But it is rarely used in analytical studies of a finite horizontal well with the consideration of wellbore storage and skin effects, except in a few petroleum studies (Ohaeri and Vo, 1991; Ozkan and Raghavan, 1991).

No studies have ever been carried out before to investigate the hydrodynamics of horizontal wells including finite-diameter sources, wellbore storage, and skin effects in porous/fractured water-table aquifers and in leaky confined aquifers that consider aquitard storage effects. The purposes of this study are as follows. First, to derive the analytical solutions that consider exact aquifer boundary conditions and aquifer media

types, and consider the effects caused by finite diameters of the horizontal wellbores. Second, through sensitivity analysis, to examine the effects caused by those boundary conditions, media types, and finite diameters of the wellbores. This study will meet these ends and provide a systematic method to analyze horizontal well pumping data.

4.2 Mathematical Model

The general geometry of the problem can be found from Figure 4.1(a) for a fractured water-table aquifer, and Figure 4.1(b) for a fractured leaky aquifer. We assume that both aquifers are finite along the vertical direction and infinite along the horizontal directions. The dashed lines in Figure 4.1 are fractures and the cubic boxes represent matrix. We must point out that the fracture model used here is idealized in order to achieve closed-form solutions, and it may be very different from actual fractures observed in real aquifers, that could be very complicated. Thus the derived results based on this simple model can be used for a screening tool of understanding flow to a horizontal well in a fractured aquifer, but it should not be used as the precise prediction of flow in a real complicated fractured aquifer system.

Because our targeting aquifer system is shallow in terms of depth, the water impeding material (skin) right outside matrix is not considered in this study (Moench, 1984). Other assumptions about the groundwater and the horizontal wellbore used in this study are identical to those used by Park and Zhan (2002). As a preliminary step to reach the finite-diameter horizontal well solution, we first consider the governing equation of ground water flow to a point sink/source in a three-dimensionally anisotropic fractured aquifer (Zhan et al., 2001; Park and Zhan, 2002),

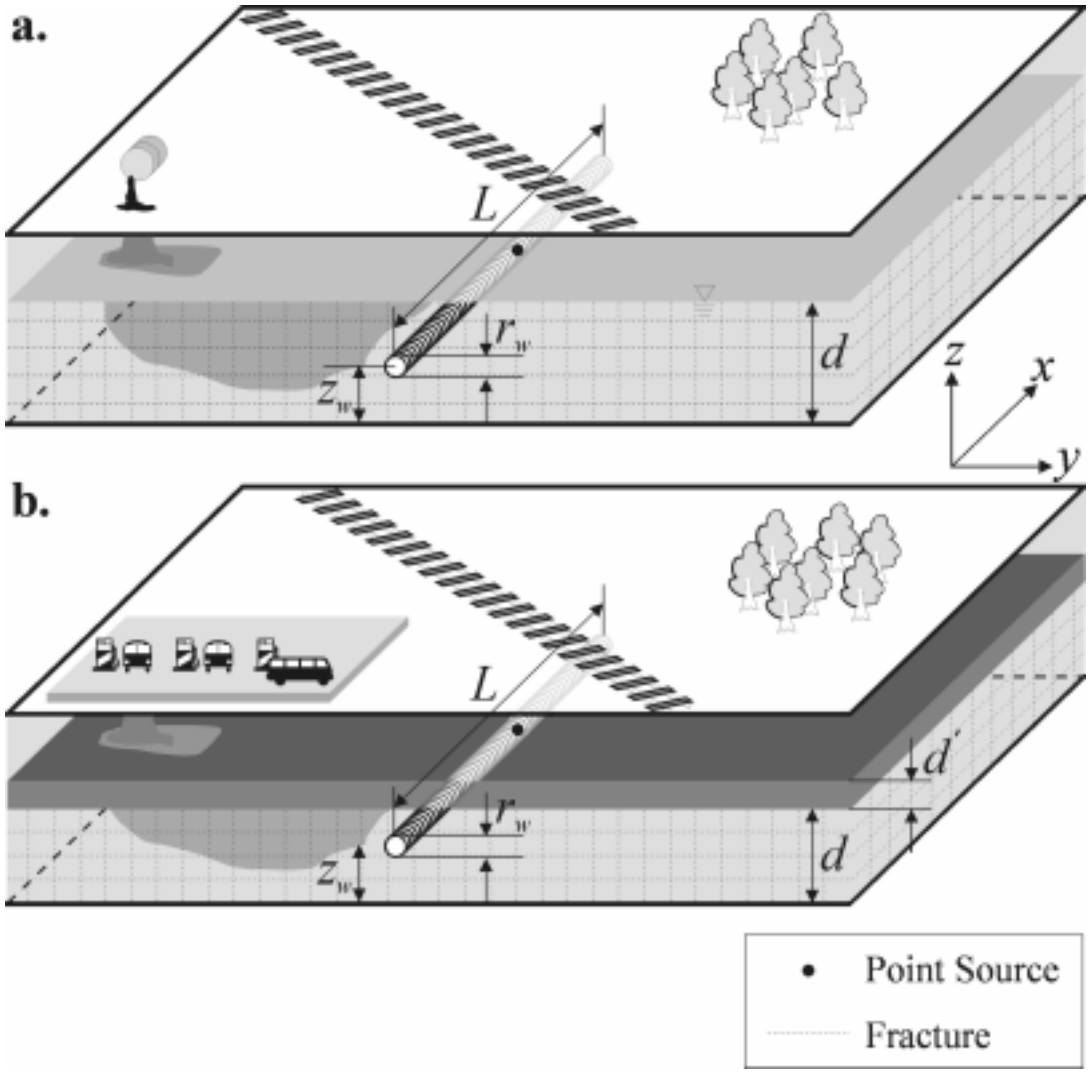

Figure 4.1. Schematic diagrams of a finite-diameter horizontal well in (a) a fractured water-table aquifer, and (b) a fractured leaky confined aquifer.

$$K_x \frac{\partial^2 h}{\partial x^2} + K_y \frac{\partial^2 h}{\partial y^2} + K_z \frac{\partial^2 h}{\partial z^2} - \Gamma_1 - \Gamma_2 - S_S \frac{\partial h}{\partial t} = q_f(t)\delta(x - x_0)\delta(y - y_0)\delta(z - z_0)\,. \tag{4.1}$$

where K_x, K_y, K_z are the principal hydraulic conductivities (m/sec) in the x-, y-, and z-directions of the fractures, respectively; h is hydraulic head (m); S_s is specific storativity (m^{-1}); t is time (sec); q_f is the aquifer pumping rate for a point sink/source (m^3/sec) (q_f>0 means pumping); $\delta(u)$ is the Dirac delta function; (x_0, y_0, z_0) is the point source location; Γ_1 is the fracture-matrix water exchange term, or the so-called surface inter-porosity flux term (1/sec); and Γ_2 is the inter-aquifer flux (leakage) term (1/sec). If $\Gamma_1 \to 0$, Eq. (4.1) converges into the governing equation of a single-porosity aquifer and if $\Gamma_2 \to 0$, Eq. (4.1) converges into the governing equation of a confined aquifer.

We separate the problem-solving process into two parts. We will first get the point source solution and superpose them to acquire our ultimate solutions of finite-diameter horizontal wells. Following Park and Zhan (2002), the finite volume horizontal wellbore can be visualized as superposition of many point sources, and the aquifer-pumping rate, Q_f, can be defined as

$$Q_f(t) = \frac{1}{V}\int_V q_f(x, y, z, t)dV\,, \tag{4.2}$$

where V is the volume of the horizontal wellbore and $q_f(x, y, z, t)/V$ is the point source strength. To apply above equation, we assume an infinite conductivity inside the wellbore and the justification for this assumption can be found from Zhan et al. (2001) and Park and Zhan (2002).

The outer boundary conditions along the x-axis and the y- axis are,

$$h(x,y,z,t)\big|_{x=\pm\infty} = h_0 \quad h(x,y,z,t)\big|_{y=\pm\infty} = h_0, \tag{4.3}$$

where, h_0 is the initial head (m). The condition at the lower boundary is,

$$\partial h(x,y,z,t)/\partial z\big|_{z=0} = 0, \tag{4.4}$$

and at the upper boundary for a leaky confined aquifer is (Fig. 1(b)),

$$\partial h(x,y,z,t)/\partial z\big|_{z=d} = 0, \tag{4.5}$$

where d is the thickness of the aquifer (m).

A horizontal well usually causes less interface movement compared to a vertical well with a given pumping rate since the pumping rate is distributed along a much longer screen. Therefore, it is safe to assume a small perturbation for the water-table boundary. In this study we apply the model of delayed drainage from unsaturated zone for a water-table boundary (Moench, 1997),

$$K_z \partial h(x,y,d,t)/\partial z = -\alpha_1 S_y \int_0^t \partial h(x,y,d,t)/\partial \tau \exp\{-\alpha_1 (t-\tau)\}\, d\tau, \tag{4.6}$$

where α_1 is an empirical constant for drainage from the unsaturated zone and S_y is the specific yield.

The initial condition of the modeled domain is

$$h(x,y,z,t)\big|_{t=0} = h_0. \tag{4.7}$$

We use a double-porosity approach to model the flux (Γ_1) between matrixes and fractures. By taking double-porosity aquifer into consideration, the subsidiary equation in the sphere shaped matrix will be (Deruyck, 1982),

$$\frac{K'}{r^2}\frac{\partial}{\partial r}\left(r^2\frac{\partial h'}{\partial r}\right)=S_S'\frac{\partial h'}{\partial t}, \tag{4.8}$$

where K' is the hydraulic conductivity (m/sec), S_s' is the specific storage (m^{-1}), and h' is the hydraulic head (m), all referring to the matrix. The inter-porosity flux is (Deruyck, 1982),

$$\Gamma_1=\frac{3K'}{r_m}\left(\frac{\partial h'}{\partial r}\right)\Bigg|_{r=r_m}, \tag{4.9}$$

where r_m is the radius (m) of the matrix block.

The initial and boundary conditions for matrixes are, respectively,

$$h'\big|_{t=0}=h_0 \text{ and } h'\big|_{r=r_m}=h. \tag{4.10}$$

The inter-aquifer flux (leakage) term is given by Γ_2. In case the aquifer is confined by an aquitard, only the vertical flux is considered and the governing equation for the vertical flow in the aquitard is (Hantush, 1960),

$$K_C\frac{\partial^2 h_C}{\partial z^2}=S_{SC}\frac{\partial h_C}{\partial t}, \tag{4.11}$$

where K_C is the hydraulic conductivity (m/sec), h_C is the hydraulic head (m), S_{SC} is the specific storativity, all referring to the aquitard (m^{-1}). The inter aquifer flux is given by

$$\Gamma_2 = \frac{K_C}{d}\frac{\partial h_C}{\partial z}\bigg|_{z=d_C}, \tag{4.12}$$

where d_c is the thickness of the aquitard (m). The initial, upper and lower boundary conditions for the aquitard are, respectively,

$$h_C\big|_{t=0} = h_0, \quad h_C\big|_{z=0} = h_0, \text{ and } h_C\big|_{z=d_C} = h. \tag{4.13}$$

For the convenience of calculation, we change the variable from head, h, to drawdown, $s=h_0-h$, and define the dimensionless parameters in Table 4.1 where all the parameters are explained in the List of Symbols. The variable for subsidiary equations, h' and h_C are also changed into $s'=h_0-h'$ and $s_C=h_0-h_C$ and converted into dimensionless parameters in the same way as h.

4.2.1 Solution in the Laplace domain

By introducing the dimensionless variables (Table 4.1) and applying Laplace transform, Eq. (4.1) becomes:

$$\frac{\partial^2 \bar{s}_D}{\partial x_D^2} + \frac{\partial^2 \bar{s}_D}{\partial y_D^2} + \frac{\partial^2 \bar{s}_D}{\partial z_D^2} - \bar{\Gamma}_{1D} - \bar{\Gamma}_{2D} - p\bar{s}_D = \frac{4\pi \bar{q}_{fD}(p)\delta(x_D - x_{0D})\delta(y_D - y_{0D})\delta(z_D - z_{0D})}{p}, \tag{4.14}$$

where a term with "bar" denotes the corresponding term in Laplace domain and the subscript "D" refers to a dimensionless term defined in Table 4.1. All the terms used hereinafter have been explained in the List of Symbols.

By solving subsidiary equations (see Hantush, 1960; Deruyck, 1982), the main governing Eq. (4.14) becomes

Table 4.1. Dimensionless parameters.

$s_D = \frac{4\pi\sqrt{K_x K_y}d}{q}s$	$\beta = \frac{4\sqrt{K_x K_y}S_S d^3}{K_z r_c^2}$
$x_D = \frac{x}{d}\sqrt{\frac{K_z}{K_x}},\ y_D = \frac{y}{d}\sqrt{\frac{K_z}{K_y}},\ z_D = \frac{z}{d}$	$\phi = \frac{K_C}{K_z}$
$t_D = \frac{K_z}{S_s d^2}t$	$\theta = \frac{S_s d}{S_y}$
$\Gamma_{1D} = \frac{4\pi d^3\sqrt{K_x K_y}}{qK_z}\Gamma_1$	$\gamma = \frac{S_{SC}K_z}{S_S K_C}$
$\Gamma_{2D} = \frac{4\pi d^3\sqrt{K_x K_y}}{qK_C}\Gamma_2$	$\mu = \frac{3K'}{r_{mD}K_z}$
$r_D = \frac{r}{d},\ r_{mD} = \frac{r}{d}, r_{wD} = \frac{r}{d}$	$\omega = \frac{K'S_S}{K_z S'_S}$
$d_{CD} = \frac{d_C}{d}$	$\sigma = \frac{S'_S}{S_S}$
$\alpha = \frac{r_w LC_s}{2d\sqrt{K_x K_y}}$	$\eta = \frac{\alpha_1 S_y d}{K_z}$

$$\nabla^2\overline{s}_D - \Psi^2\overline{s}_D = \frac{4\pi\overline{q}_{fD}(p)\delta(x_D - x_{0D})\delta(y_D - y_{0D})\delta(z_D - z_{0D})}{p} \tag{4.15}$$

where

$$\Psi = \sqrt{\phi\sqrt{\gamma p}\coth\left(d_{CD}\sqrt{\gamma p}\right) + \mu\left\{\sqrt{\frac{p}{\omega}}\coth\left(\sqrt{\frac{p}{\omega}}r_{mD}\right) - \frac{1}{r_{mD}}\right\} + p}\,, \tag{4.16}$$

where the first term inside the square root sign is related to the leakage through the aquitard, and the second term inside the square root sign is related to the flow between matrix and fracture.

By applying dimensionless parameter conversion (Table 4.1) and Laplace transform, Eqs. (4.3)-(4.7) become

$$\overline{s}_D\left(x_D, y_D, z_D, p\right)\Big|_{x_D=\pm\infty} = 0\,,\ \overline{s}_D\left(x_D, y_D, z_D, p\right)\Big|_{y_D=\pm\infty} = 0\,. \tag{4.17}$$

$$\partial\overline{s}_D\left(x_D, y_D, z_D, p\right)/\partial z_D\Big|_{z_D=0} = 0\,. \tag{4.18}$$

The upper boundary condition can be either no-flow boundary (leaky confined aquifer)

$$\partial\overline{s}_D\left(x_D, y_D, z_D, p\right)/\partial z_D\Big|_{z_D=1} = 0\,, \tag{4.19}$$

or free boundary (water-table aquifer) (Moench, 1997)

$$\frac{\partial\overline{h}_D\left(x_D, y_D, 1, p\right)}{\partial z_D} = -\eta\frac{p\overline{h}_D\left(x_D, y_D, 1, p\right)}{p + \eta\theta} \tag{4.20}$$

The solutions for Eqs. (4.15) and (4.17)-(4.20) are derived in Appendix and is given below.

$$\begin{aligned}\bar{s}(x_D, y_D, z_D, p) &= \frac{\bar{Q}_{fD}}{V}\int_V \bar{g}_0 dV \\ &= \frac{\bar{Q}_{fD}}{V}\int_V 2K_0\left(r_D\Psi\right) + 4\sum_{n=1}^{\infty}\cos\left(n\pi z_D\right)\cos\left(n\pi z_{0D}\right)K_0\left(r_D\sqrt{\Psi^2+n^2\pi^2}\right)dV\end{aligned}, \tag{4.21}$$

for a leaky confined aquifer, and

$$\bar{s}(x_D, y_D, z_D, p) = \frac{\bar{Q}_{fD}}{V}\int_V \sum_{m=0}^{\infty}\frac{4\cos\left(\varepsilon_m z_{0D}\right)\cos\left(\varepsilon_m z_D\right)}{1+0.5\sin\left(2\varepsilon_m\right)/\varepsilon_m}K_0\left(r_D\sqrt{\Psi^2+\varepsilon_m^2}\right)dV, \tag{4.22}$$

for a water-table aquifer, where

$$\varepsilon_m \tan\left(\varepsilon_m\right) = \frac{\eta p}{p+\eta\theta}.$$

4.2.2 Aquifer pumping rate

The wellbore storage is one of the important parameters that mask the early time or the near field pressure data. In most horizontal well applications, fairly long wellbores are used to enlarge the contact area with the targeting aquifer systems. Therefore, the effect of disturbing the early time aquifer response is much severe in horizontal well applications than that in vertical wells. The analytical approach of wellbore storage effect of a finite-diameter horizontal well is well introduced in the previous study (Park and Zhan, 2002). In the present study, our interests are about leaky confined aquifer with aquitard storage and water-table aquifer in fractured or non-fractured aquifers, and we need to develop new solutions considering different aquifer

conditions. Park and Zhan (2002) have given the aquifer-pumping rate by a finite diameter horizontal wellbore in the Laplace domain, $\bar{Q}_{fD}$, as

$$\bar{Q}_{fD}(p) = \frac{\alpha\beta}{p\left[p\left\{1+\alpha\bar{g}^*(p)\right\}+\alpha\beta\right]}, \tag{4.23}$$

for a monitoring piezometer outside of the wellbore. The aquifer-pumping rate inside the wellbore is independent of the location within the wellbore and based on the work of Park and Zhan (2002) [Eq. (18)], it is given by,

$$\bar{Q}_{fD} = \frac{\beta\left\{1+\bar{g}^*(p)\right\}}{p\left[p\left\{1+\alpha\bar{g}^*(p)\right\}+\alpha\beta\right]}. \tag{4.24}$$

The skin is assumed to be infinitesimally thin when using Eqs. (4.23)-(4.24). This treatment is similar to those used by Dougherty and Babu (1984), Kabala and Cassiani (1997), and many others in studying vertical wells. The arguments with and relationship between the infinitesimal and the finite thickness skins are well defined by Moench and Hsieh (1985) and Park and Zhan (2002).

In this study, the surface average of the geometric functions, $\bar{g}^*$, differs from the previous case of a leaky confined aquifer without aquitard storage. The point source solutions derived through this study, Eqs. (4.21)-(4.22), are the foundation for the following work. The relationship between the point source solution and the surface average of the geometric function is defined in the following Eq. (4.25).

$$\bar{g}^*(p) = \frac{1}{VA}\int_A\int_V \bar{g}_0\left(x_D, y_D, z_D; x_{0D}, y_{0D}, z_{0D}, p\right) dV dA, \tag{4.25}$$

where V is the volume of the horizontal wellbore and A is the area right outside of the wellbore.

For most of the horizontal well applications, the lengths of the wellbores are reasonably long and the wellbore storages and skin effects are profound during the early time. Under those conditions, we can approximate Eq. (4.25) by employing several identities used in previous studies (Hantush, 1964; Zhan et al, 2001; Park and Zhan, 2002). For leaky confined and confined aquifers, we can approximate the surface average of the geometric function as

$$\bar{g}^*(p) \approx \frac{2\pi}{L_D}\left\{\frac{1}{\sqrt{p+\Psi^2}} + 2\sum_{n=1}^{\infty}\cos^2\left(n\pi z_{wD}\right)\frac{1}{\sqrt{p+\Psi^2+n^2\pi^2}}\right\}, \tag{4.26}$$

and for water-table aquifers, it is

$$\bar{g}^*(p) \approx \frac{4\pi\cos\left(\varepsilon z_{0D}\right)^2}{L_D\left\{1+0.5\sin\left(2\varepsilon\right)/\varepsilon\right\}\sqrt{p+\Psi^2+\varepsilon^2}}. \tag{4.27}$$

The derivations of Eqs. (4.26)-(4.27) follow the same procedure presented in Park and Zhan (2002).

For most of the practical calculations, we can simplify the geometric function of a finite diameter horizontal wellbore by reducing the dimension of the integration (Park and Zhan, 2002). Park and Zhan (2002) point out that the finite-diameter geometric function is computationally demanding but its effect only exists during very early time and converges to the line geometric function at $t_D/(x_D^2+y_D^2)=0.01$ in an isotropic aquifer if excluding the wellbore storage. Therefore, we can safely substitute the finite-diameter

geometric function by the line geometric function. The numerical evaluation of the analytical solutions is accomplished using a MATLAB script developed by the authors. This numerical algorithm is used to conduct the Laplace inversion to get the drawdowns in real time (Stehfest, 1970; de Hoog et al, 1982; Hollenbeck, 1998). The MATLAB script used for this study is denoted FINHOW2 and is available by individual contact.

This program can handle six types of aquifer conditions: confined, leaky confined, and water-table aquifers, and each of them can be either fractured or non-fractured. This program uses up to twenty-one controllable hydrogeologic parameters: d, d_c, K_x, K_y, K_z, K', K_c, r_m, S_s, S_y, S_s', S_{sc}, α_1, and well parameters C_w, L, r_w, Q, x, y, z, z_w. All these parameters are explained in the List of Symbols.

4.3 Sensitivity Analyses

In the following, we conduct sensitivity analyses of the theoretical model. The default parameter values used in the sensitivity analyses are presented in Table 4.2. For all the sensitivity analyses, the monitoring piezometer is located at (1 m, 1 m, 5 m).

Table 4.2. Hypothetical default parameters used for sensitivity analyses.

Parameter	Default value
D	10 m
K_x, K_y, K_z	0.0001 m/sec (isotropic if not specified)
S_s	0.00002 m^{-1}
Q	0.001 m^3/sec
L	100 m
z_w	5 m
r_w	0.1 m
C_s	0.0001 sec^{-1}
Fractured aquifer	
K'	0.00001 m/sec (if not specified)
S_S'	0.001 m^{-1} (if not specified)
r_m	1 m
Leaky aquifer	
K_C	0.000001 m/sec
S_{SC}	0.0001 m^{-1}

Table 4.2. Continued

Parameter	Default value
d_C	1 m
Water-table aquifer	
S_y	0.2
α_1	100 m/sec

4.3.1 Comparison of hydraulics between confined and water-table aquifers

The hypothetic response of confined and water-table aquifers considering fractured and non-fractured aquifer media is presented in Figure 4.2. Notice that the drawdowns in a fractured aquifer always refer to those in the fractures, not in the matrixes. As expected, horizontal well pumping in a water-table aquifer causes much less drawdown especially after the mid-time when the water is supplied from the unsaturated zone. In a confined aquifer that is either fractured or non-fractured, there is an appreciable difference between a fractured aquifer and a non-fractured aquifer in later time drawdown history. That is because water is extracted from the storage in a confined aquifer; a fractured confined aquifer has extra storage water from the matrixes in additional to the fractures, thus should has less drawdowns compared with a non-fractured confined aquifer. In a water-table aquifer, the drawdowns for both fractured and non-fractured cases converge in later time and no appreciable effect of matrix flow can be found. The reason for this is that after the mid-time, the unsaturated zone plays its role as a main reservoir that supplies water to the aquifer. Such a main water source substantially surpasses any difference of storage water contributions from a fractured or non-fractured aquifer. Therefore, the difference caused by matrix flow during the early time disappears after the mid-time and the two curves, one for fractured and one for non-fractured merge at the later time.

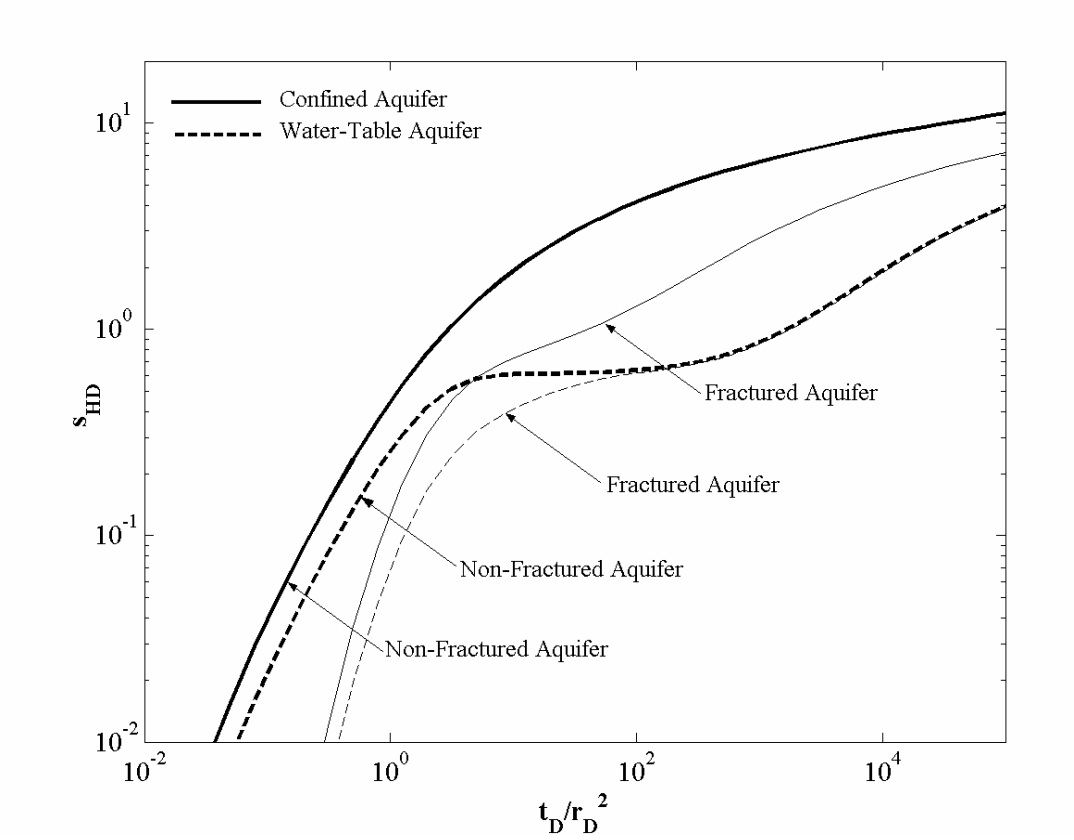

Figure 4.2. Comparison of dimensionless drawdowns versus dimensionless times in a log-log scale (type curves) for different aquifer types and media. Non-fractured confined aquifer is bold solid line; fractured confined aquifer is thin solid line; Non-fractured water-table aquifer is bold dash line; and fractured water-table aquifer is thin dash line.

4.3.2 Wellbore storage and skin effects

To verify the wellbore storage effects, we test several different dimensionless radii of horizontal wellbores of 0.001, 0.01, 0.02, 0.03, and 0.1 with a given skin conductance of 0.0001 sec^{-1} in a fractured confined aquifer and a fractured water-table aquifer (Figure 4.3). We find that the wellbore storage effects in both fractured confined aquifers and fractured water-table aquifer are very similar to what we have seen in non-fractured confined aquifers (Park and Zhan, 2002). That is: the wellbore storage effects mask the early time responses and a larger dimensionless wellbore radius represents a greater and longer lasting wellbore storage effect. This finding indicates that the wellbore storage effect substantially surpasses the matrix-fracture flow effect at the early pumping stage.

In regard to the skin effect, the results of fractured confined aquifers and fractured water-table aquifers are also very similar to those in non-fractured confined aquifers (Park and Zhan, 2002). Figure 4.4 compares the solutions of different skin effects (α) with an ideal case solution of Zhan and Zlotnik (2002) that does not account for the wellbore storage and skin effects in water-table aquifers. This figure shows that the type curves depart from that of Zhan and Zlotnik (2002) at early and intermediate times, but converge to that of Zhan and Zlotnik (2002) at the late time. Furthermore, the smaller the α, the longer it takes to converge.

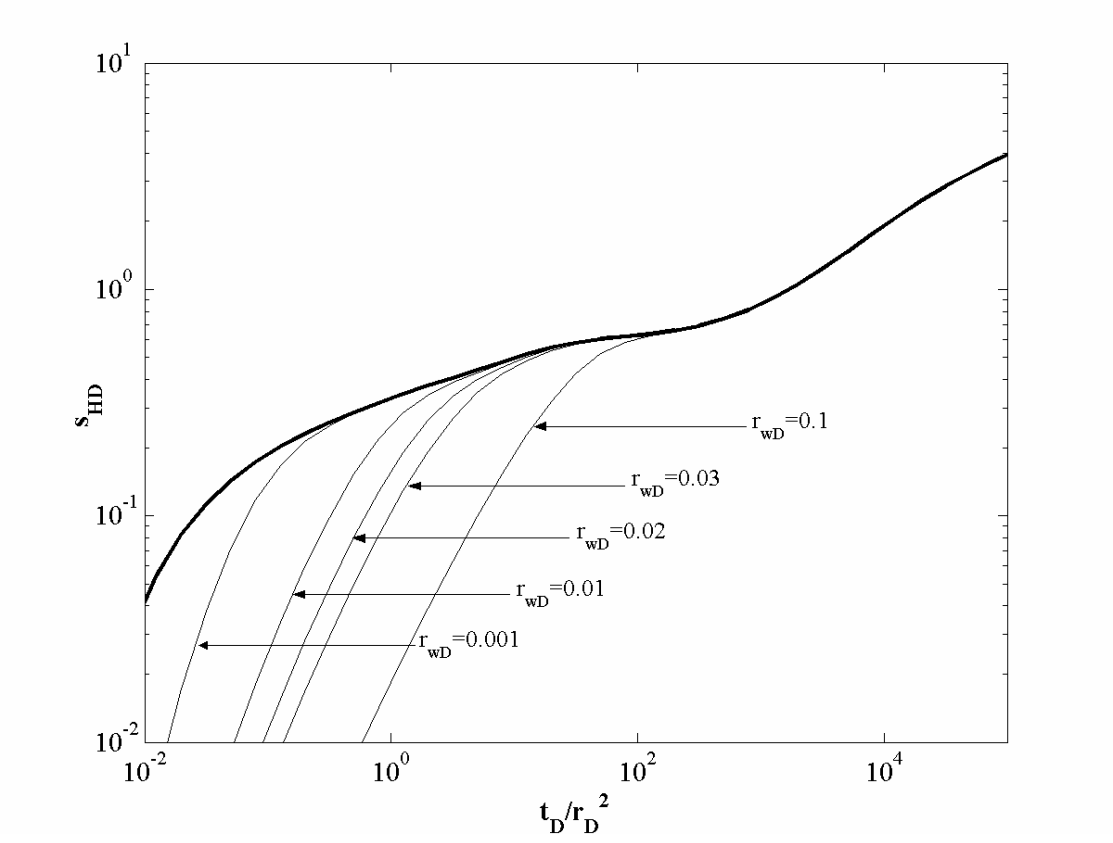

Figure 4.3. Comparison of different wellbore radius in a fractured water-table aquifer. Ideal response of the aquifer (bold line) is compared with several different finite wellbore solutions (thin line) with different dimensionless wellbore radius (r_{wD}=0.001, 0.01, 0.02, 0.03, and 0.1).

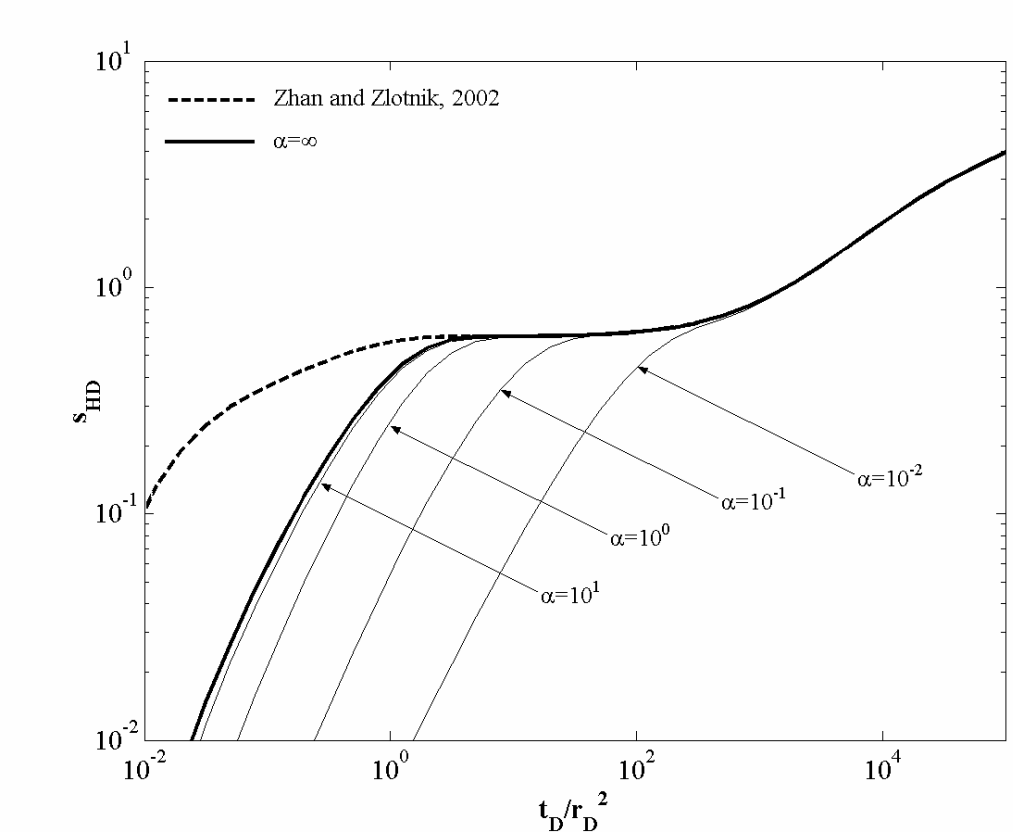

Figure 4.4. Comparison of different skin parameters (α) in porous water-table aquifer. Ideal response of the aquifer (bold line) and the previous study (bold dash line) is compared with several different dimensionless skin parameters of this study (α=0.01, 0.1, 1, and 10).

For instance, for $\alpha=10^0$ and 10^{-2}, the type curves converge to the type curve of Zhan and Zlotnik (2002) at approximately at t_D / r_D^2 =10 and 10^3 respectively. Using the parameters in Table 4.1, these are corresponding to t=4 sec and 400 sec, respectively. This indicates that after the first several minutes of pumping, the Zhan and Zlotnik (2002) can be safely used for practical purpose.

4.3.3 Specific storativity of the aquitard

We make sensitivity analysis on dimensionless aquitard storage parameters (γ), which is proportional to the aquitard specific storativity. In a case that the aquitard storage is non-negligible (silt/clay), the water supply from the aquitard storage plays a role during the mid-time of the type curve when compared to the case excluding the aquitard storage (See Figure 4.5). The highest value of dimensionless aquitard storage parameter shows the greatest deviation from negligible aquitard storage model. It is interesting to find out that at the late time, the storage water from the aquitard is depleted and the type curves corresponding to different aquitard storage coefficients merge to the type curve of the case excluding the aquitard storage.

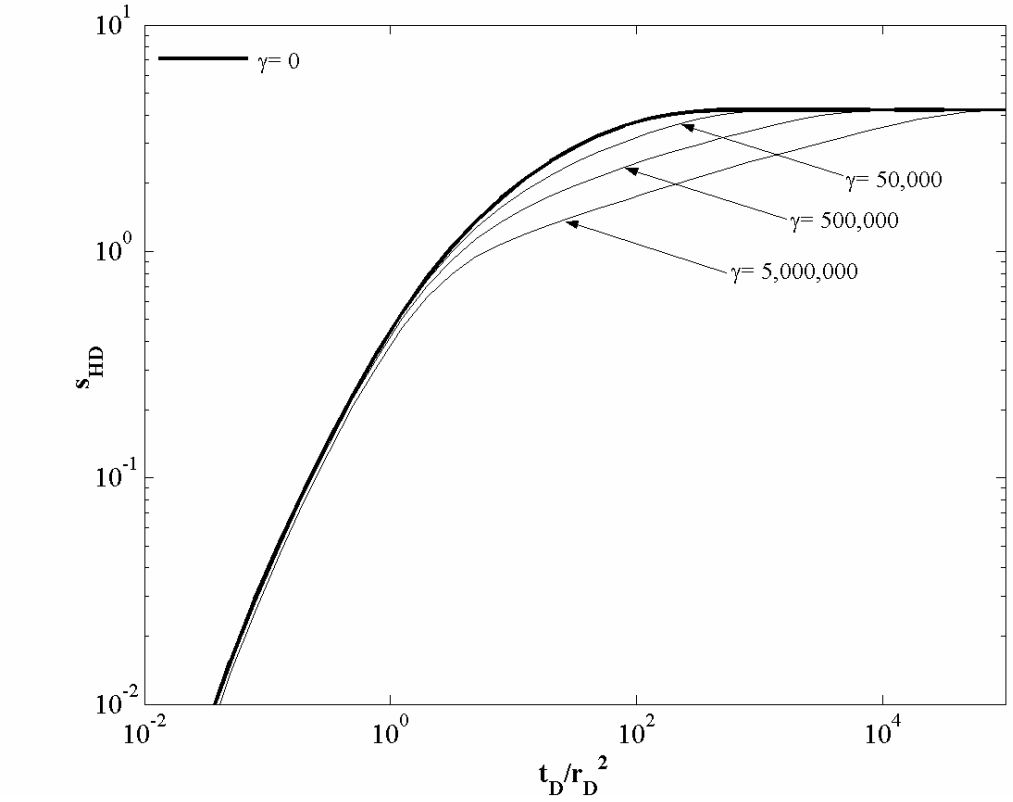

Figure 4.5. Comparison of different aquitard storage parameters (γ). No aquitard storage case (bold line) (Park and Zhan, 2002) is compared with several different dimensionless aquitard storage parameters (γ=5,000,000, 500,000, and 50,000).

4.3.4 Hydraulic conductivity of the matrix

We test several hydraulic conductivity ratios (v) of 10^{-1}, 10^{-3}, 10^{-5}, and 10^{-7} under S'_s/S_s=50. Figure 4.6 shows a few interesting results for a confined aquifer. First, the higher hydraulic conductivity of the matrix (higher v value) results in the lower drawdown at a given time. Second, the type curves with different v values converge at the late time, and the smaller the v value, the longer it takes to converge. Third, the type curves with different v values depart from the non-fractured type curve developed by Park and Zhan (2002), and the larger the v value, the earlier it starts to depart.

Using the same hydraulic conductivity ratios and S'_s/S_s as that used in Figure 4.6, Figure 4.7 shows the result for a water-table aquifer. In Figure 4.7, one can see that the trends are similar to that of a fractured confined aquifer. However, the effect caused by the hydraulic conductivity of the matrix is more prominent at the early time, but less prominent at the late time. That is because at the late time, most of the water is supplied from the unsaturated zone, thus the contribution from the matrix becomes much less important. Figure 4.7 shows that one can apply the non-fractured aquifer solution to the fractured aquifer system in a water-table aquifer if the contrast of the hydraulic conductivity between fracture and matrix is very large ($v \le 10^{-5}$). According to this analysis, we generally cannot ignore the water flow from matrix to fracture even if the hydraulic conductivity of the matrix is almost negligible compare to that of fracture.

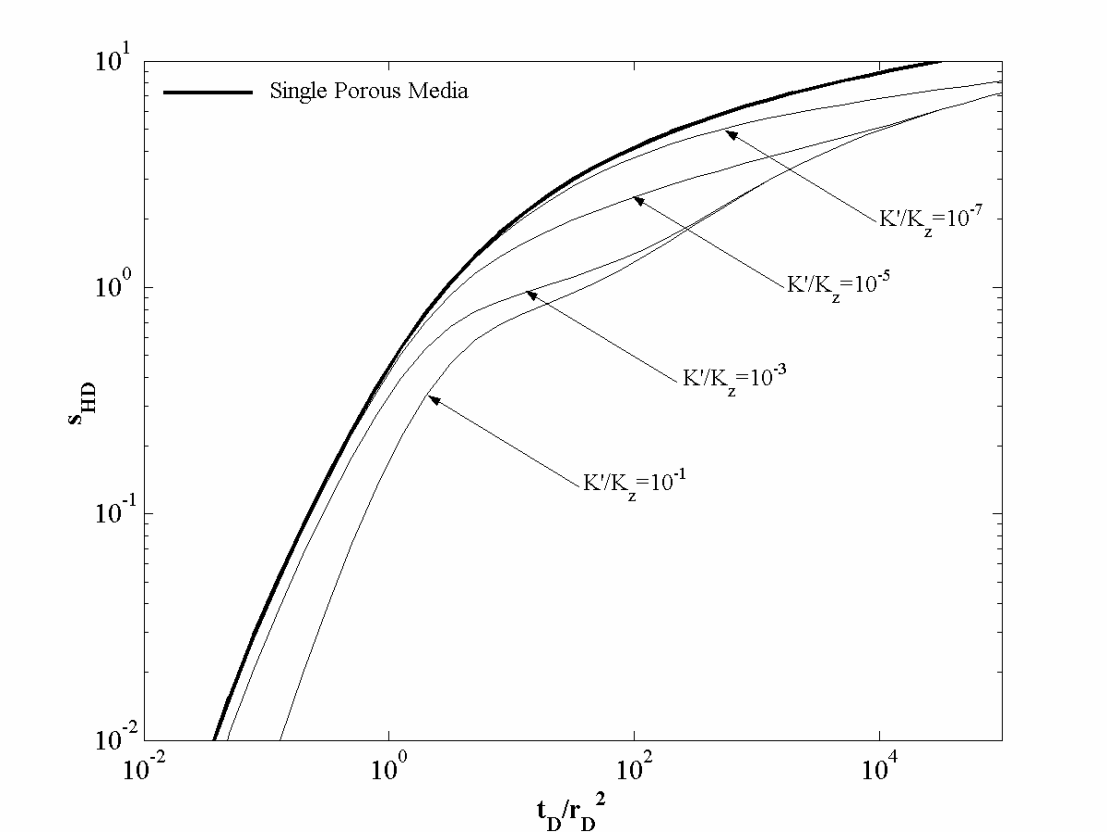

Figure 4.6. Comparison of different hydraulic conductivities of the matrix in fractured confined aquifer system. Non-fractured aquifer solution (bold line) (Park and Zhan, 2002) is compared with several different hydraulic conductivity ratios between matrix and fracture (v=10^{-1}, 10^{-3}, 10^{-5}, and 10^{-7}).

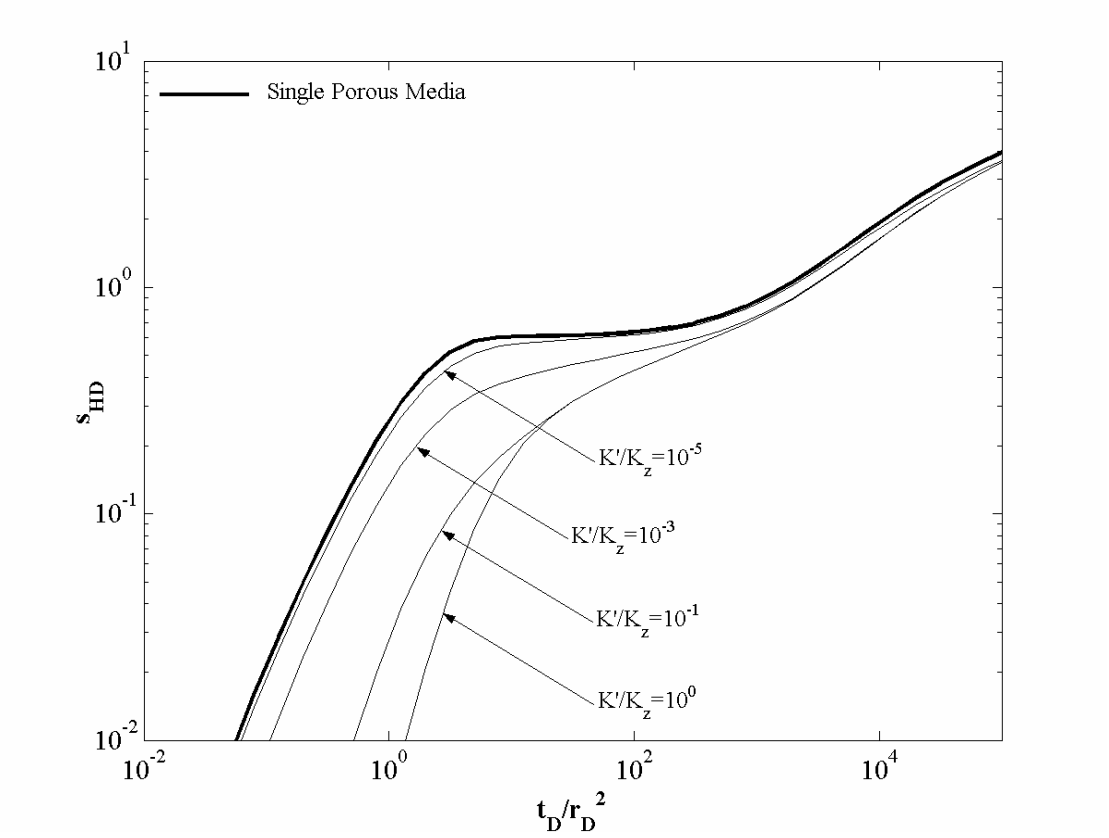

Figure 4.7. Comparison of different hydraulic conductivities of the matrix in fractured water-table aquifer system. Non-fractured aquifer solution (bold line) is compared with several different hydraulic conductivity ratios between matrix and fracture (ν=10^{-1}, 10^{-3}, 10^{-5}, and 10^{-7}).

4.3.5 Specific storativity of the matrix

We test several specific storativity ratios (σ) of 5,000, 500, 50, and 5 under $K'/K_z=10^{-5}$. In Figure 4.8, one can see that after a certain time, drawdown curves start to depart from the early single porosity curve. One can see that the departing times and depressions of the drawdown curves depend on specific storativity ratios. Our analysis shows that when the specific storativity of the matrix is very small, the fractured aquifer solution converges into the non-fractured aquifer solution. However, in many real cases, the matrix systems have much higher capabilities to store water than fracture systems, thus the fractured aquifer solutions are substantially different from the non-fractured aquifer solutions. On the contrary, in a fractured water-table aquifer system, the solution is much less sensitive to the specific storativity ratio. This is because the drawdown depends more on the water from the unsaturated zone than from the matrix after the mid-time.

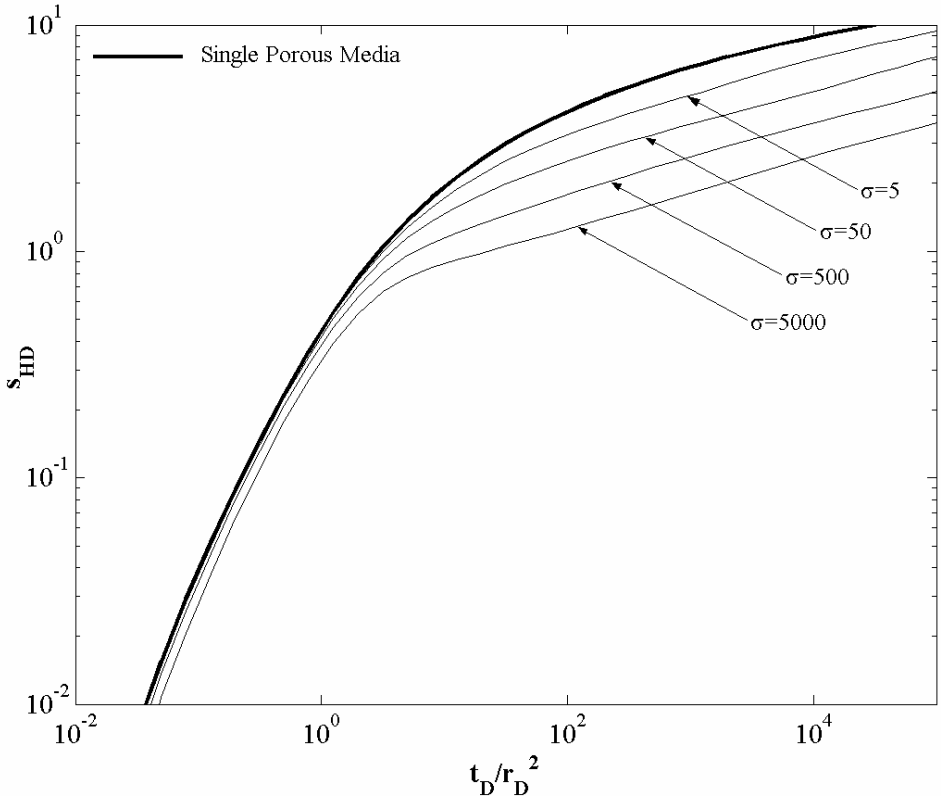

Figure 4.8. Comparison of different specific storativity of the matrix in fractured confined aquifer system. Non-fractured aquifer solution (bold line) is compared with several different specific storativity ratios between matrix and fracture (ν=5,000, 500, 50, and 5).

4.4 Conclusions

Three-dimensional semi-analytical solutions for finite-diameter horizontal wells in fractured shallow aquifer systems, i.e. water-table aquifers and leaky confined aquifers, are derived through this study. They have more applicability on many realistic aquifer systems including fractured/non-fractured aquifers. The derived solutions improve previous finite diameter aquifer solutions (Park and Zhan, 2002) by considering fractured media and also including aquitard storage. Also, the solutions improve previous horizontal well solutions for water-table aquifers (Zhan and Zlotnik, 2002) by including wellbore storage and skin effects.

The solutions are derived base on the method of superposition by integrating the point-source solutions. A graphically integrated numerical MATLAB program named FINHOW2 is developed to facilitate the input and output handling. This program can handle six types of aquifer conditions and twenty-one controllable hydrogeologic and well parameters.

In general, the drawdowns are more sensitive to the hydraulic conductivity and storativity of the matrix in a fractured confined aquifer than that in a fractured water-table aquifer.

In a confined aquifer that is either fractured or non-fractured, there is an appreciable difference between a fractured aquifer and a non-fractured aquifer at the later time. In a water-table aquifer, the drawdowns for both fractured and non-fractured cases converge at the later time and no appreciable effect of matrix flow can be found.

We find that the wellbore storage effects in both fractured confined aquifers and fractured water-table aquifer are very similar to what we have seen in non-fractured confined aquifers (Park and Zhan, 2002). This finding indicates that the wellbore storage effect substantially surpasses the matrix-fracture flow effect at the early pumping stage in a fractured aquifer. In regard to the skin effect, the results of fractured confined aquifers and fractured water-table aquifers are also very similar to those in non-fractured confined aquifers (Park and Zhan, 2002). We find that for practical purpose, the skin effect is usually negligible after the first several minutes of pumping in a water-table aquifer.

In a case that the aquitard storage is non-negligible (silt/clay), the water supply from the aquitard storage plays a role during the mid-time of the type curve when compared to the case excluding the aquitard storage.

Several interesting results are found with different matrix/fracture hydraulic conductivity ratios (v) in a confined aquifer. The type curves with different v values depart from the non-fractured type curve developed by Park and Zhan (2002). In a fractured water-table aquifer, the effect caused by the hydraulic conductivity of the matrix is more prominent at the early time, and less prominent at the late time. We can apply the non-fractured aquifer solution to the fractured aquifer system in a water-table aquifer if the contrast of the hydraulic conductivity between fracture and matrix is very large ($v \leq 10^{-5}$). We generally cannot ignore the water flow from matrix to fracture even if the hydraulic conductivity of the matrix is almost negligible compare to that of fracture.

In a fractured confined aquifer, the solution is sensitive to the specific storativity ratio; but in a fractured water-table aquifer, the solution is much less sensitive to the specific storativity ratio.

CHAPTER V

SUMMARY AND FUTURE WORKS

5.1 Summary

In this dissertation, we have investigated the contaminant transport problems from finite sources in a finite thickness aquifer with consideration of point, line, area, and volume sources. We have also studied well hydraulics of finite diameter horizontal wells in finite thickness confined, leaky confined, and water table aquifers with consideration of porous or fractured media.

In Chapter II, we generated analytical solutions of multidimensional concentration fields originated from one- two-, and three-dimensional, finite sources within finite-thickness aquifers using the Green's function method. Based on our findings, a library of analytical solutions for different source shapes is compiled. To facilitate the calculation, a computational code integrated with the library of many different source shapes and the graphical user interface is developed. The derived analytical solutions show that the upper and lower aquifer boundaries have a profound influence upon the concentration distribution. We also find that the concentration at a near field point is sensitive to the source geometry when the dispersion coefficients are anisotropic; it is less sensitive to the source geometry when the dispersion coefficients are isotropic. The concentration at a far field is found to be almost independent of the source geometry.

In Chapter III, we provided solutions on groundwater flow to a finite-diameter horizontal well including wellbore storage and skin effect. These solutions offer better

physical insights than previous line source solutions into the hydraulics of horizontal wells in three-dimensionally anisotropic leaky aquifers. They are more useful for describing the near field drawdown behavior. A graphically integrated numerical MATLAB program FINHOW is written to evaluate the developed semi-analytical solutions and to provide the type curves of groundwater flow to a finite-diameter horizontal well.

Our solution shows that the finite-diameter of the well only influences the near field at the early flow time. The finite-diameter solution converges to the line source solution at very early dimensionless time in an isotropic aquifer if excluding the wellbore storage. If the wellbore storage is included, it will take a much longer time for the finite-diameter solution to converge to the line source solution. The skin effect impacts flow through the conductance of the wellbore skin. A higher skin conductance means easier flow from the aquifer to the well and quicker response of the aquifer to the pumping. When the skin conductance increases, the drawdown becomes less sensitive to the skin conductance, and the type curves approach the asymptotic limit that is corresponding to an infinite conductance case. The anisotropy controls the relative strength of vertical and horizontal flows at the early time, and thus shows a strong influence on the early time near-field drawdown. The leakage parameter influences the late pseudo-radial flow substantially but has limited impact on the early and intermediate flows when excluding the storage in the leaky confining layer.

In Chapter IV, three-dimensional semi-analytical solutions for finite-diameter horizontal wells in fractured shallow aquifer systems, i.e. water-table aquifer and leaky

confined aquifer, are derived. They have more applicability on many realistic aquifer systems including fractured/non-fractured aquifers. The derived solutions improve previous finite diameter aquifer solutions developed in the Chapter III by considering fractured media and also including aquitard storage. Also, the solutions improve previous horizontal well solutions for water-table aquifers by including wellbore storage and skin effects. A graphically integrated numerical MATLAB program named FINHOW2 is developed to facilitate the input and output handling. This program can handle six types of aquifer conditions and twenty-one controllable hydrogeologic and well parameters.

In general, the drawdowns are more sensitive to the hydraulic conductivity and storativity of the matrix in a fractured confined aquifer than that in a fractured water table aquifer. In a confined aquifer that is either fractured or non-fractured, there is an appreciable difference between a fractured aquifer and a non-fractured aquifer in later time drawdown history. In a water-table aquifer, the drawdowns for both fractured and non-fractured cases converge in later time and no appreciable effect of matrix flow can be found. We find that the wellbore storage effects in both fractured confined aquifers and fractured water table aquifer are very similar to what we have seen in non-fractured confined aquifers. This finding indicates that the wellbore storage effect substantially surpasses the matrix-fracture flow effect at the early pumping stage in a fractured aquifer. In regard to the skin effect, the results of fractured confined aquifers and fractured water table aquifers are also very similar to those in non-fractured confined aquifers. We find that for practical purpose, the skin effect is usually negligible after the first several

minutes of pumping in a water table aquifer. In a case that the aquitard storage is non-negligible (silt/clay), the water supply from the aquitard storage plays a role during the mid-time of the type curve when compared to the case excluding the aquitard storage. Several interesting results are found with different matrix/fracture hydraulic conductivity ratios in a confined aquifer. The type curves with different matrix-fracture hydraulics conductivity ratio, ν, values depart from the non-fractured type curve developed by Chapter III. In a fractured water table aquifer, the effect caused by the hydraulic conductivity of the matrix is more prominent in the early time, and less prominent in the late time. We can apply the non-fractured aquifer solution to the fractured aquifer system in a water-table aquifer if the contrast of the hydraulic conductivity between fracture and matrix is very large. We generally cannot ignore the water flow from matrix to fracture even if the hydraulic conductivity of the matrix is almost negligible compare to that of fracture. In a fractured confined aquifer, the solution is sensitive to the specific storativity ratio; but in a fractured water table aquifer, the solution is much less sensitive to the specific storativity ratio.

Finally, I expect our works will be used for many practical problems related with contaminant transport, and application of horizontal wells in environmental and hydrological problems. Our ultimate goal are keeping our invaluable resources, groundwater, from deteriorations and depletions and finding better ways to manage groundwater resources.

5.2 Future Works

Based on this study, the finite contaminant source model in contaminant transport theory will be improved to be closer to reality. The mixed type boundary condition will be considered to simulate more realistic contaminant solute effluent phenomenon from source zone.

The horizontal wells have very high potential to be experienced the heterogeneity of the aquifer system due to its long wellbore. On the basis of this study, the new methods to figure out field heterogeneity using horizontal wells will be developed. Also, in analytical simulation, horizontal wells have been treated as constant flux boundary with no internal impedance of water flow but, in reality, we need to consider it as a constant head boundary and also need to consider the internal impedance of water flow. In the following study, all the problems mentioned will be addressed.

NOMENCLATURE

1. CHAPTER II

C	concentration of point at time (kg/m^3)
d	aquifer thickness (m)
K_x, K_y, K_z	longitudinal, transverse horizontal and vertical dispersion coefficients (m^2/day)
G	Green's function
q_0	constant source strength (kg/(m^3·day))
q_a	area source strength function (kg/(m^2·day))
q_f	line source strength function (kg/(m·day))
q_p	point source strength function (kg/day)
q_v	volume source strength function (kg/(m^3·day))
$S(M,t)$	source function
t	time (day)
v	velocity of groundwater (m/day)
x, y, z	coordinates of the point where concentration is measured (m)
x_0, y_0, z_0, z_1	sources dimensions along the x, y-, and z-axis (m)
$\delta(\ )$,	Dirac Delta function
λ	first-order decay factor (day^{-1})

2. CHAPTER III

B_D	Dimensionless leakage coefficient
C_s	Conductance of wellbore skin (sec^{-1})
d	Thickness of leaky confined aquifer (m)
d'	Thickness of leaky confining layer (m)
d_s	Thickness of skin (m)
f	Averaged drawdown outside of the skin (m)
f_D	Dimensionless averaged drawdown outside of the skin
$\bar{f}_D$	Dimensionless averaged drawdown outside of the skin in Laplace domain
g_0	Dimensionless point geometric function
$\bar{g}$	Dimensionless geometric function of horizontal well in Laplace domain
$\bar{g}_0$	Dimensionless point geometric function in Laplace domain
$\bar{g}^*$	Dimensionless averaged geometric function of horizontal well in Laplace domain
h	Hydraulic head (m)
h_0	Initial hydraulic head (m)
K	Hydraulic conductivity of an isotropic aquifer (m/sec)
K'	Hydraulic conductivity of leaky confining layer (m/sec)
$K_0(\ )$	Modified Bessel function second kind zero order

K_s	Hydraulic conductivity of skin zone (m/sec)
K_x, K_y, K_z	Principal hydraulic conductivities along *x*-, *y*-, and *z*- axis, respectively (m/sec)
L	Screen length of horizontal wellbore (m)
L_D	Dimensionless Screen length of horizontal wellbore
$L^{-1}( )$	Inverse Laplace transform, respectively
p	Laplace transform variable with respect to dimensionless time
Q	Total pumping rate (m^3/sec)
Q_f	Total aquifer pumping rate (m^3/sec)
Q_w	Total wellbore storage pumping rate (m^3/sec)
Q_{fD}	Dimensionless total aquifer pumping rate
Q_{wD}	Dimensionless total wellbore storage pumping rate
$\bar{Q}_{fD}$	Dimensionless total wellbore storage pumping rate in Laplace domain
q	Reference pumping rate (m^3/sec)
q_f	Aquifer pumping rate (m^3/sec)
q_{fD}	Dimensionless aquifer pumping rate
$\bar{q}'_{fD}$	Modified dimensionless aquifer pumping rate in Laplace domain
q'_{fD}	Modified dimensionless aquifer pumping rate in real time domain
r_c	Radius of the casing connected with the horizontal well screen (m)
r_D	Dimensionless horizontal distance from point source to monitoring location

r_s	$=r_w+d_s$, outer radius of the skin (m)
r_w	Wellbore radius (m)
r_{wD}	Dimensionless wellbore radius
S_s	Specific storativity (m^{-1})
s	Drawdown outside wellbore (m)
s_D	Dimensionless drawdown outside wellbore
s_{HD}	Dimensionless drawdown caused by a horizontal well
s'_D	Modified dimensionless drawdown outside wellbore
$\bar{s}'_D$	Modified dimensionless drawdown outside wellbore in Laplace domain
s_w	Drawdown inside wellbore (m)
s_{wD}	Dimensionless drawdown inside wellbore
t	Time (sec)
t_D	Dimensionless time
V	Volume of finite diameter horizontal wellbore (m^3)
x, y, z	Longitudinal, transversal, and vertical coordinates, respectively (m)
x_0, y_0, z_0	Coordinates of the point source along the *x*-, *y*-, and *z*- axis (m)
x_{0D}, y_{0D}, z_{0D}	Dimensionless coordinates of the point source along the *x*-, *y*-, and *z*- axis
x_D, y_D, z_D	Dimensionless coordinates of the monitoring point along the *x*-, *y*-, and *z*-axis

z_w	Depth from the central axis of the horizontal well to the lower boundary (m)
α	Dimensionless skin conductance coefficient
β	Dimensionless wellbore storage coefficient
$\delta( )$	Dirac delta function
η	Skin effect parameter

3. CHAPTER IV

A,	area along outside of the horizontal wellbore (m^2)
d,	thickness of the aquifer (m)
d_c,	thickness of the aquitard (m)
C_w,	conductance of wellbore skin (s^{-1})
$\bar{g}_0$	Dimensionless point geometric function in Laplace domain
$\bar{g}^*$	Dimensionless averaged geometric function of horizontal well in Laplace domain
h,	hydraulic head (m)
h',	hydraulic head in the matrix (m)
h_0,	initial hydraulic head (m)
h_C,	hydraulic head in the aquitard (m)
$K_0( )$,	second kind zero-order modified Bessel function
K_x, K_y, K_z,	principal hydraulic conductivities along x-, y-, and z- axis, respectively (m/s)

K',	hydraulic conductivity of the matrix (m/s)
K_c,	hydraulic conductivity of the aquitard (m/s)
L,	screen length of horizontal wellbore (m)
p,	Laplace transform variable with respect to dimensionless time
Q,	total pumping rate (m^3/s)
$\bar{Q}_{fD}$	Dimensionless total wellbore storage pumping rate in Laplace domain
r,	variable in spherical coordinate (m)
r_D,	dimensionless horizontal radial distance
r_m,	radius of the matrix (m)
r_w,	well radius (m)
S_s,	specific storativity (m^{-1})
S_y,	specific yield
S_s',	specific storativity of the matrix (m^{-1})
S_{sc},	specific storativity of the aquitard (m^{-1})
s,	drawdown (m)
s',	drawdown in matrix (m)
s_C,	drawdown in aquitard (m)
t,	time (s)
V,	volume of finite diameter horizontal wellbore (m^3)
x, y, z,	longitudinal, transversal, and vertical coordinates, respectively (m)
x_0, y_0, z_0,	coordinates of the point source along x-, y-, and z- axis (m)

z_w,	depth from the central axis of the horizontal well to the lower boundary (m)
α,	dimensionless skin conductance coefficient
β,	dimensionless wellbore storage coefficient
α_1,	empirical constant for drainage from the unsaturated zone (s^{-1})
δ( ),	Dirac Delta function
Γ_1,	inter-porosity flux between matrixes and fractures (s^{-1})
Γ_2,	leakage flux from adjacent aquifer (s^{-1})

REFERENCES

Abramowitz, M., Stegun, I.A., 1972. Handbook of Mathematical Functions. Dover Publications, New York, USA.

Agarwal, R.G., Al-Hussainy, R., Ramey, H.J., 1970. An investigation of wellbore storage and skin effect in unsteady liquid flow: I. Analytical treatment. Soc. Pet. Eng. J. 10, 279-290.

Arfken, G.B., Weber, H.J., 1995. Mathematical Methods for Physicists. 4th ed., Academic Press, San Diego, USA.

Barenblatt, G.I., Zheltov, I.P., Kocina, I.N., 1960. Basic concepts in the theory of seepage of homogeneous liquids in fissured rocks. J. Appl. Math. Mech. Engl. Transl. 24, 1286-1303.

Batu, V., 1989. A generalized two-dimensional analytical solution for hydrodynamic dispersion in bounded media with the first-type boundary condition at the source, Water Resour. Res. 25 (6), 1125-1132.

Batu, V., 1993. A generalized two-dimensional analytical solute transport model in bounded media for flux-type finite multiple sources. Water Resour. Res. 29 (8), 2881-2892.

Bear, J., 1972. Dynamics of Fluids in Porous Media. Elsevier, New York, USA.

Bear, J., 1979. Hydraulics of Groundwater. McGraw-Hill, New York, USA.

Boulton, N.S., Streltsova, T.D., 1977. Unsteady flow to a pumped well in a fissured water-bearing formation. J. Hydrol. 35, 257-270.

Carslaw, H.S., Jaeger, J.C., 1959. Conduction of Heat in Solids. Clarendon Press, Oxford, UK.

Cassiani, G., Kabala, Z.J., 1998. Hydraulics of a partially penetrating well: solution to a mixed-type boundary value problem via dual integral equations. J. Hydrol. 211 (1-4), 100-111.

Cassiani, G., Kabala, Z.J., Medina, M.A., 1999. Flowing partially penetrating well: solution to a mixed-type boundary value problem. Adv. Water Resour. 23 (1), 59-68.

Cleveland, T.G., 1994. Recovery performance for vertical and horizontal wells using semianalytical simulation. Ground Water 32(1), 103-107.

Cole, K., Zlotnik, V., 1994. Modification of Dagan's numerical method for slug and packer test interpretation, in "Computational Methods in Water Resources X". Kluwer Academic Publishers, Dordrecht, Netherlands.

Daviau, F., Mouronval, G., Bourdarot, G., Curutchet, P., 1988. Pressure analysis for horizontal wells. SPE Formation Evaluation 3 (4), 716-724.

de Hoog, F.R., Knight, J.H., Stokes, A.N., 1982. An improved method for numerical inversion of Laplace transforms. SIAM J. Sci. and Stat. Comp. 3, 357-366.

Deruyck, B.G., Bourdet, D.P., DaPrat, G., Ramey, H.J., Jr., 1982. Interpretation of interference tests in reservoirs with double porosity behavior, theory and field examples. SPE Paper 11025, Soc. of Pet. Eng. of AIME, Dallas, TX.

Domenico, P.A., Robbins, G.A., 1984. A new method of contaminant plume analysis. Ground Water 23, 476-485.

Domenico, P.A., 1987. An analytical model for multidimensional transport of a decaying contaminant species. J. Hydrol. 91, 49-58.

Domenico, P.A., Schwartz, F.W., 1998. Physical and Chemical Hydrogeology (2nd ed.). John Wiley & Sons, New York, USA.

Dougherty, D.E., Babu, D.K., 1984. Flow to a partially penetrating well in a double-porosity reservoir. Water Resour. Res. 20(8), 1116-1122.

Ehlig-Economides, C., Joseph, J., 1987. A new test for determination of individual layer porosities in a multilayered reservoir. SPE Formation Evaluation 2 (3), 261-283.

Falta, R.W., 1995. Analytical solutions for gas flow due to gas injection and extraction from horizontal wells. Ground Water 33 (2), 235-246.

Fetter, C.W., 1999. Contaminant Hydrogeology (2nd ed.). Prentice Hall, Upper Saddle River, NJ, USA.

Gelhar, L.W., 1993. Stochastic Subsurface Hydrology. Prentice Hall, Englewood Cliffs, NJ, USA.

Goode, P.A., Thambynayagam, R.K.M., 1987. Pressure drawdown and buildup analysis of horizontal wells in anisotropic media. SPE Formation Evaluation 2 (4), 683-697.

Gringarten, A.C., Ramey, H.J. Jr., 1973. The use of source and Green's functions in solving unsteady-flow problems in reservoirs. Soc. Pet. Eng. J. 13, 285-296.

Haitjema, H.M., Kraemer, S.R., 1988. A new analytic function for modeling partially penetrating wells. Water Resour. Res. 24 (5), 683-690.

Hantush, M.S., 1960. Modification of the theory of leaky aquifers. J. Geophy. Res. 65(11), 3713-3716.

Hantush, M.S., Papadopulos, I.S., 1962. Flow of ground water to collector wells. J. Hydraulics Division, Proc. Am. Soc. Civil Engrs. HY 5, 221-244.

Hantush, M.S., 1964. Hydraulics of Wells, in Advances in Hydroscience. Academic Press, New York, USA.

Hemker, C.J., 1999. Transient well flow in vertically heterogeneous aquifers. J. Hydrol. 225, 1-18.

Hollenbeck, K.J., 1998. INVLAP.M, A MATLAB function for numerical inversion of Laplace transforms by the de Hoog algorithm. http://www.isva.dtu.dk/staff/karl/invlap.htm.

Hunt, B., Massmann, J.W., 2000. Vapor flow to trench in leaky aquifer. J. Evir. Engr. 126, 375-380.

Jargon, J.R., 1976. Effect of wellbore storage and wellbore damage at the active well on interference test analysis. J. Pet. Technol. 28, 851-858.

Jiao, J.J., Rushton, K.R., 1995. Sensitivity of drawdown to parameters and its influence on parameter estimation for pumping tests in large-diameter wells. Ground Water 33 (5), 794-800.

Joshi, S.D., 1988. Augmentation of well productivity with slant and horizontal wells. J. Pet. Tech., 729-739.

Kabala, Z.J., Cassiani, G., 1997. Well hydraulics with the Weber-Goldstein transforms. Transport in Porous Media 29 (2), 225-246.

Kazemi, H., 1969. Pressure transient analysis of naturally fractured reservoirs with uniform fracture distribution. Trans. Soc. Pet. Eng. AIME 246, 451-462.

Kirkham, D., 1959. Exact theory of flow into a partially penetrating well. J. Geophys. Res. 64, 1317-1327.

Kuchuk, F.J., Habashy, T., 1996. Pressure behavior of horizontal wells in multilayer reservoirs with crossflow. SPE Formation Evaluation 11 (1), 55-64.

Lai, R.Y.S., Su, C.W., 1974. Nonsteady flow to a large well in a leaky aquifer. J. Hydrol. 22, 333-345.

Leij, F.J., Toride, N., van Genuchten, M.T., 1993. Analytical solutions for non-equilibrium solute transport in three-dimensional porous media. J. Contam. Hydrol. 151, 193-228.

Leij, F.J., Priesackand, E., Schaap, M. G., 2000. Solute transport modeled with Green's functions with application to persistent solute sources. J. Contam. Hydrol. 41, 155-173.

MathWorks, Inc., 2000. MATLAB (software), website: http://www.mathworks.com/. Natick, MA, USA.

Maurer W.C., 1995. Recent advances in horizontal drilling. J. Can. Pet. Tech. 34 (9), 25-33.

Moench, A.F., 1984. Double-porosity models for a fissured groundwater reservoir with fracture skin. Water Resour. Res. 20 (7), 831-846.

Moench, A.F., Hsieh, P., 1985. Comment on "Evaluation of slug tests in wells containing a finite-thickness skin" by C.R. Faust, J.W. Mercer. Water Resour. Res. 21 (9), 1459-1461.

Moench, A.F., 1985. Transient flow to a large-diameter well in an aquifer with storative semiconfining layers. Water Resour. Res. 21 (8), 1121-1131.

Moench, A.F., 1997. Flow to a well of finite diameter in a homogeneous, anisotropic water table aquifer. Water Resour. Res. 33 (6), 1397-1407.

Moench, A.F., 1998. Correction to “Flow to a well of finite diameter in a homogeneous, anisotropic water table aquifer” by AF Moench. Water Resour. Res. 34 (9), 2431-2432.

Morgenau, M., Murphy, G. M., 1956. The Mathematics of Physics and Chemistry. Van Nostrand Company, Princeton, NJ, USA.

Murdoch, L.C., 1994. Transient analyses of an interceptor trench. Water Resour. Res. 30 (11), 3023-3031.

Muskat, M., 1937. The Flow of Homogeneous Fluids Through Porous Media. J.W. Edwards, Ann Arbor, USA.

Ng, M.C., Aguilera, R., 1999. Well test analysis of horizontal wells in bounded naturally fractured reservoirs. J. Can. Pet. Technol. 38 (7), 20-24.

Novakowski, K.S., 1989. A composite analytical model of analysis of pumping tests affected by well bore storage and finite thickness skin. Water Resour. Res. 25 (9), 1937-1946.

Ogata, A. and Banks, R. B., 1961. A solution of differential equation of longitudinal dispersion in porous media. U. S. Geological Survey, Prof. Paper no. 411-A.

Ohaeri, C.U., Vo, D.T., 1991. Practical solutions for interactive horizontal well test analysis. SPE Paper 22729, Soc. of Pet. Eng. of AIME, Dallas, TX.

Ozkan, E., Raghavan, R., 1991. New solutions for well-test-analysis problems: Part 1-Analytical consideration. SPE Formation Evaluation 6 (3), 359-368.

Papadopulos, I.S., Cooper, H.H., 1967. Drawdown in a well of large diameter. Water Resour. Res. 3 (1), 241-244.

Park, E., Zhan, H., 2002. Hydraulics of a finite diameter horizontal well with wellbore storage and skin effect in leaky aquifers. Adv. Water Resour. 25(4), 389-400.

Parmentier, P.P., Klemovich, R.M., 1996. A New Direction in Remediation. Civil Engr.66, 55-57.

Press, W.H., Flannery, B.P., Teukolsky, S.A., Vetterling, W.T., 1989. Numerical Recipes, the Art of Scientific Computing. Cambridge University Press, New York, USA

Ramey, H.J., 1965. Non-Darcy flow and wellbore storage effects in pressure buildup and drawdown of gas wells. J. Pet. Tech. 17, 223-233.

Ramey, H.J., 1970. Short-time well test data interpretation in the presence of skin effect and wellbore storage. J. Pet. Tech. 22, 97-104.

Ramey, H.J., Agarwal, R.G., 1972. Annulus unloading rates as influenced by wellbore storage and skin effect. Soc. Pet. Eng. J. 12 (10), 453-459.

Rosa, A.J., Carvalho, R.D.S., 1989. A mathematical model for pressure evaluation in an infinite-conductivity horizontal well. SPE Formation Evaluation 4 (4), 559-566.

Rund, N.C., Kabala, Z.J., 1997. Response of a partially penetrating well in a heterogeneous aquifer: integrated well-face flux vs. uniform well-face flux boundary conditions. J. Hydrol. 194, 76-94.

Sauty, J.P., 1980. An analysis of hydrodispersive transfer in aquifers. Water Resour. Res. 16, 145-158.

Sawyer, C.S., Lieuallen-Dulam, K.K., 1998. Productivity comparison of horizontal and vertical ground water remediation well scenarios. Ground Water 36 (1), 98-103.

Seines, K., Lieu, S.C., Haug, B.T., 1994. Troll horizontal well tests demonstrate large production potential from thin oil zones. SPE Reservoir Engineering 9 (2), 133-139.

Sen, Z., 1992. Drawdown distribution around a large diameter well with nonlinear groundwater flow. J. Environ. Sci. Health 27 (7), 1817-1833.

Stehfest, H., 1970. Numerical inversion of Laplace transforms, Communications of the ACM 13 (1), 47-49.

Streltsova, T.D., 1988. Well Testing in Heterogeneous Formations. John Wiley&Sons, New York, USA.

USEPA, 1994. Manual Alternative Methods for Fluid Delivery and Recovery. EPA/625/R-94/003.

van Everdingen, A.F., Hurst, W., 1949. The application of the Laplace transformation to flow problems in reservoirs. Trans AIME 186, 305-324.

van Genuchten, M.T., 1981. Analytical solutions for chemical transport with simultaneous adsorption, zero-order production and first-order decay. J. Hydrol. 49, 213-233.

Warren, J.E., Root, R.J., 1963. The behavior of naturally fractured reservoirs. Trans. Am. Inst. Min. Metall. Pet. Eng. 228, 245-255.

Wexler, E.J., 1992. Analytical solutions for one-, two-, and three-dimensional solute transport in ground-water systems with uniform flow. U.S. Geological Survey, Techniques of Water-Resources Investigations, Book 3, Chap. B7.

Wilkinson, D., Hammond, P.S., 1990. A perturbation method for mixed boundary value-problems in pressure transient testing. Transport in Porous Media 5 (6), 609-636.

Yeh, G. T., 1981. AT123D: analytical transient one-, two-, and three-dimensional simulation of waste transport in an aquifer system. Rep. ORNL-5602. Oak Ridge National Laboratory, Oak Ridge, TN.

Zhan, H., 1998. Transport of waste leakage in heterogeneous stratified formations, Adv. in Water Resour. 22 (2), 159-168.

Zhan, H., 1999. Analytical study of capture time to a horizontal well. J. Hydrol. 217, 46-54.

Zhan, H., Cao, J., 2000. Analytical and semi-analytical solutions of horizontal well capture times under no-flow and constant-head boundaries. Adv. Water Resour. 23 (8), 835-848.

Zhan, H., Wang, L.V., Park, E., 2001. On the horizontal-well pumping tests in anisotropic confined aquifers. J. Hydrol. 252(1-4), 37-50.

Zhan, H., Park, E., 2002. Vapor flow to horizontal wells in vadose zones. Soil Sci. Soc. Am. J. 66(3), 710-721.

Zhan, H., Zlotnik, V.A., 2002. Groundwater flow to horizontal and slanted wells in unconfined aquifers. Water Resour. Res., In Press.

Zheng, C., Bennett, G. D.,1995. Applied Contaminant Transport Modeling, Theory and Practice. Van Nostrand Reinhold, New York, USA.

APPENDIX A

Eqs. (3.5)- (3.8) are solved using the procedure described in the Appendix of Zhan et al. (2001). The solution satisfying boundary conditions (3.6) and (3.7) can be written (eg. Dougherty DE, Babu (1984) and Moench (1997)):

$$\overline{s}'_D(p) = \sum_{n=0}^{\infty} H_n(x_D, y_D, p)\cos(\omega_n z_D)\,. \tag{A.1}$$

where H_n is a function depending on the horizontal coordinates and p, and ω_n is the spatial frequency term. The solution is (Zhan et al., 2001):

$$H_0 = 2\overline{q}'_{fD}(p)K_0(r_D\sqrt{p})\,, \tag{A.2}$$

$$H_n = 4\overline{q}'_{fD}(p)\cos(n\pi z_{0D})K_0(r_D\sqrt{n^2\pi^2 + p})\,,\ \text{n>0,} \tag{A.3}$$

where $r_D = [(x_D - x_{0D})^2 + (y_D - y_{0D})^2]^{1/2}$ is the dimensionless horizontal radial distance between the source point and measuring point, and $K_0(u)$ is the second kind, zero order modified Bessel function. Substituting (A.2) and (A.3) into (A.1) results in the solution of $\overline{s}'_D$. Applying inverse Laplace transform to the solution of $\overline{s}'_D$ and using the following identities (Hantush, 1964, p. 303)

$$L^{-1}\left(K_0(r_D\sqrt{p})\right) = \frac{1}{2t_D}\exp(-\frac{r_D^2}{4t_D})\,,\ L^{-1}\left(K_0(r_D\sqrt{p+n^2\pi^2})\right) = \frac{1}{2t_D}\exp(-n^2\pi^2 t_D - \frac{r_D^2}{4t_D})\,, \tag{A.4}$$

and the convolution theorem, where L^{-1} is the inverse Laplace operator, one obtains

$$s'_D(t_D)=\int_0^{t_D} q'_{fD}(t_D-\tau)\exp\left[-\frac{r_D^{\,2}}{4\tau}\right]\left[1+2\sum_{n=1}^{\infty}\cos[n\pi z_D]\cos[n\pi z_{0D}]\exp\left[-n^2\pi^2\tau\right]\right]\frac{d\tau}{\tau}. \qquad \text{(A.5)}$$

Combining (A.5) and definitions of s'_D and q'_{fD} in List of Symbols, one obtains the dimensionless drawdown

$$s_D(t_D)=\int_0^{t_D} q_{fD}(t_D-\tau)\exp\left[-\frac{\tau}{B_D^2}-\frac{r_D^{\,2}}{4\tau}\right]\left[1+2\sum_{n=1}^{\infty}\cos[n\pi z_D]\cos[n\pi z_{0D}]\exp\left[-n^2\pi^2\tau\right]\right]\frac{d\tau}{\tau}. \quad \text{(A.6)}$$

APPENDIX B

Eq. (4.15) can be solved based on the boundary conditions, Eqs. (4.17)-(4.20). According to previous studies (Dougherty and Babu, 1984; Moench, 1997; Zhan et al., 2001; Park and Zhan, 2002), the proposed solution that satisfies the boundary conditions is

$$\overline{s}_D(x_D, y_D, z_D, p) = \sum_{n=0}^{\infty} \overline{f}_n(x_D, y_D; x_{0D}, y_{0D}, p)\cos(\varepsilon_n z_D), \tag{B.1}$$

where $\overline{s}_D$ is the dimensionless drawdown in Laplace domain, $\overline{f}_n$ is the function that depends on the horizontal coordinate and p, and ε_n is the spatial frequency term. For the boundary conditions given by Eqs. (4.17)-(4.19), the solution procedure is same as Park and Zhan (2002). For the boundary conditions given by Eqs. (4.17)-(4.18) and (4.20), by applying Eq. (B.1) into Eq. (4.20), one has

$$\varepsilon_n \tan(\varepsilon_n) = \frac{\eta p}{p + \eta\theta}, \tag{B.2}$$

and from Eq. (B.2), one can find the value of ε_m by a simple root finding routine.

By applying Eq. (B.1) into Eq. (4.15), multiplying $\cos(\varepsilon_m z_{0D})$, and integrating from dimensionless location of lower (z_D=0) to upper (z_D=1) boundaries along z-axis, one has

$$\left(\Psi^2 + \varepsilon_n^2\right)\overline{f}_D = \frac{\partial^2 \overline{f}_D}{\partial x_D^2} + \frac{\partial^2 \overline{f}_D}{\partial y_D^2} + \frac{8\pi \overline{q}_{fD}(p)\delta(x_D - x_{0D})\delta(y_D - y_{0D})\cos(\varepsilon_n z_{0D})}{1 + 0.5\sin(2\varepsilon_n)/\varepsilon_n}. \tag{B.3}$$

The solution for Eq. (B.3) is

$$\bar{g}_0(x_D, y_D, z_D; x_{0D}, y_{0D}, z_{0D}, p) = \sum_{m=0}^{\infty} \frac{4\cos(\varepsilon_n z_{0D})\cos(\varepsilon_n z_D)}{1+0.5\sin(2\varepsilon_n)/\varepsilon_n} K_0\left(r_D\sqrt{\Psi^2+\varepsilon_n^2}\right), \tag{B.4}$$

where $r_D = [(x_D - x_{0D})^2 + (y_D - y_{0D})^2]^{1/2}$ is the dimensionless horizontal radial distance between the source point, (x_{0D}, y_{0D}, z_{0D}), and the measuring point, (x_D, y_D, z_D), and K_0( ) is the second kind, zero order, modified Bessel function.

VITA

Eungyu Park was born in Seoul, Korea, on February 20, 1971. He received a Bachelor of Science degree and a Master of Science degree in Geology from Yonsei University, Seoul, Korea, in February 1997 and February 1999, respectively. Then he was an intern researcher at Yonsei University, Seoul, Korea, specializing in groundwater contaminant transport modeling until starting the doctoral program at Texas A&M University in September 1999. He received his doctoral degree in August 2002. His permanent address is Samsung-Dong, Gangnam-Gu, Seoul, Korea.

This dissertation was typed by the author.